THE UNIVERSITY OF CHICAGO

LANTIBIOTIC-PRODUCING BACTERIA IMPACT MICROBIOME RESILIENCE AND COLONIZATION RESISTANCE

A DISSERTATION SUBMITTED TO
THE FACULTY OF THE DIVISION OF THE BIOLOGICAL SCIENCES
AND THE PRITZKER SCHOOL OF MEDICINE
IN CANDIDACY FOR THE DEGREE OF
DOCTOR OF PHILOSOPHY

COMMITTEE ON MICROBIOLOGY

BY
CODY GENE COLE

CHICAGO, ILLINOIS
JUNE 2025

ABSTRACT

Bacteria utilize bacteriocins as a mechanism to maintain a competitive advantage in their niche. Lantibiotic-producing bacteria have been investigated for their ability to kill opportunistic pathogens such as vancomycin-resistant *Enterococcus faecium* (VRE). However, not much is known about the impact that lantibiotic-producing bacteria can have on the broader microbiome. We find that lanthipeptide genes, including previously characterized lantibiotics, are common among clinical patient gut microbiomes. Using a mouse model, we show the lantibiotic-producing bacterium, *Blautia pseudococcoides* SCSK, is capable of preventing recolonization of keystone species in the gut microbiota post antibiotic treatment. This results in prolonged dysbiosis that leave mice susceptible to *Klebsiella pneumoniae* and *Clostrioides difficile* infection weeks after antibiotic treatment has been suspended. These findings demonstrate the ability bacteria capable of producing broad-spectrum lantibiotics have in shaping the microbiota and may explain a possible mechanism for prolonged dysbiosis observed by patients in the clinic after taking antibiotics.

This dissertation is dedicated to my family, friends, mentors, and all those that have helped me get to where I am today.

TABLE OF CONTENTS

LIST OF PUBLICATIONS

Cody G. Cole, Zhenrun J. Zhang, Shravan R. Dommaraju, Qiwen Dong, Rosemary L. Pope, Sophie S. Son, Emma J. McSpadden, Che K. Woodson, Nicholas P. Dylla, Huaiying Lin, Ashley M. Sidebottom, Anitha Sundararajan, Douglas A. Mitchell, Eric G. Pamer. Lantibiotic-producing bacteria impact microbiome resilience and colonization resistance. *bioAxiv*, 2025. doi:10.1101/2025.05.06.652565.

Zhenrun J. Zhang, **Cody G. Cole**, Michael J. Coyne, Huaiying Lin, Nicholas Dylla, Rita C. Smith, Téa E. Pappas, Shannon A. Townson, Nina Laliwala, Emily Waligurski, Ramanujam Ramaswamy, Che Woodson, Victoria Burgo, Jessica C. Little, David Moran, Amber Rose, Mary McMillin, Emma McSpadden, Anitha Sundararajan, Ashley M. Sidebottom, Eric G. Pamer, Laurie E. Comstock. Comprehensive analyses of a large human gut Bacteroidales culture collection reveal species- and strain-level diversity and evolution. *Cell Host & Microbe*, 32(10):1853-1867.e5, 2024. ISSN 1931-3128. doi:10.1016/j.chom.2024.08.016.

Matthew A. Odenwald, Huaiying Lin, Christopher Lehmann, Nicholas P. Dylla, **Cody G. Cole**, Jake D. Mostad, Téa E. Pappas, Ramanujam Ramaswamy, Angelica Moran, Alan L Hutchison, Matthew R. Stutz, Mark Dela Cruz, Emerald Adler, Jaye Boissiere, Maryam Khalid, Jackelyn Cantoral, Fidel Haro, Rita A. Oliveira, Emily Waligurski, Thomas G. Cotter, Samuel H. Light, Kathleen G. Beavis, Anitha Sundararajan, Ashley M. Sidebottom, K. Gautham Reddy, Sonali Paul, Anjana Pillai, Helen S. Te, Mary E. Rinella, Michael R. Charlton, Eric G. Pamer, and Andrew I. Aronsohn. Bifidobacteria metabolize lactulose to optimize gut metabolites and prevent systemic infection in patients with liver disease. *Nature Microbiology*, 8(11):2033–2049, 2023. doi:10.1038/s41564-023-01493-w.

Zhenrun J. Zhang, **Cody G. Cole**, Huaiying Lin, Chunyu Wu, Fidel Haro, Emma McSpadden, Wilfred A. van der Donk, and Eric G. Pamer. Exposure and resistance to lantibiotics impact microbiota composition and function. *bioAxiv*, 2023. doi:10.1101/2023.12.30.573728.

Zhenrun J. Zhang, Christopher J. Lehmann, **Cody G. Cole**, and Eric G. Pamer. *Annual Reviews in Microbiology*, 76(1):435-460, 2022. ISSN 0066-4227. doi:10.1146/annurev-micro-041020-022206.

LIST OF FIGURES

LIST OF TABLES

LIST OF ACRONYMS/ABBREVIATIONS

ABC: ATP-binding cassette

Amp: Ampicillin

ARM: Ampicillin-resistant Microbiota

ASV: Amplicon Sequence Variants

ATP: Adenosine Triphosphate

BGC: Biosynthetic Gene Cluster

BHI: Brain Heart Infusion

BpSCSK: *Blautia pseudococcoides* SCSK

BpKH6: *Blautia producta* KH6

C-dox: Chlorine Dioxide-based Disinfectant

CBBP: *Enterocloster* [*Clostridium*] *bolteae*, *Phocaeicola* [*Bacteroides*] *sartorii*, BpSCSK, and *Parabacteroides distasonis*

CFU: Colony-forming Unit

DPBS: Dulbecco's Phosphate-buffered saline

FDA: Food and Drug Administration

FMT: Fecal Microbiota Transplant

GC-MS: Gas Chromatography-Mass Spectrometry

GI: Gastrointestinal

GMM: Gut Metabolite Modules

GRAS: Generally Regarded as Safe

GTP: Guanosine Triphosphate

HIV: Human Immunodeficiency Virus

HMP: Human Microbiome Project

HSV: Herpes Simplex Virus

IP: Intraperitoneal

LC-MS: Liquid Chromatography-Mass Spectrometry

LPS: Lipopolysaccharide

MIC: Minimum Inhibitory Concentration

MICU: Medical Intensive Care Unit

NMVC: Neomycin, Metronidazole, Vancomycin, and Clindamycin

NRP: Non-ribosomal Peptide

NSR: Nisin Resistant Protein

NTP: Nucleoside Triphosphate

OMM^{12}: Oligo-Mouse-Microbiota

PBS: Phosphate-buffered Saline

PFBBr: Pentafluorobenzyl-bromide

P.I.: Post Infection

QTOF: Quadrupole Time-of-flight

RiPP: Ribosomally Synthesized and Post-translationally-modified Peptides

RODEO: Rapid ORF Description and Evaluation Online

RSV: Respiratory Syncytial Virus

SCFA: Short-chain Fatty Acid

SCG: Single-copy Core Gene

SIHUMI: Simplified Human Intestinal Microbiota

SPF: Specific-pathogen-free

TIM1: T-cell Ig mucin domain protein

TPS: Two-component System

VRE: Vancomycin-resistant *Enterococcus*

ACKNOWLEDGMENTS

My time in graduate school has truly been some of the best years of my life, and it was all thanks to the incredible people I have had the pleasure of learning and working with.

I would first like to express my deepest gratitude to my advisor Eric Pamer for giving the opportunity to work in the Pamer lab. The skills and knowledge I have acquired from your mentorship has far exceeded anything I could have ever hoped for in graduate school. It has been incredible to watch the Duchossois Family Institute grow and become one of the leading microbiome institutions in the world under your leadership.

I would especially like to thank all the Pamer lab members and all the others at the Duchossois Family Institute for their help with my graduate research. Much of my work was done alongside Jerry Zhang who also worked extensively on lanthipeptides. Getting to know everyone both professionally and personally while you all built your families and excelled in your careers has been a highlight my time in the Pamer lab. I am extremely glad that I did not have to be the only graduate student in the Pamer lab, and instead got to go through it with Rosemary Pope and Sophie Son.

To all the incredible friends I have made in graduate school, particularly those in my cohort and other in the Committee on Microbiology, I will forever be grateful making graduate school such a enjoyable time. I am going to miss hanging out with you all and playing broomball, volleyball, and softball.

I would like to extend thanks to my thesis committee Mark Mimee, Cathy Pfister, Sam Light, and Phoebe Rice for all the invaluable input you all have given to me throughout my thesis work. I am particularly grateful to Cathy Pfister for allowing me to help establish the Microbiome Symposium and help with the Microbiome Conference at the University of Chicago.

I would like to thank my family for all their continued support throughout my life. Although moving to Chicago has made it difficult to visit, you have all made fill connected

to home. I also would like to thank Ying Huang for being by my side during most of my time in graduate school.

Lastly, I would like to thank my high school science teacher, Diana Turner, for setting me down my path of microbiology research. I could not even imagine what I would do as career other than something related to microbiology and scientific discovery.

CHAPTER 1

INTRODUCTION

In nature, bacteria rarely live in isolation from other bacteria and microbes. Typically, they can be found in complex communities that lead to a vast array of microbe-microbe interactions. These close interactions, however, can lead to strong competitive pressures between microbes, especially in environments with limited space and nutrients. To maintain a competitive advantage within their niche, many bacteria have evolved the ability to produce narrow- and broad-spectrum antibiotics to inhibit or kill neighboring bacteria by targeting specific cellular components or disrupting the bacterial cell wall and/or membrane [Heilbronner et al., 2021]. Antibiotics can come in the form of small molecules or larger bacteriocins. Unlike small-molecule antibiotics, bacteriocins are made up of peptides and consist of antimicrobial non-ribosomal peptides (NRPs), ribosomally synthesized and post-translationally modified peptides (RiPPs), and proteins. These categories are further broken down into groups based on the type of structure and chemical bonds the peptides or proteins contain as well as the enzymes required to produce them.

The mammalian gut microbiota is home to trillions of bacteria and is an environment where space and nutrients can quickly diminish. Metagenomic analysis of the Human Microbiome Project (HMP) has revealed that biosynthetic gene clusters (BGCs) responsible for the production of RiPPs are among the most prevalent BGCs encoded in the human microbiome [Donia et al., 2014, King et al., 2023, Walsh et al., 2015]. Of the RiPPs detected, BGCs for production of lanthipeptides, named after the lanthionine bonds they contain, were the most abundant. Although lanthipeptides can serve various functions, those that have antimicrobial activity are referred to as lantibiotics. The bacterial composition of the gut microbiota can be influenced by many factors such as nutrient competition, quorum-sensing, host defenses, and metabolites. However, the effects of bacteriocins, including lantibiotics, on the gut microbiota as a whole is still largely unknown.

Since their discovery, lantibiotics have been one of the longest studied RiPP types. While extensive work has gone into characterizing the properties of lantibiotics—and lanthipeptides in general—the work outlined in this thesis aims to contribute to our understanding of how lantibiotic-producing bacteria impact the colonization of other gut commensals.

1.1 Structure of lanthipeptides

Lanthipeptides represent all lanthionine- and methyllanthionine-containing peptides. Before the mature peptide has been created, lanthipeptides are made up of an N-terminal leader and C-terminal core peptide, which together are referred to as the precursor peptide **(Fig. 1.1a)**. The precursor peptide generally ranges from 50-100 amino acid residues. The leader peptide sequences are typically around 25 amino acids and serve multiple functions in the generation of the mature core peptide. Following translation, the leader peptide contains the binding sites for post-translational modification enzymes that modify the core peptide. Once the core peptide has been modified, the leader peptide directs the core peptide to the cell membrane to transport it out of the cell. Upon secretion, the leader peptide is cleaved from the core peptide, yielding the mature core lanthipeptide.

To generate a lanthionine or methyllanthionine bond, serine and threonine residues in the core sequence are modified and bound to a cysteine residue **(Fig. 1.1a and 1.1b)**. A lanthionine synthetase activates the hydroxyl groups on the side chains of serine or threonine residues through ATP-dependent phosphorylation or glutamylation, depending on the lanthipeptide class and its biosynthesis genes [Repka et al., 2017]. A subsequent β-elimination reaction removes the phosphate or glutamate along with the hydroxyl group, yielding 2,3-dehydroalanine from serine and (Z)-2,3-dehydrobutyrine from threonine. Next, a Michael-type addition reaction occurs, in which a cysteine thiol attacks the electrophilic dehydroalanine or dehydrobutyrine, forming a thioether linkage and creating two alanine residues that are bound together with a lanthionine bond. However, for dehydrobutyrine, the β-methyl

group is typically retained in this reaction, resulting in an alanine and α-aminobutyric acid residue bound together with a 3-methyllanthionine bond. In some lanthipeptides, a carbon-carbon cross-linkage can be formed between two dehydroalanine residues to make a labionin bond.

Apart from cyclization of the core peptide, lanthipeptides can also undergo additional tailoring modifications before the mature peptide is formed [Funk and Donk, 2017, Repka et al., 2017]. Epimerization has been described in some lanthipeptides where dehydroalanine is converted to D-alanine through stereospecific reduction. Some peptides undergo halogenation adding a chlorine atom to tryptophan residues generating 5-chlorotryptophan. Although disulfide bridges are less common in bacterial RiPPs, some lanthipeptides may have disulfide linkages in place of lanthionine rings. Hydroxylation of asparagine and proline residues have also been observed in a subset of lanthipeptides. Lastly, lanthipeptides may have N- and C-terminal modifications such as lactyl or acetyl groups added to the N-terminus or oxidatively decarboxylated cysteine added to an internal dehydroalanine or dehydrobutyrine to create aminovinyl(methyl)cysteine at the C-terminus.

Together, these modifications give lanthipeptides their unique structures that are important for their activity, stability, and resistance to peptidase degradation.

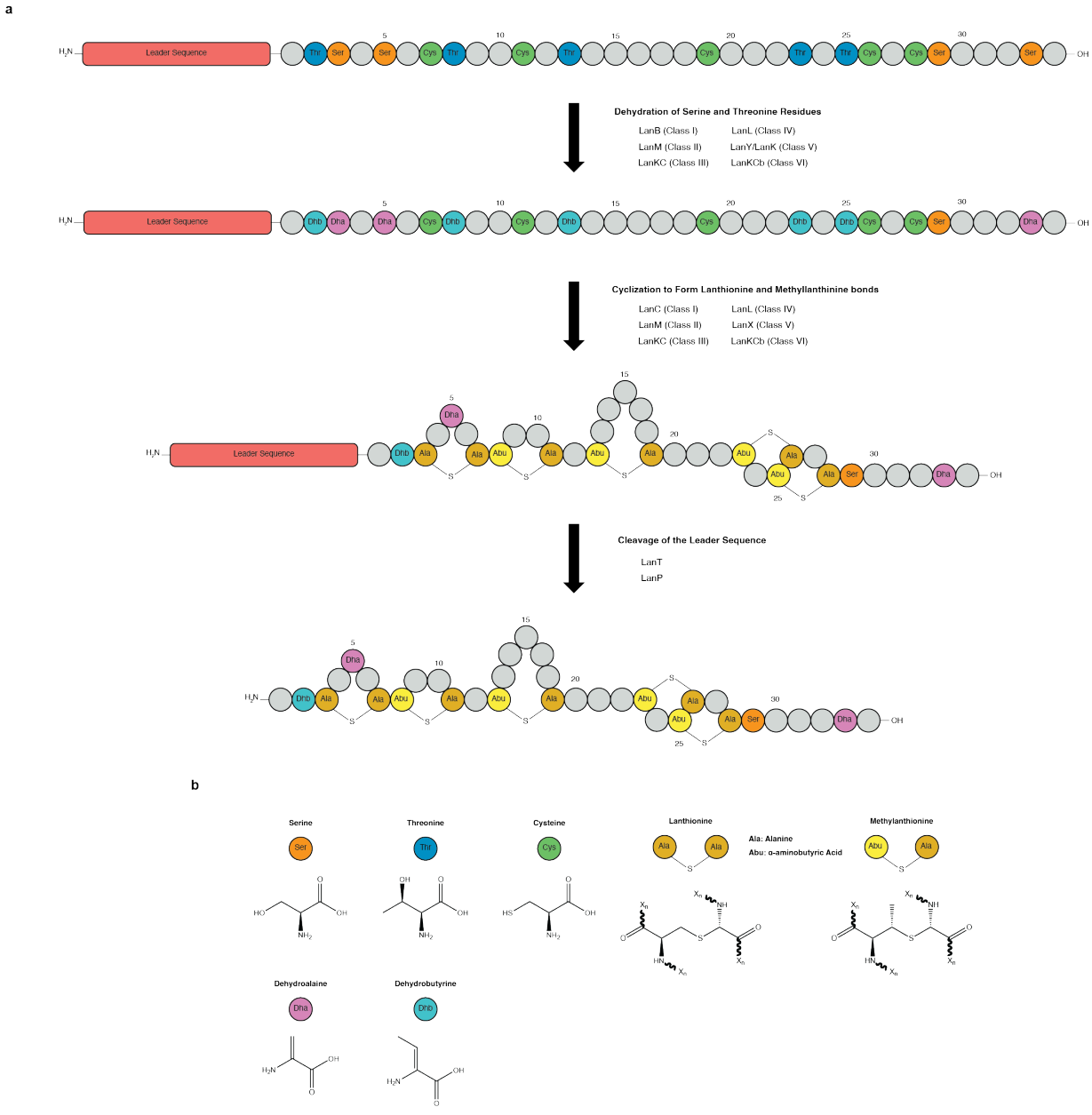

Figure 1.1: Biosynthesis pathway and structure of lanthipeptides. **a,** Processing pathway of a hypothetical lanthipeptide to generate lanthionine and methyllanthionine bonds. Gray represents unspecified amino acid residues. Additional tailoring modifications to the lanthipeptide structure are not depicted. **b,** Structure of residues and bonds that are critical to lanthipeptides.

1.2 Lanthipeptide classification

The classes of lanthipeptides are determined based on the enzyme(s) in the BGC required for the dehydration and cyclization steps that form the lanthionine and methyllanthionine bonds **(Fig. 1.1a and Fig. 1.2a-f)**. Currently, there are six different classes for lanthipeptides that have been described. However, much less is known about class III-VI due to their more recent discoveries compared to I and II. The following sections outline the distinctions between the different lanthipeptide classes.

1.2.1 Class I lanthipeptides

Class I lanthipeptide BGCs contain two separate enzymes for dehydration and cyclization of the core peptide **(Fig. 1.2a)** [Funk and Donk, 2017, Repka et al., 2017]. The first is the LanB dehydratase that is comprised of an N-terminal glutamylation domain followed by a C-terminal glutamate elimination domain that correspond to the Pfam domains PF04738 and PF14028, respectively. LanB recognizes a motif in leader sequence to directly bind and modify. Glutamyl-tRNA was determined to be the source of glutamate for the glutamylation reaction in class I lanthipeptides. Furthermore, it was found that LanB works best with specific glutamyl-tRNAs from the producing strain. Therefore, when expressing heterogeneously in different species, it may be necessary to also express the cognate glutamyl-tRNAs and glutamyl-tRNA synthetase of the original producer.

Cyclization of class I lanthipeptides is carried out by the LanC cyclase **(Fig. 1.2a)** [Funk and Donk, 2017, Repka et al., 2017]. Like LanB, LanC also recognizes a motif in the leader sequence of the precursor peptide. The exact mechanism of cyclization has yet to be explained; however, the current model is a zinc site activates the thiol found in the cysteine residues for a subsequent attack on the dehydroalanine and dehydrobutyrine residues. A key hallmark of the LanC protein is the lanthionine sythetase C Pfam domain PF05147. Although not yet confirmed, evidence suggests that the LanB and LanC proteins work in a

multi-enzyme complex with the precursor peptide.

1.2.2 Class II lanthipeptides

The dehydration and cyclization in production of class II lanthipeptides is performed by a single enzyme, LanM, rather than two separate proteins **(Fig. 1.2b)** [Funk and Donk, 2017, Repka et al., 2017]. LanM phosphorylates the hydroxyl groups of serine and threonine using adenosine triphosphate (ATP) in place of glutamylation for dehydration followed by β-elimination. The N-terminal side of the LanM protein is responsible for this reaction, and it does not contain the same Pfam domains as observed in LanB. Instead, it has the Pfam domain PF13575, which is currently annotated as a domain of unknown function. The C-terminal cyclase domain, however, shares the Pfam domain as LanC, PF05147.

1.2.3 Class III lanthipeptides

Similar to class II lanthipeptides, class III lanthipeptides also have a single enzyme, LanKC, for dehydration and cyclization **(Fig. 1.2c)** [Funk and Donk, 2017, Repka et al., 2017]. LanKC is made up of an N-terminal lyase domain for β-elimination, a central serine and threonine kinase domain for phosphorylation, and a C-terminal cyclase domain, like in LanC and lanM, for cyclization. Unique to LanKC, the kinase domain uses Guanosine triphosphate (GTP) for phosphorylation. However, some have reported LanKC proteins capable of using a range of nucleoside triphosphates (NTPs) including ATP. In addition to the lanthionine and methyllanthionine bonds, LanKC can also form labionin bonds in certain lanthipeptides. The determining factors that lead to labionin bonds over the formation of lanthionine bonds are not yet known. Unlike LanC and LanM, the cyclase domain in LanKC does not have a zinc-binding site. Therefore, it employs a different mechanism for cyclization.

1.2.4 Class IV lanthipeptides

Class IV lanthipeptides are made with the LanL synthetase **(Fig. 1.2d)** [Funk and Donk, 2017, Repka et al., 2017]. Like LanKC in class III lanthipeptides, LanL has a lyase, kinase, and cyclization domain. However, the C-terminal cyclase domain of LanL resembles LanC and LanM more closely than that of LanKC. It also contains the zinc-binding residues seen in LanC and LanM.

1.2.5 Class V lanthipeptides

Class V lanthipeptides are a combination of features from lanthipeptides and linaridins, another RiPP family bacteriocin [Ramírez-Rendón et al., 2023]. In addition to the typical lanthipeptide features, class V lanthipeptides contain an N-terminal dimethylation found in linaridins. Dehydration and cyclization of the precursor peptide requires three separate enzymes **(Fig. 1.2e)**. LanK, a serine/threonine kinases with the Pfam domain PF01636, and LanY, an enzyme that catalyzes the phosphate elimination from phoshothreonine with the Pfam domain PF17914, carry out the dehydration steps, while a LanC-like enzyme, LanX, catalyzes the cyclization.

1.2.6 Class VI lanthipeptides

Class VI lanthipeptides have only recently been described, and currently, they have only been identified in *Streptococcus* spp [He et al., 2023]. Interestingly, the core sequence of these lanthipeptides is much smaller than other lanthipeptides, typically ranging from 4-9 amino acids. Like class III lanthipeptides, dehydration and cyclization are done with a single protein, LanKCb **(Fig. 1.2f)**. However, the lyase and cyclase domains are truncated. Given their short core sequence, only a single lanthionine moiety is generated in the final peptide at a conserved TxxC region on the C-terminus of the peptide. The functions of these lanthipeptides remains unknown.

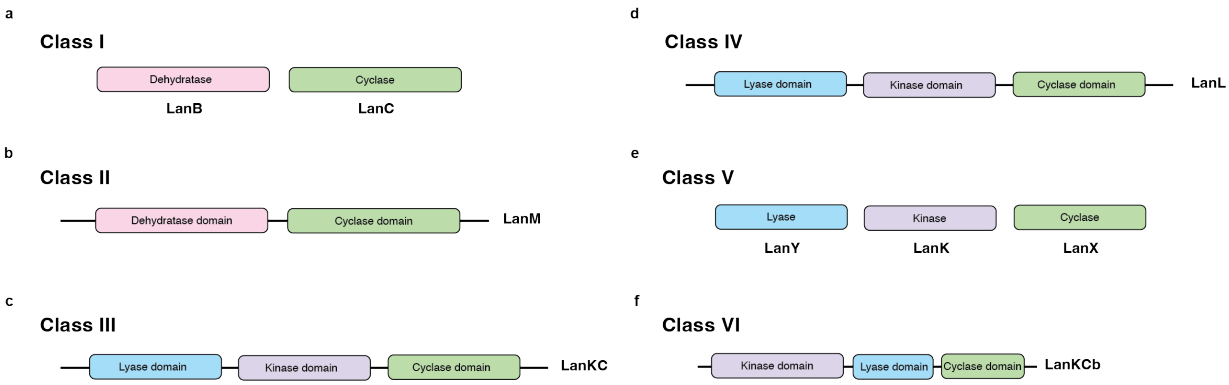

Figure 1.2: Class determining lanthipeptide genes. a-f, Genes that determine class I-VI lanthipeptides. These genes are responsible for the dehydration and cyclization steps of lanthipeptide synthesis. The lines indicate a continuous gene.

1.3 Other lanthipeptide biosynthesis genes

In addition to the lanthipeptide genes responsible for dehydration and cyclization of the precursor peptide, other genes may be present in the BGC that facilitate further modifications, transport, and regulation of lanthipeptide biosynthesis. While the genes that define the lanthipeptide classes are required for production of the active core peptide, these genes may or may not be required depending on the lanthipeptide and the producer.

For modifications, the currently described proteins include LanJ, LanD, LanO, and LanX [Arnison et al., 2012, Repka et al., 2017]. LanJ is an enzyme that converts dehydroalanine residues to D-alanine. LanD is an oxidoreductase flavoprotein that performs the oxidative decarboxylation reactions on cystine residues at the C-terminus of the core peptide. LanO denotes various oxidation enzymes that include a monooxygenase that catalyzes the formation of sulfoxide bonds, reduction of an N-terminal pyruvate to lactate using NADPH, and reduction of N-terminal oxopropionyl groups to hydroxypropionyl. LanX is an α-ketoglutarate/Fe(II)-dependent hydroxylase that can hydroxylate aspartate.

Once modified, some lanthipeptides, such as nisin, are directed to a dedicated transmembrane transporter, LanT, via the leader sequence of the precursor peptide. The peptide

is then transported across the cell membrane in an ATP-dependent manner [Repka et al., 2017]. Some *lanT* genes also encode an N-terminal cysteine protease that cleaves the leader peptide from the final core peptide after transport. However, not all LanT transporters contain a protease. When absent, the BGC will typically contain a serine protease that is secreted through the general secretory (Sec) pathway outside the cell and cleaves the leader peptide. These reactions can also occur in a stepwise order, such as the production of the lantibiotics cytolysin L and S, whereby LanT cleaves most of the leader sequence and a LanP protease removes the remaining peptides of the leader sequence. Dedicated LanT and/or LanP proteins are not always necessary. Studies have shown that some lanthipeptides are capable of utilizing other transport pathways in the lanthipeptide-encoding strain.

Since lanthipeptide production can be toxic for the producer, proper regulation of the lanthipeptide BGC can be critical. Although different mechanisms have evolved in lanthipeptide BGC regulation, many lanthipeptide BGCs contain a two-component signaling pathway that consists of a cellular surface histidine kinase protein receptor, LanK, and a transcriptional response regulator, LanR. Lanthipeptides, generally the lanthipeptides found in the same BGC, are detected extracellularly by LanK. This results in auto-phosphorylation of a histidine residue. A phosphoryl group is then transferred to LanR, which in turn bind to operators within the BGC and can activate transcription of the lanthipeptides, synthesis genes, and lantibiotic immunity genes. This system can be highly sensitive with as little as 5 nisin peptides being sufficient to activate transcription in the case of nisin production. It is not uncommon to see multiple LanK and LanR systems in the same BGC. General transcriptional regulators have also been shown to be involved in expression of lanthipeptide genes. Lacticin 481 produced by *Lactococcus lactis* is regulated by a general regulator outside the BGC that responds to acidic pH [Hindré et al., 2004].

1.4 Lantibiotic immunity

While proper regulation of lantibiotic genes is important to avoid toxicity for the producing strain, the concentrations at which lantibiotics are effective at inhibiting other bacteria can still be inhibitory for the producer, especially for lantibiotics that target closely related species. For this reason, lantibiotic-producing bacteria have evolved mechanisms of immunity to their own lantibiotics [Draper et al., 2015, Hill et al., 2008]. Targeted bacteria also need mechanisms of resistance to avoid getting outcompeted in their niche. To achieve this, bacteria may encode dedicated immunity genes for lantibiotics, acquire natural immunity, or utilize existing general defense mechanisms [Draper et al., 2015, Hill et al., 2008, Draper et al., 2015].

One of the primary mechanisms of immunity for lantibiotics is the ATP-binding cassette (ABC) transporter complex known as LanFEG [Hill et al., 2008, Alkhatib et al., 2012]. LanF forms a dimer in the cytosol of the cell at the LanFEG complex and contains the nucleotide binding domain where ATP hydrolysis occurs to provide the energy to transport lantibiotics. LanE and LanG have hydrophobic domains and form a heterodimeric structure in the cell membrane. Together, these proteins pump lantibiotics out and away from the cell without modification or degradation to the peptide itself. For lantibiotic producers, the *lanFEG* genes are typically located in the same BGC as the lantibiotic. However, non-lantibiotic producing bacteria may also harbor *lanFEG* genes for lantibiotic resistance.

In addition to *lanFEG*, some bacteria encode a neighboring *lanI* immunity gene [Hill et al., 2008, Alkhatib et al., 2012]. In some rare cases, the *lanI* gene may be the only immunity factor. LanI is a lipoprotein with an N-terminal signal sequence that directs the protein to be anchored to the extracellular side of the cell membrane. The signal sequence is cleaved from the final protein during this process. Interestingly, research with the *lanI* found in the nisin BGC has shown that around 50% of LanI proteins do not undergo lipid modifications, resulting in soluble LanI proteins in the surrounding extracellular matrix.

LanI functions by using its C-terminal domain to bind to the lantibiotic peptide hindering its activity. Unlike LanFEG, LanI proteins are usually highly specific to the lantibiotic found in their corresponding BGC.

Certain non-lantibiotic producing bacteria make use of a separate dedicated system to obtain resistance to lantibiotics known as the nisin resistance protein (NSR) [Sun et al., 2009, Draper et al., 2015]. Like LanI, NSR also contains a signal sequence that allows it to localize at the cell membrane. However, rather than only binding to specific lantibiotics, NSR uses a C-terminal tail-specific protease to cleave and inactivate a broader range of lantibiotics. The *nsr* locus is sometimes located next to an ABC transport that works in conjunction with NSR to increase resistance to lantibiotics.

Apart from dedicated systems for lantibiotics, there are several other broad mechanisms bacteria can take advantage of to resist lantibiotic-mediated inhibition [Draper et al., 2015]. Modifications to the cell envelope such as thickening of the cell wall, alterations to the net charge, and/or changes to the composition. As with other antibiotics, formation of biofilms can make it difficult for lantibiotics to reach bacteria. Furthermore, antimicrobial efflux pumps can be effective in providing resistance to lantibiotics. Several regulatory two-component systems (TPS) that are not specific to lantibiotics have been identified that are able to modulate these mechanisms. Gram-negative bacteria are generally more resistant to lantibiotics due to their outermembrane layer particularly with lipopolysaccharide (LPS).

1.5 Lanthipeptide functions and mechanisms of action

The majority of lanthipeptides characterized today are classified as lantibiotics, which have antimicrobial properties [Ongpipattanakul et al., 2022]. Most of the lantibiotic testing for inhibition has been conducted on bacteria, but there are examples of antiviral, antifungal, and even antitumor lantibiotics. The activity of lantibiotics can range from narrow- to broad-spectrum making them of particular interest for potential therapeutic applications.

While not all lanthipeptides contain observed antimicrobial properties, our knowledge of the functions of these lanthipeptides is limited. Some lanthipeptides have been shown to act as biosurfactants or function as quorum sensing signals. It should be noted, however, that most of the lanthipeptide functional research has been focused on antimicrobial activity, and non-antimicrobial functions can be challenging to prove. Therefore, the full range of lanthipeptide functions may be far greater than currently appreciated, and known lantibiotics may have more functions for the producing bacteria beyond antimicrobial activity.

Lantibiotics that are known to have activity against other bacteria often target the cell membrane or components of the cell surface likely due to its accessibility [Ongpipattanakul et al., 2022]. The cellular surface of bacteria typically contains a net negative charge and lantibiotics are generally cationic peptides. Thus, lantibiotics are naturally directed to the cell surface. The most common mechanism of inhibition stems from pore formation at the cell membrane. For some lantibiotics, including nisin and nisin-like lantibiotics, cell surface molecules such as lipid II, which is involved in peptidoglycan synthesis, can be specifically targeted to aid in inhibition. The binding of nisin to lipid II prevents the addition of peptidoglycan to the cell wall during cell division, and nisin bound lipid II has been observed at nisin-induced pores, indicating that binding to lipid II may contribute to pore formation by acting as an anchor. The pores permit solutes and ions in the cytoplasm to exit the cell. Some lantibiotics, such as microbisporicin and mutacin 1140, bind to lipid II without the formation of pores demonstrating that pore formation is not always required for inhibition by lipid II binding lantibiotics.

Another known target of lantibiotics is phosphatidylethanolamine, which can be found in the membrane of all living cells [Ongpipattanakul et al., 2022]. Phosphatidylethanolamine is the primary phospholipid in bacteria and second most abundant in mammalian cells. The class II lantibiotic cinnamycin found in species of *Streptomyces*, for example, binds to phosphatidylethanolamine and causes transbilayer movement of phospholipids that results in

membrane permeabilization. Binding of phosphatidylethanolamine by cinnamycin, and similar lantibiotics, have demonstrated antiviral properties by preventing viral entry of viruses that rely on phosphatidylethanolamine. These lantibiotics can also be potent inhibitors of phospholipase A_2, likely as an indirect effect of phosphatidylethanolamine binding. Interestingly, phosphatidylethanolamine is predominately found in the inner leaflet of membranes, and it is not yet known how lantibiotics reach them.

Certain class II lantibiotics have been shown to inhibit bacteria via a two-component mechanism of action [Ongpipattanakul et al., 2022]. These lantibiotics often consist of an α- and β-peptide encoded within the same BGC that work synergistically. For lacticin 3147 α/β produced by *Lactococcus lactis* and haloduracin α/β, the α-peptide binds to lipid II and recruits the β-peptide to the cell surface to induce pore formation. The two peptides work synergistically for inhibition with little individual activity. Cytolysin L and S is another two-component lantibiotic found in *Enterococcus faecalis*. While the mechanism of action is not yet known, the two peptides have been shown to be an important virulence factor with activity against bacteria and red blood cells. Cytolysin L appears to be important for binding to red blood cells as it has 7-fold greater affinity compared to cytolysin S. Cytolysin S also serves as the quorum-sensing signal that activates genes in the cytolysin BGC.

The functions of lanthipeptides that have little or no observable antimicrobial activity are much less understood. One of the most notable examples, however, is the class III lanthipeptide SapB produced by *Streptomyces coelicolor* [Ongpipattanakul et al., 2022, Kodani et al., 2004]. SapB has been found to act as a biosurfactant that reduces surface tension to facilitate the formation of aerial hyphae in the *S. coelicolor* development cycle. In addition, it appears to be an important factor for sporulation. Lanthipeptides that share sequence homology with SapB can be found throughout *Streptomyces* species.

1.6 Lanthipeptide producers

The first lantibiotic discovered was nisin, in *Lactococcus lactis* isolated from cow milk. Since then, *in silico* mining of lanthipeptides in metagenomic databases has revealed a great deal about lanthipeptide producers. One of the largest screenings was conducted by Walker et al. in 2020 in which they screened over 100,000 genomes from bacteria and archaea in the RefSeq databases for the presence of lanthipeptide BGCs [Walker et al., 2020]. Their analysis identified 2698 class I lanthipeptides, 3002 class II lanthipeptides, 2304 class III lanthipeptides, and 401 class IV lanthipeptides. While the lanthipeptide BGCs were predominantly found in Gram-positive bacteria, there were some examples of Gram-negative lantibiotic-producers and even 33 class II lanthipeptide BGCs encoded by Archaea.

Lanthipeptide genes have been detected across 14 phyla that includes Actinomycetota [Actinobacteria], Bacillota [Firmicutes], Pseudomonadota [Proteobacteria], Bacteroidota [Bacteroidetes], Cyanobacteria, Chlamydiota [Chlamydiae], Chloroflexota [Chloroflexi], Planctomycetota [Planctomyces], Gemmatimonadetes, Acidobacteriota [Acidobacteria], Deinococcota [Deinococcus-Thermus], Rhodothermota [Rhodothermaeota], Thermotogota, and Euryarchaeota [Walker et al., 2020]. Among the 14 phyla, Actinomycetota and Bacillota harbored more than 75% of the lanthipeptides across all four classes. Actinomycetota represented more than half of the lanthipeptides for class I, III, and IV. Bacillota, on the other hand, encoded more than half of the class II lanthipeptides. Additionally, Actinomycetota and Bacillota were the only phyla with detectable class IV lanthipeptides. Importantly, Pseudomonadota, Actinobacteria, and Bacillota represented a larger portion of the genomes that were analyzed. Therefore, it is possible that Actinomyceotota and Bacillota only contained the largest proportion of lanthipeptides due to a greater number of sequenced genomes from these phyla, and a more balanced distribution of genomes may yield different lanthipeptide proportions.

An area of particular interest are lantibiotic producers found in the microbiomes of Eu-

karya, which often contain several of Acinomycetota and Bacillota species. In ruminants a common gut commensal, *Ruminococcus flavefaciens*, was found to encode various class II lantibiotics known as flavecins [Zhao and van der Donk, 2016]. The nisin-like lantibiotic, Suicin, was found in *Streptococcus suis* that colonizes the swine tonsil microbiome [Vaillancourt et al., 2015]. Lanthipeptides have also been characterized from the fish gut microbiome including Carnolysins made by *Carnobacterium maltaromaticum* and formicin made by *Bacillus paralicheniformis* [Tulini et al., 2014, Uniacke-Lowe et al., 2024]. Commensals of the human microbiome also serve as a rich source for lanthipeptide producers. The skin microbiome can contain various *Staphylococcus* and *Streptococcus* species that encode lantibiotics capable of preventing sensitive skin commensals from colonizing [Donia et al., 2014]. *Streptococcus* species, such as *Streptococcus salivarius*, in the human oral microbiome have also been found to encode lanthipeptides [Wescombe et al., 2006]. The largest source for lanthipeptides in the human microbiome, however, is the colon [Walsh et al., 2015, Zheng et al., 2015, King et al., 2023, Donia et al., 2014]. Some notable examples include species from *Blautia*, *Enteroccocus*, *Bifidobacterium*, *Bacteroides*, and *Mediterraneibacter*.

1.7 Lantibiotics for therapeutic use

The foundational discovery of nisin in 1928 coincided with the discovery of penicillin by Alexander Fleming [Field et al., 2023]. The antibacterial properties nisin has against clinical pathogens like *Mycobacterium tuberculosis* quickly garnered interest for use as an antibiotic to treat infections. Due to its low solubility and reduced stability at physiological pH, however, it was deemed an unlikely candidate. Instead, an alternative use case was later discovered in the 1950s when nisin added to processed cheese prevented spoilage by clostridia species. Since then, it continues to be used as a food preservative in a range of foods such as dairy, canned goods, beer, processed meats, and baked goods. Given that nisin was widely used prior to the establishment of the Food and Drug Administration (FDA), it received the

generally regarded as safe (GRAS) designation for use as a food additive by the FDA. It has also been approved for use in over 80 other countries.

Given its long history of use, nisin has continued to be investigated as a potential therapeutic. A particular area where nisin treatment has shown promising results is in veterinarian medicine to treat bovine mastitis, inflammation of the mammary gland often caused by bacteria infections [Roy et al., 2016]. Bovine mastitis is one of the most common diseases associated with dairy cattle. Infectious mastitis generally results from infections of *Staphylococcus aureus*, *Streptococcus agalactiae*, or *Streptococcus uberis* that occur after milking. Currently, the primary treatment for bovine mastitis are conventional antibiotics, which account for the most annual antibiotic use among veterinary care. This has led to high rates of antibiotic resistance on dairy farms that can potentially carry over to human pathogens. ImmuCell Corporation has been seeking FDA approval for their product that uses nisin via intramammary infusion as an alternative to current antibiotic treatments. In studies, it has shown similar efficacy to gentamicin treatment. Additionally, they have made nisin infused wipes to inhibit mastitis related bacteria prior to milking. In humans, topically applied nisin has also shown potential in treating mastitis [Fernández et al., 2008].

While few clinical trials exploring the use of lantibiotics exist, some have begun to investigate their use to treat infections [Ongey et al., 2017]. Novacta, for example, has been working with two derivatives of the lantibiotic actagardine made by *Actinoplanes liguriae* to treat *Clostridioides difficile* infection via oral and intravenous administration. Oragenics is a company working with mutacin 1140 produced by *Streptoccocus mutans* to treat multi-drug resistant infections through intravenous dosing. Naicons SRL and Sentinella Pharmaceuticals are attempting the same with the *Microbispora corallina* lantibiotic NAI-107. Interestingly, Lantibio/AOP Orphan Pharmaceuticals are working on a cystic fibrosis treatment using a *Streptomyces cinnamoneum* lantibiotic moli1901 given daily through aerosol inhalation. Because cystic fibrosis is the result of abnormal chloride transport into cells, moli1901 is being

administered to cause chloride efflux from epithelial cells through moli1901's interaction with phosphatidylethanolamine.

In addition to treating cystic fibrosis, lanthipeptides have seen potential in other non-antimicrobial applications. Lanthipeptides, such as labyrinthopeptin and NAI-112, appear to possess pain relief capacities including antiallodynic, antinociceptive, and antihyperalgesia properties [Staden et al., 2021]. Mice given intravenous injections of labyrinthopeptide, for example, exhibited significantly reduced tactile allodynia that lasted for six hours post-treatment with efficacy eventually diminishing after 24 hours. Likewise, NAI-112 can reduce pain in mice after intrapreneurial injection. However, the mechanism of action for these properties have yet to be elucidated.

Efforts are currently underway to use lanthipeptides as new anticancer agents [Staden et al., 2021]. Experiments with nisin has provided evidence of apoptosis induction in head and neck carcinoma without having much of an impact on primary keratinocytes. It is hypothesized that this is due to binding to phosphatidylcholine, which has an increased presence in cancer cells. Nisin binding then causes calcium influx that leads to caspase 3-independent apoptosis through calpain-1 activation. The treatment can be even more effective when used in combination with other cancer drugs like doxorubicin or 5-fluorouracil. The lantibiotic Duramycin has been proposed as a potential anticancer treatment by fusing it with IgG antibodies. Using the duramycin part to bind phosphatidylethanolamine, which is greater in cancer cells, allows immune cells to detect the free Fc region of the IgG antibody.

The targets of duramycin and labyrinthopeptin have also led to the growing interest of lanthipeptide use as effective antiviral therapeutics [Staden et al., 2021]. In particular, duramycin has demonstrated the ability to inhibit the viral entry of flaviviruses and filoviruses in host cells. Its inhibition stems from interruption of the T-cell Ig mucin domain protein (TIM1), a protein used by some viruses to attach to host cells during viral entry, by binding the ligand of TIM1, phosphatidylethanolamine. Rather than interacting with the host cell,

labyrinthopeptin appears to disrupt viruses directly by targeting phosphatidylethanolamine in the membrane of enveloped viruses. Labyrinthopeptin has shown activity against human immunodeficiency virus (HIV), herpes simplex virus (HSV), and repiratory syncytial virus (RSV).

The previously described therapeutic applications of lanthipeptides are focused on purified lanthipeptides. Work by Caballero et al. found that a consortia of four bacteria could restore colonization resistance to vancomycin-resistant *Enterococcus faecium* (VRE) and clear VRE after it has colonized the gastrointestinal (GI) tract of mice [Caballero et al., 2017]. Later, Kim et al. demonstrated that VRE inhibition was dependent on *Blautia pseudococcoides* SCSK (BpSCSK), which was found to encode a lantibiotic BGC [Kim et al., 2019]. Purified forms of the lantibiotic, blauticin, were also capable of inhibiting VRE *in vitro*. These findings have given rise to possibility of using lantibiotic-producing bacteria as a probiotic therapeutic as opposed to purifying lantibiotics for treatment. This method has the added benefit of constant lantibiotic production in the GI tract which may be important for overcoming lantibiotic degradation that can happen before the lantibiotic reaches the desired target.

1.8 Influence of lantibiotics on the microbiome

Although metagenomic mining of lantibiotics, and other bacteriocins, has revealed that they are present in a variety of microbiomes found throughout nature, there is significantly less knowledge about the impact they can have on a microbiota. Studies investigating activity of lantibiotics often have a strong focus on activity against pathogens or a small set of target bacteria. Furthermore, the activity is typically assessed using *in vitro* culturing methods with purified lantibiotics. Some of these tests have revealed that lantibiotics from commensals can inhibit growth of various gut commensals, which indicates that they are likely to play an important role in shaping the microbiota [Kim et al., 2019, Zhang et al., 2024b, King

et al., 2023]. However, only a few studies have begun to provide evidence that both purified lantibiotics and lantibiotic-producers can have noticeable impacts on the composition of a microbiota *in vivo*.

Since nisin is a broad-spectrum lantibiotic used as a preservative in various processed foods, there has been interest in determining whether nisin consumption has an impact on the gut microbiota. Using a porcine model, O'Reilly et al. was able to demonstrate that orally-ingested nisin can transverse the GI tract. Additionally, it was found that when treated with nisin, there is reduced abundance of Gram-positive Bacillota coupled with an increase in abundance of Gram-negative Pseudomonadota [O'Reilly et al., 2023]. Subsequently, there was an observable decrease in butyrate and increase in propionate. Similar experiments conducted in mice also resulted in a decrease of Bacillota species and shifts in short-chain fatty acids (SCFAs) [Zhang et al., 2023].

One of the best examples of investigating the impact of bacteriocin-producers, including lantibiotic-producers, on a bacterial community was performed by Ríos Colombo et at. using a simplified human intestinal microbiota (SIHUMI), a collection of seven well characterized and culturable human gut commensals [Eun et al., 2014, Colombo et al., 2023]. They cultured the SIHUMI consortia in solid and liquid media with *Lactococcous lactis* strains expressing different bacteriocins and measured their impact on the SIMUMI community. *L. lactis* expressing the lantibiotic lacticin 3147 lead to significant shifts in the SIMUMI strains. Specifically, *Mediterraneibacter gnavus*, *Faecalibacterium prausnitzii*, and *Bifidobacterium longum* were inhibited, which matched the individual susceptibilities to lacticin 3147. *Lactiplantibacillus plantarum* was also inhibited in the SIMUMI culture when *L. lactis* expressing lacticin 3147 is present, but unlike the other strains, *L. plantarum* was resistant to lacticin 3147 inhibition when co-cultured with *L. lactis*. This highlights the potential of off-target, indirect inhibition of bacteria in the presence of lantibiotic-producing bacteria.

1.9 Thesis scope

Since lantibiotics can inhibit a range of bacteria and are found throughout the gut microbiota, we hypothesized that lantibiotic-producing bacteria, when present, can shape the colonization of the gut microbiota. Here I provide evidence that BpSCSK, the lantibiotic-producing bacterium that provides colonization resistance against VRE, prolongs antibiotic-induced dysbiosis by preventing recolonization of the gut microbiota with gut commensals [Caballero et al., 2017, Kim et al., 2019] and reduces fecal metabolite concentrations associated with epithelial barrier function and mucosal immune defenses. In antibiotic-treated mice, BpSCSK prolongs susceptibility to gut colonization by *Klebsiella pneumoniae* and *Clostrioides difficile*. These findings highlight the potentially detrimental role bacteriocin-producing commensal bacteria can play in microbiota diversification and function.

Moreover, lanthipeptide-encoding genes can be detected across fecal metagenomes from healthy humans and hospitalized patients with varying degrees of dysbiosis. Bacterial strains encoding lanthipeptides generally have higher relative abundance with the microbiota compared to the same species lacking lanthipeptide-encoding genes, suggesting they contribute to fitness in the gut. Lanthipeptide genes were detected in several species including *Blautia* species and probiotic species such as *Streptococcus thermophilus*, *Bifidobacterium longum*, *Bifidobacterium breve*, *Lactiplantabacillus plantarum*, and *Lactococcus lactis*, which have been shown to prolong dysbiosis after antibiotic treatment by an undefined mechanism [Suez et al., 2018]. Although further testing is required to confirm, lantibiotics provide a possible mechanism for this observation.

Overall, lantibiotic-producing bacteria represent an underappreciated layer of complexity to the factors that make up microbiome resilience and colonization in the GI tract. While lantibiotics and lantibiotic-producing bacteria have promising applications in the treatment of human diseases, it is important to continue investigating their potential contributions to other diseases.

CHAPTER 2

MURINE STUDIES ON LANTHIPEPTIDE IMPACTS ON THE INTESTINAL MICROBIOME AND METABOLOME

2.1 Characteristics of the lantibiotic-producer BpSCSK

Blautia pseudococcoides SCSK (BpSCSK) is an anaerobic, Gram-positive, spore-forming strain of *Blautia* in the *Lachnospiraceae* family. It was isolated from MyD88$^{-/-}$ C57BL/6 mice that had been continuously treated with Augmentin, a combination of the β-lactam amoxicillin and β-lactamase inhibitor clavulanate, in drinking water for over 10 years [Caballero et al., 2017]. Originally, it was classified as *Blautia producta* SCSK; however, it was reclassified in 2021 to *B. pseudococcoides* along with *Blautia coccoides* YL58, a *Blautia* species used in the Oligo-Mouse-Microbiota (OMM^{12}) to confer colonization resistance to *Salmonella enterica* serovar Typhimurium [Brugiroux et al., 2016, Maturana and Cárdenas, 2021].

Analysis performed by Kim et al. revealed that BpSCSK encodes a BGC that is responsible for producing the class I lantibiotic blauticin. The blauticin BGC consists of six lantibiotic (*lanA*) genes, the *lanP* protease for cleavage of the leader peptide, *lanFEGI* genes to confer immunity, two sets of *lanKR* genes to regulate expression through two-component signaling, *lanBC* genes for dehydration and cyclization of the lantibiotic peptides, and a *lanT* gene responsible for transporting the lantibiotics out of the cell **(Fig. 2.1a)**. Although there are six *lanA* genes, the amino acid sequences of the inner four genes are identical and are responsible for the blauticin lantibiotic that has been purified and tested for activity [Kim et al., 2019, Zhang et al., 2023, 2024b]. While activity and expression of the other two *lanA* genes has not yet been assessed, the last *lanA* gene in the BGC, as well as the inner four genes, contain the gallidermin Pfam domain (PF02052) that is characteristic of some class I lantibiotics.

In addition to the blauticin BGC, the BpSCSK genome has three *lanM* genes that are each located next to small hypothetical proteins that are presumed to be class II lanthipeptide genes **(Fig. 2.1b-d)**. Whether they are expressed or have any antimicrobial properties is unknown. Interestingly, in cluster 4, the predicted *lanA* gene overlaps with the predicted *lanK* histidine kinase **(Fig. 2.1d)**. Furthermore, the *lanM* gene of cluster 4 appears to have partially split as there is a smaller neighboring gene that has the same serine/threonine dehydration Pfam domain, PF13575, found in *lanM* genes. However, the larger *lanM* gene contains both the PF13575 domain and the cyclization domain PF05147. While all three *lanM* genes have predicted *lanKR* genes, other lanthipeptide genes could not be readily determined.

Because genetic tools to inactivate specific genes in BpSCSK are lacking, Kim et al. used *Blautia producta* KH6 (BpKH6), which does not encode any known lantibiotic genes, as a negative control for *in vivo* mouse experiments [Kim et al., 2019]. Unlike BpSCSK, it was unable to inhibit VRE colonization. Based on single-copy core genes (SCGs), BpSCSK and BpKH6 show a similar phylogenetic relatedness compared to other *Blautia* species isolated from healthy human stool samples **(Fig. 2.2a)**. Analysis of the gut metabolite modules (GMMs) determined by Omixer-RPM[Brugiroux et al., 2016], a tool that uses KEGG annotations to detect metabolic pathways, revealed that BpSCSK and BpKH6 share many of the same metabolite modules **(Fig. 2.2b)**. However, BpKH6 has a few additional metabolic pathways that were not complete in BpSCSK, which include allose, rhamnose, ribose, arginine, 4-aminobutyrate, and urea degradation pathways. Out of the 103 modules, the mannose degradation pathway was the only one detected in BpSCSK that wasn't also present in BpKH6.

To assess how growth of BpSCSK and BpKH6 compare, the two were grown anaerobically at 37 °C in brain heart infusion (BHI) liquid media. BpKH6 had pronounced log-phase growth reaching a final OD_{600} of approximately 1.38 after 32 hours **(Fig. 2.2c)**. However,

there was a small decrease in OD_{600} at 16 hours before continuing at a slower growth rate to its final OD_{600}. BpSCSK exhibited a much slower growth rate over 32 hours and only reached an OD_{600} of .25, suggesting that lantibiotic production may carry a strong fitness cost. When BpSCSK and BpKH6 were cultured together at an equivalent starting OD_{600}, the final OD_{600} was slightly higher than BpSCSK alone, but it was markedly lower than BpKH6 alone. This indicates that BpSCSK can impact BpKH6 growth, which may result from the lantibiotics produced by BpSCSK.

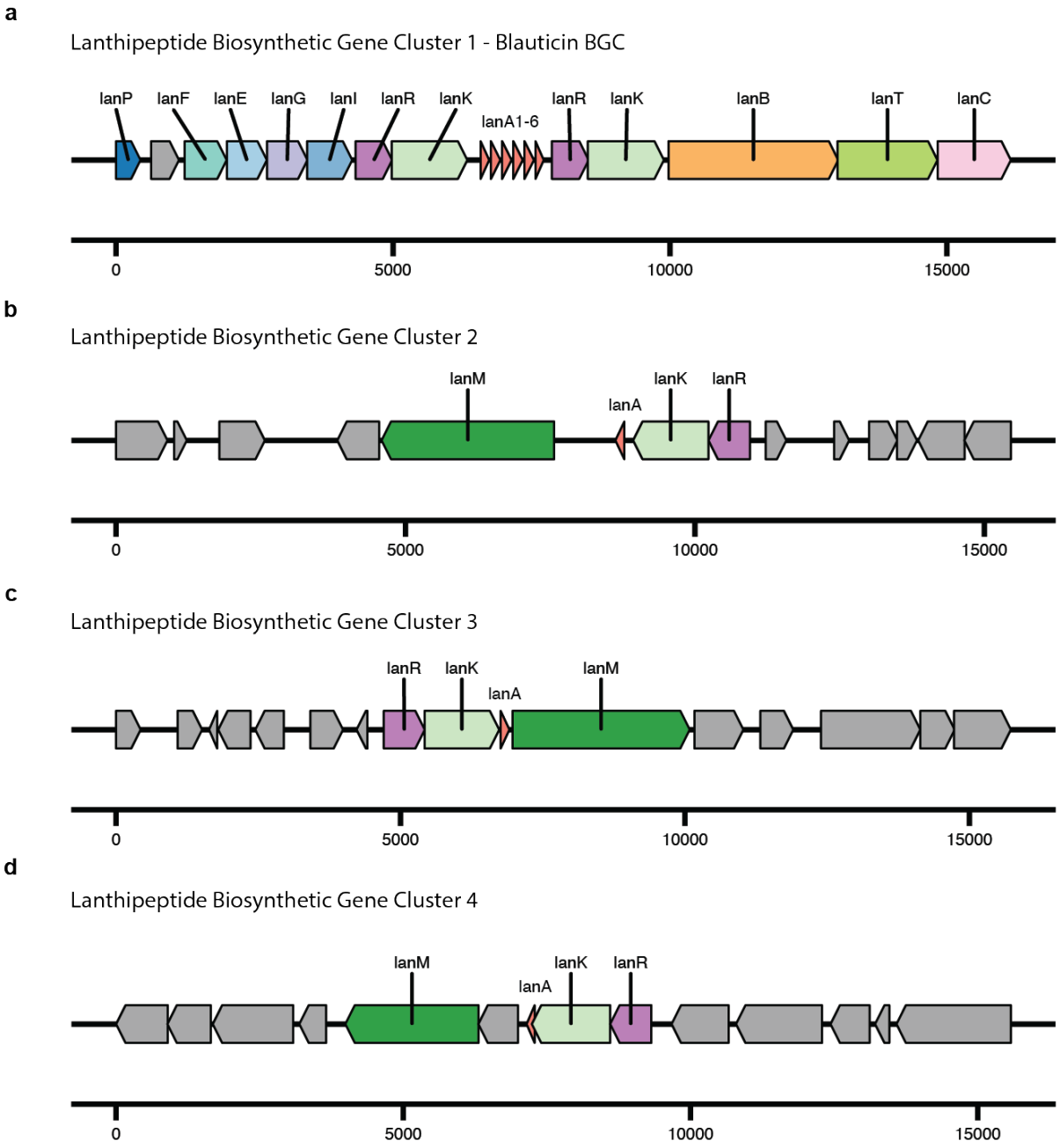

Figure 2.1: Lanthipeptide biosynthetic gene clusters in BpSCSK. a, Class I blauticin biosynthetic gene cluster. **b-d,** Class II lanthipeptide biosynthetic gene clusters. Predicted genes that could not be identified as part of the biosynthetic gene clusters appear in gray. Scales beneath each biosynthetic gene cluster represents the length of nucleotides.

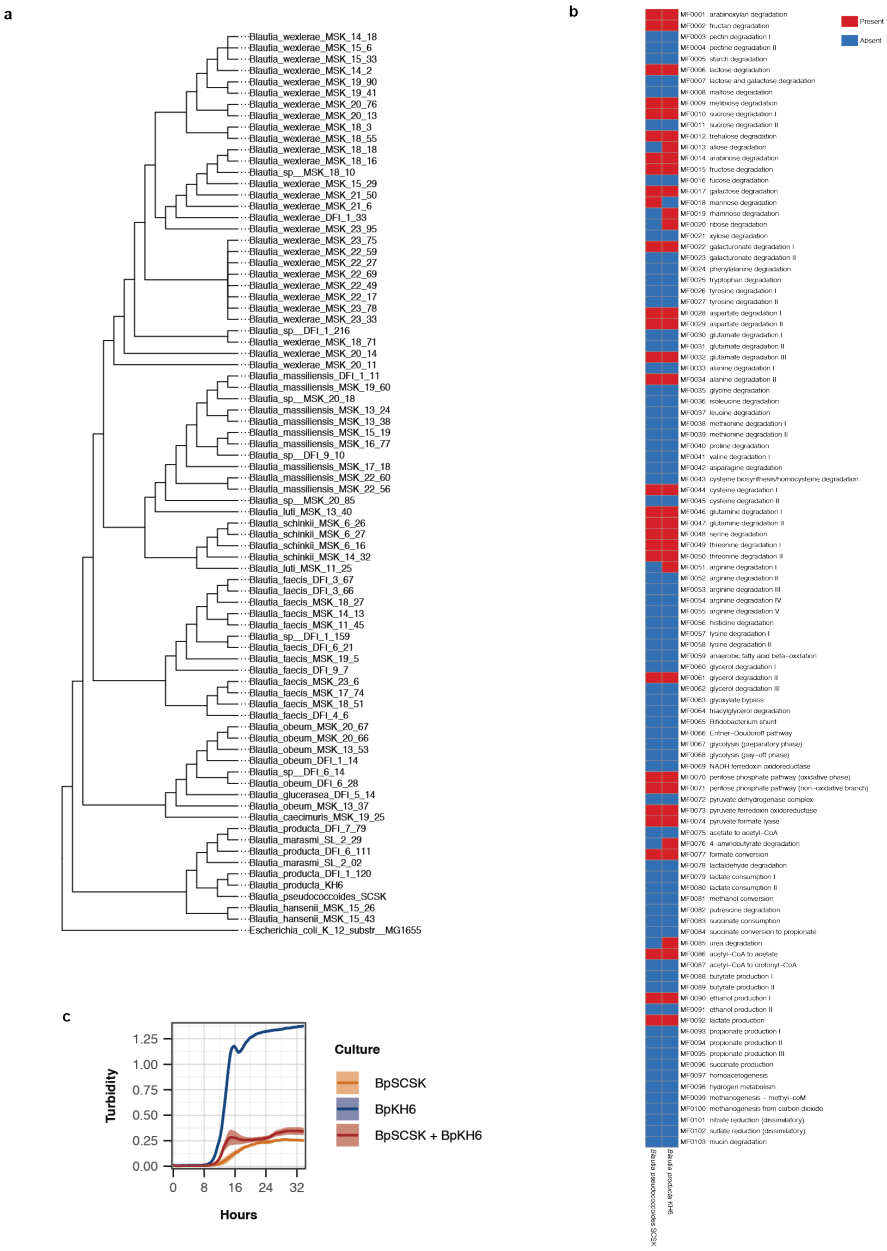

Figure 2.2: Growth rates and metabolite pathways of BpSCSK and BpKH6 **a,** Phylogenetic tree of BpSCSK, BpKH6, and *Blautia* spp. isolated from healthy human donors and rooted with *Escherichia coli* K12 substr. MG1655. **b,** Gut metabolite modules of BpSCSK and BpKH6 determined by Omixer-RPM. **c,** Growth curve of BpSCSK, BpKH6, and both grown together in BHIS liquid media ($n = 6$). Lines represent the average across biological replicates and ribbons represent the 95% confidence intervals.

2.2 BpSCSK suppresses microbiota recolonization following antibiotic treatment

Lantibiotic expression by BpSCSK promotes VRE clearance from the gut [Caballero et al., 2017, Kim et al., 2019], but the extent to which it suppresses commensal bacterial populations and potentially enables BpSCSK to invade a diverse microbiota is unclear. To address this, we administered BpSCSK by oral gavage daily for three days to specific-pathogen-free (SPF) C57BL/6 mice from Jackson Laboratories **(Fig. 2.3a)**. We also gavaged mice with BpKH6 as a negative control and phosphate-buffered saline (PBS) as a vehicle control. Neither BpSCSK nor BpKH6 were detected in fecal samples by 16S rRNA gene sequencing in recipient mice harboring the SPF microbiota **(Fig. 2.3b)**. Furthermore, there was no significant changes in α-diversity, as evidenced by a similar number of amplicon sequence variants (ASVs) and consistent Shannon diversity index for each group, and the samples had similar Bray-Curtis dissimilarities **(Fig. 2.3c-e)**. Thus, BpSCSK's ability to express blauticin did not enable it to invade and colonize a diverse SPF microbiota following repeated oral gavage.

To reduce microbiota-mediated colonization resistance, mice were treated with 0.5 g/L ampicillin in drinking water for four days to deplete the gut microbiota. Two days after ampicillin treatment was stopped, mice were oral gavaged of BpSCSK, BpKH6, or a PBS vehicle control for three consecutive days **(Fig. 2.4a)**. Following oral gavage, both BpSCSK and BpKH6 colonized the gut post-ampicillin treatment and persisted for up to 28 days **(Fig. 2.4b)**. BpSCSK represented >50% of the 16s rRNA gene relative abundance of fecal pellets collected on all days following oral gavage, while BpKH6 had a lower abundance upon colonization and continued to decrease overtime. Unlike the PBS- and BpKH6-treated groups, all mice colonized with BpSCSK maintained a significantly lower α-diversity for the 28 days mice were monitored **(Fig. 2.4c and 2.4d)**. PBS- and BpKH6-treated mice reached similar levels of α-diversity after 1-3 days post-colonization; however, both remained slightly lower than those of untreated, antibiotic-naive SPF mice after 28 days. Furthermore, PBS-

and BpKH6-treated groups clustered more closely with SPF mice than BpSCSK-colonized mice based on their Bray-Curtis dissimilarity **(Fig. 2.4e)**. Despite the differences observed in diversity, all mice had similar overall bacterial densities in feces, as determined by RT-qPCR **(Fig. 2.4f)**.

Following ampicillin treatment, *Enterococcus* and *Turicibacter* were among the most abundant genera detected in fecal pellets **(Fig. 2.4b)**. In BpSCSK-colonized mice, *Turicibacter* diminished over the 28-day period while the *Enterococcus* and *Lactobacillus* ASVs persisted along with *Akkermansia*, which was detected from day 1 post gavage. Among ASVs across all groups, ASVs that belong to the Eubacteriales order and particularly within the *Lachnospiraceae* and *Oscillospiraceae* families represented the majority of ASVs that did not recolonize mice containing BpSCSK after 28 days, including the ASVs for *Lachnospiraceae* and *Oscillospiraceae* that were present prior to the introduction of BpSCSK **(Fig. 2.4b; Table 2.1)**. Of the *Lachnospiraceae* ASVs that remained in BpSCSK-colonized mice after 28 days, all 12 belonged to the *Blautia* genus. These findings demonstrate that the lantibiotic-producing BpSCSK strain markedly impairs recolonization by gut commensals following antibiotic treatment.

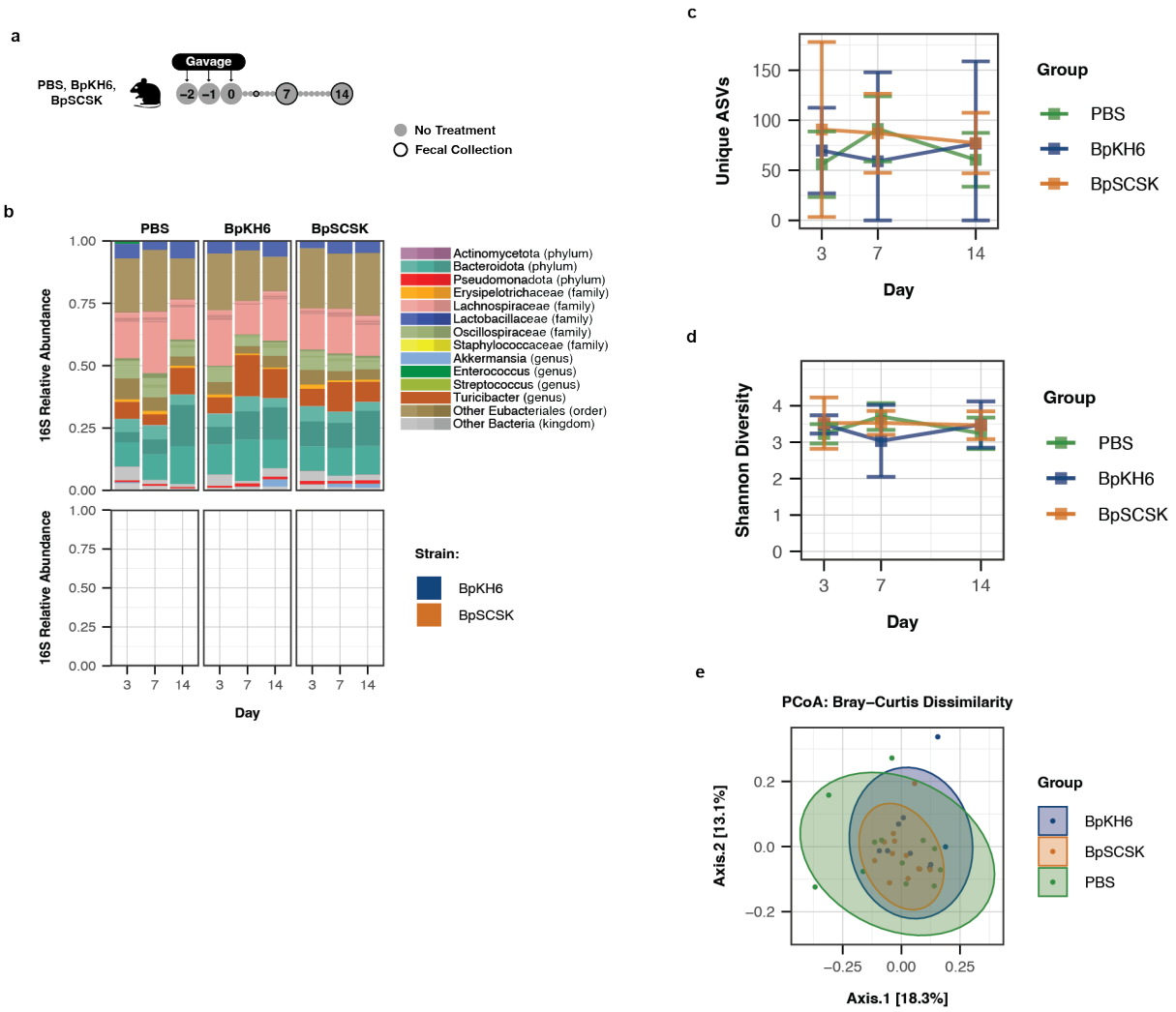

Figure 2.3: BpSCSK colonization in wild-type SPF mice. a, Schematic of experimental groups and time points. Female wild-type SPF C57BL/6 mice 9-10 weeks old were given PBS, BpKH6, or BpSCSK via oral gavage. Fecal samples were collected at indicated timepoints. Each group contains 3 mice. **b,** Average fecal microbiota 16S rRNA gene relative abundance. ASVs with greater than >0.01% abundance are plotted. Specific ASVs for BpSCSK and BpKH6 are plotted below. **c,** Average number of unique ASVs detected. Error bars indicate 95% confidence intervals. **d,** Average Shannon diversity. Error bars indicate 95% confidence intervals. **e,** Bray-Curtis dissimilarity principal coordinates analysis (PCoA) for all time points.

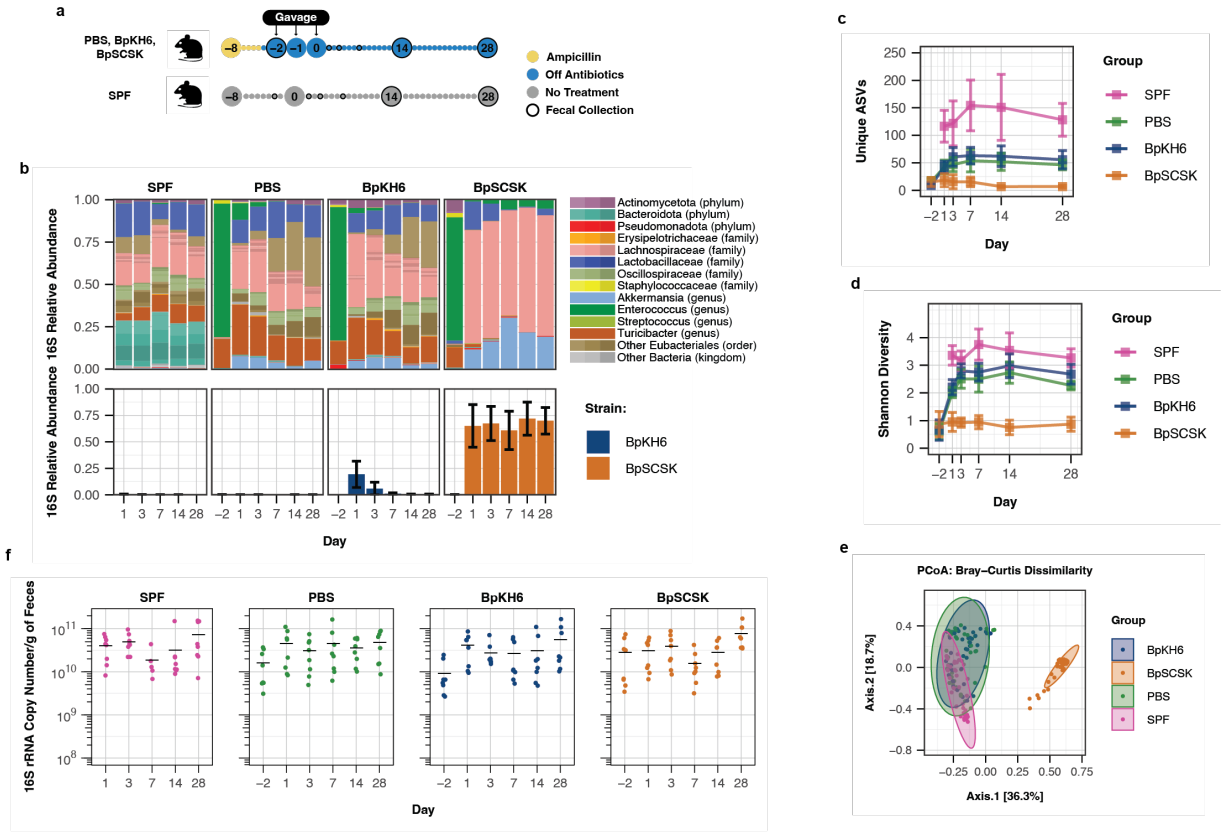

Figure 2.4: BpSCSK suppresses microbiota recolonization following antibiotic treatment. a, Schematic of experimental groups and time points. Female wild-type SPF C57BL/6 mice 9-10 weeks old were treated with 0.5 g/L ampicillin (Amp) in their drinking water for 4 days and given PBS, BpKH6, or BpSCSK via oral gavage. Fecal samples were collected at indicated time points. Each group contains 8 mice. **b,** Average fecal microbiota 16S rRNA gene relative abundance. ASVs with greater than >0.01% abundance are plotted. Specific ASVs for BpSCSK (orange) and BpKH6 (blue) are plotted below. Error bars indicate standard deviation. **c,** Average number of unique ASVs detected. Error bars indicate 95% confidence intervals. **d,** Average Shannon diversity. Error bars indicate 95% confidence intervals. **e,** Bray-Curtis dissimilarity principal coordinates analysis (PCoA) for all time points excluding day -2. **f,** 16S rRNA gene copy number per g of feces determined via qPCR. Black bars indicate the mean.

Phylum	Class	Order	Family	SPF	PBS	BpKH6	BpSCSK
Actinomycetota	Actinobacteria	Bifidobacteriales	*Bifidobacteriaceae*	1	1	1	1
		Micrococcales	*Microbacteriaceae*	-	1	-	-
	Coriobacteriia	Coriobacteriales	*Atopobiaceae*	1	1	-	-
		Eggerthellales	*Eggerthellaceae*	4	-	-	-
Bacillota	Bacilli	Lactobacillales	*Enterococcaceae*	-	1	1	1
			Lactobacillaceae	4	4	3	3
	Clostridia	Eubacteriales	*Christensenellaceae*	2	-	-	-
			Clostridiaceae 1	3	7	9	1
			Eubacteriaceae	1	-	-	-
			Eubacteriales Family XIII Incertae Sedis	1	-	1	-
			Lachnospiraceae	202	94	137	12
			Oscillospiraceae	74	36	41	-
			Peptococcaceae	4	-	-	-
			Peptostreptococcaceae	3	3	3	1
			Unclassified	48	8	8	1
	Erysipelotrichia	Erysipelotrichales	*Coprobacillaceae*	1	1	1	-
			Erysipelotrichaceae	3	2	4	-
			Turicibacteraceae	4	5	6	-
			Unclassified	1	-	1	-
	Unclassified	Unclassified	Unclassified	1	1	1	-
Bacteroidota	Bacteroidia	Bacteroidales	*Muribaculaceae*	15	1	-	-
Mycoplasmatota	Mollicutes	Acholeplasmatales	*Acholeplasmataceae*	3	1	-	-
		Anaeroplasmatales	*Anaeroplasmataceae*	1	-	1	-
		Unclassified	Unclassified	3	-	1	-
Pseudomonadota	Gammaproteobacteria	Enterobacterales	*Erwiniaceae*	-	-	-	3
Unclassified	Unclassified	Unclassified	Unclassified	11	1	3	-
Verrucomicrobiota	Verrucomicrobiia	Verrucomicrobiales	*Akkermansiaceae*	-	3	2	6
			Total ASVs:	**391**	**171**	**224**	**29**

Table 2.1: Unique ASVs detected on day 28 of colonization. Taxonomic distribution of ASVs from 16S rRNA gene sequencing of mice at day 28 in Figure 2.4. Values indicate the number of unique ASVs at the family level detected at >0.01% relative abundance.

2.3 The fecal metabolome is rendered deficient by BpSCSK colonization

Lachnospiraceae and *Oscillospiraceae* encode genes that enable production of microbiota-derived metabolites, including short-chain fatty acids (SCFAs) and a range of bile acid variants [Sorbara et al., 2019]. Since the species from these families were not well represented in the fecal pellets of mice harboring BpSCSK compared to the PBS and BpKH6 controls, we investigated the metabolomic profiles of fecal pellets collected over 28 days from these mice.

Using gas chromatography-mass spectrometry (GC-MS) with pentafluorobenzyl-bromide (PFBBr) derivatization, we determined the concentrations of a panel of 8 compounds that include amino acids, fatty acids, and organic acids. As expected, 4-day treatment with

ampicillin led to the marked reduction of SCFA concentrations in all mouse groups compared to SPF mice **(Fig. 2.5a)**. In contrast, proline and tyramine concentrations increased after ampicillin treatment compared to SPF mice, while glycine concentrations only changed minimally. Within the first week following PBS- or BpKH6-treatment, concentrations of proline, butyrate, and acetate returned to those detected in SPF mice. Concentrations of 5-aminovalerate exceeded the relative concentrations in SPF mice by day 1 and continued to day 28, suggesting that antibiotic treatment resulted in the expansion of bacterial species that produce this metabolite. In contrast, mice colonized with BpSCSK had consistently lower concentrations of 5-aminovalerate and butyrate compared to SPF mice over the 28 days samples were collected. In addition, concentrations of glycine, proline, and succinate remained elevated for 28 days. The absolute concentrations of metabolites at day 28 revealed that BpSCSK-colonized mice did not have any detectable butyrate in their fecal pellets and confirmed the higher concentrations of glycine and proline **(Table 2.2)**.

Next, we investigated the concentration changes of bile acids in fecal pellets using liquid chromatography-mass spectrometry (LC-MS). Before oral gavage, ampicillin treatment resulted in increased concentrations of conjugated primary bile acids, taurocholic and taurochenodeoxycholic acid, and decreased unconjugated primary bile acids compared to SPF mice **(Fig. 2.5b)**. In conjunction, the secondary bile acid concentrations began to decrease and secondary bile acids recovered and reached concentrations approaching those of SPF mice after termination of ampicillin treatment and were unaffected by BpKH6 or control PBS administration. In BpSCSK-colonized mice, in contrast, taurocholic and taurochenodeoxycholic acid levels remained elevated and secondary bile acid concentrations remained low up to 28 days after termination of ampicillin treatment. The relative abundance of *Turicibacter*, a genus with species previously shown to deconjugate taurine-conjugated primary bile acids, decreased during the course of BpSCSK colonization **(Fig. 2.5c)** [Lynch et al., 2023]. Absolute concentrations of bile acids revealed that deoxycholic and isodeoxycholic

acid were below the limits of detection, while other secondary bile acids were near zero except for ursodeoxycholic and allocholic acid **(Table 2.2)**. Taurocholic acid concentrations were more than 10-fold greater in BpSCSK colonized mice than PBS- or BpKH6-treated mice.

Together, these metabolomic panels demonstrate that, in addition to decreased microbiota α-diversity, BpSCSK-colonized mice fail to recover critical producers of microbiota-derived metabolites. Therefore, BpSCSK prolongs both the compositional and functional dysbiotic state of mice up to 28 days after ampicillin treatment has ceased.

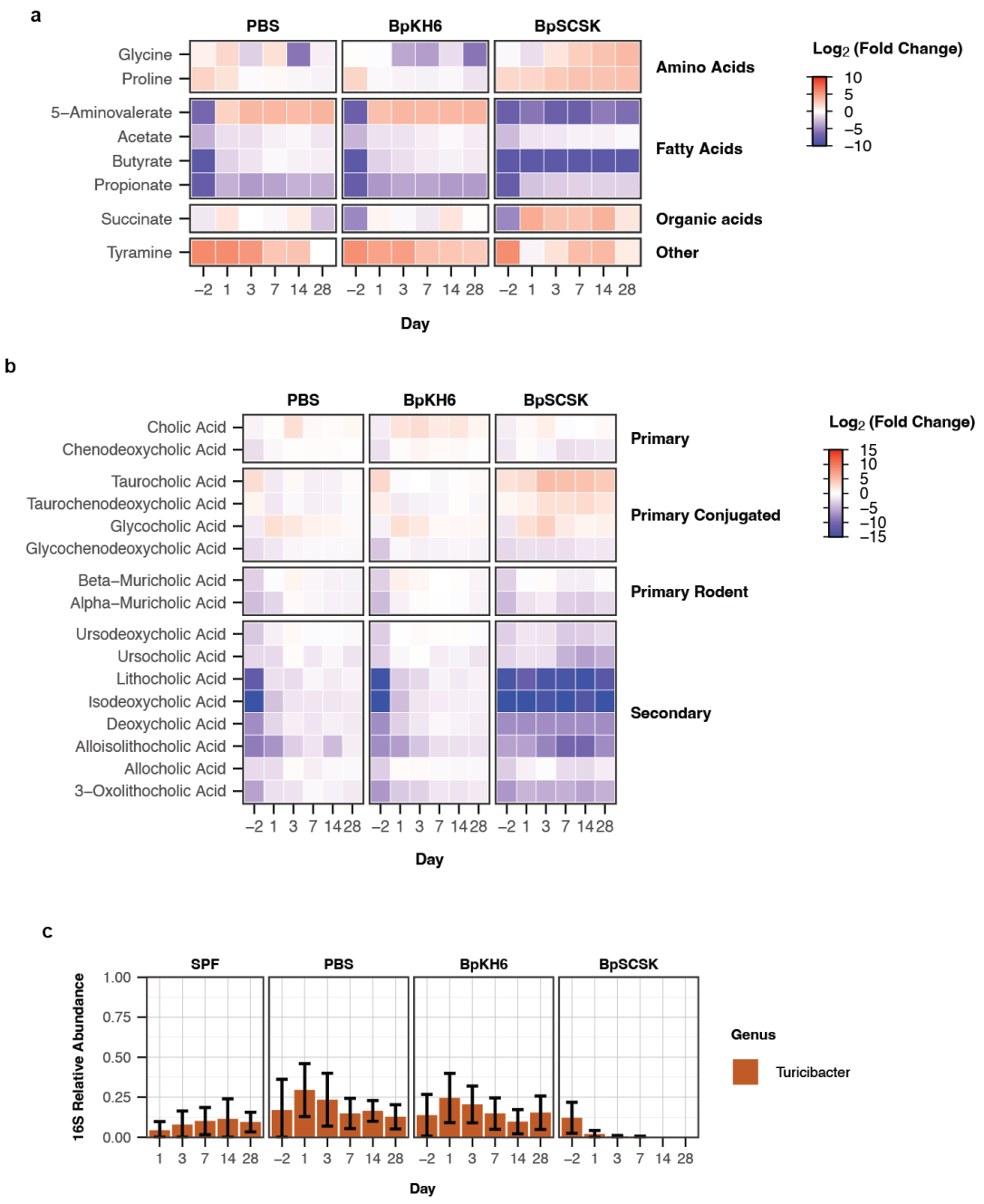

Figure 2.5: The fecal metabolome is rendered deficient by BpSCSK colonization. Fecal pellets collected from mice at the same time as 16S rRNA gene sequencing in Figure 2.4 were also subject to metabolics. **a, b,** $\log_2$ fold change of metabolites are calculated as the ratio of the average concentration of metabolites for indicated groups by the average concentration of metabolites across all days for SPF mice. **c,** Average 16S rRNA gene relative abundance for *Turicibacter*. Error bars indicate standard deviation.

Compound	Compound Class	SPF	PBS	BpKH6	BpSCSK
PFBBr Metabolomic Panel					
Glycine	Amino Acids	0.0625 ± 0.0981 mM	0.035 ± 0.099 mM	0 ± 0 mM	0.757 ± 0.261 mM
Proline	Amino Acids	0.188 ± 0.118 mM	0.133 ± 0.155 mM	0.0888 ± 0.0656 mM	1.95 ± 0.51 mM
5-Aminovalerate	Fatty Acids	0.375 ± 0.349 mM	4.93 ± 1.82 mM	4.94 ± 2.4 mM	0.0025 ± 0.00463 mM
Acetate	Fatty Acids	10.3 ± 3.93 mM	5.48 ± 2.03 mM	6.45 ± 2.5 mM	9.29 ± 0.62 mM
Butyrate	Fatty Acids	4.87 ± 3.49 mM	2.39 ± 0.691 mM	2.16 ± 0.347 mM	0 ± 0 mM
Propionate	Fatty Acids	2.28 ± 0.749 mM	0.184 ± 0.21 mM	0.104 ± 0.126 mM	0.534 ± 0.304 mM
Succinate	Organic acids	0.0938 ± 0.195 mM	0.0425 ± 0.12 mM	0.329 ± 0.38 mM	0.739 ± 1.71 mM
Tyramine	Other	0.00125 ± 0.00354 mM	0.0025 ± 0.00463 mM	0.0213 ± 0.0376 mM	0.00625 ± 0.00744 mM
Bile Acid Metabolomic Panel					
Cholic Acid	Primary	83.6 ± 116 μM	320 ± 425 μM	381 ± 384 μM	293 ± 217 μM
Chenodeoxycholic Acid	Primary	7.26 ± 4.48 μM	7.9 ± 7.65 μM	7.44 ± 5.56 μM	2.89 ± 1.88 μM
Taurocholic Acid	Primary Conjugated	10.3 ± 6.19 μM	31.4 ± 63 μM	32.8 ± 63 μM	400 ± 213 μM
Taurochenodeoxycholic Acid	Primary Conjugated	1.3 ± 0.825 μM	1.47 ± 1.81 μM	1.22 ± 1 μM	8.6 ± 2.8 μM
Glycocholic Acid	Primary Conjugated	0.433 ± 0.242 μM	0.681 ± 0.389 μM	0.767 ± 0.324 μM	1.04 ± 0.386 μM
Glycochenodeoxycholic Acid	Primary Conjugated	0.221 ± 0.0624 μM	0.123 ± 0.0751 μM	0.104 ± 0.0875 μM	0.0677 ± 0.0496 μM
Beta-Muricholic Acid	Primary Rodent	753 ± 313 μM	428 ± 265 μM	477 ± 266 μM	685 ± 420 μM
Alpha-Muricholic Acid	Primary Rodent	271 ± 153 μM	118 ± 55.7 μM	139 ± 58.8 μM	50.1 ± 28.6 μM
Ursodeoxycholic Acid	Secondary	12.7 ± 3.68 μM	8.57 ± 5.71 μM	10.2 ± 3.96 μM	2.37 ± 1.49 μM
Ursocholic Acid	Secondary	2.07 ± 1.08 μM	1.27 ± 0.664 μM	1.29 ± 0.669 μM	0.122 ± 0.0898 μM
Lithocholic Acid	Secondary	68.9 ± 27.4 μM	23.9 ± 26 μM	22.9 ± 24.6 μM	0.00443 ± 0.00947 μM
Isodeoxycholic Acid	Secondary	79.5 ± 41.6 μM	25.2 ± 29.8 μM	31.4 ± 37.8 μM	0 ± 0 μM
Deoxycholic Acid	Secondary	745 ± 275 μM	266 ± 298 μM	291 ± 317 μM	0 ± 0 μM
Alloisolithocholic Acid	Secondary	4.55 ± 3.23 μM	1.27 ± 3.38 μM	0.794 ± 1.26 μM	0.0155 ± 0.0302 μM
Allocholic Acid	Secondary	21.5 ± 19 μM	29.1 ± 29.8 μM	25.7 ± 18.8 μM	16.2 ± 7.35 μM
3-Oxolithocholic Acid	Secondary	2.04 ± 1.29 μM	0.559 ± 0.53 μM	0.567 ± 0.619 μM	0.0434 ± 0.0493 μM

Table 2.2: Metabolite concentrations on day 28 of colonization. Metabolite concentrations of mice from Figure 2.5. Concentrations are listed as the average concentration ± standard deviation across 8 mice.

2.4 Fecal microbiota transplantation fails to restore gut microbiota diversity and key metabolite producers

Recolonization of the gut microbiota following ampicillin treatment is driven by bacterial species that persist at low densities within the host or that are acquired from the surrounding environment. Therefore, it is possible that BpSCSK-colonized mice do not achieve the same level of diversity observed in PBS- and BpKH6-treated mice because they are unable to acquire commensal species from the environment. To address this, we attempted to recolonize mice by administering a fecal microbiota transplant (FMT) from antibiotic-naive SPF donor mice. Fecal pellets from four separate SPF mice were pooled and administered to BpSCSK-colonized mice via oral gavage. The process was repeated once a day for three consecutive days starting 28 days after the final gavage of PBS, BpKH6, or BpSCSK **(Fig. 2.6a)**. To

ensure the FMT was viable, a separate group of mice were treated with ampicillin, in the same manner as the other groups, for four days starting six days before the first FMT **(Fig. 2.7a)**.

In BpKH6-colonized mice, BpKH6 represented <0.5% of the relative abundance on day 28 and further decreased following FMT **(Fig. 2.4b and 2.6b)**. The PBS- and BpKH6-treated mice gained slightly more α-diversity after the FMT and reached a similar level of ASVs and Shannon diversity as FMT control mice **(Fig. 2.6c, 2.6d, and 2.7b)**. After three daily FMTs, BpSCSK still represented approximately 40% of the relative abundance of ASVs in fecal pellets after two weeks **(Fig. 2.6b)**. ASVs for *Muribaculaceae* and *Erysipelotrichaceae*, which were not detected before the FMT, made up approximately 35% in abundance on day 44. To a lesser extent, ASVs for *Oscillospiraceae* and an unknown Eubacteriales species were also detected on day 44. Although the Shannon diversity of BpSCSK-colonized mice was almost two-fold greater one day after the final FMT was administered, it remained at a Shannon diversity index of approximately 2 on day 44 while other groups had an average Shannon diversity index above 3 **(Fig. 2.6c and 2.6d)**. This was further highlighted by the Bray-Curtis dissimilarity between samples where the BpSCSK samples remained distinct from all other groups while PBS- and BpKH6-treated mice overlapped with samples from SPF and FMT control mice **(Fig. 2.6e)**.

Metabolomic profiling of mice before and after FMT treatment revealed that metabolites in PBS- and BpKH6-treated mice returned to the concentrations observed in SPF and FMT control **(Fig. 2.8a and 2.8b)**. BpSCSK-colonized mice had increased concentrations of propionate, ursocholic acid, ursodeoxycholic acid, α-muricholic acid, β-muricholic acid, and chenodeoxycholic acid and decreased concentrations of taurocholic and taurochenodeoxycholic acid. Interestingly, the decrease in taurocholic and taurochenodeoxycholic acid was not associated with reestablishment of *Turicibacter* species **(Fig. 2.6b)**. Therefore, there may be other bacteria among the *Muribaculaceae* and *Erysipelotrichaceae* that recolonized

with the ability to deconjugate taurine. Other metabolites in the two panels were within similar ranges to the starting concentrations on day 28 in BpSCSK-colonized mice two weeks after FMT treatment **(Fig. 2.8a and 2.8b)**. Thus, BpSCSK, once established in the gut, prevents colonization by many bacterial species following FMT from SPF mice.

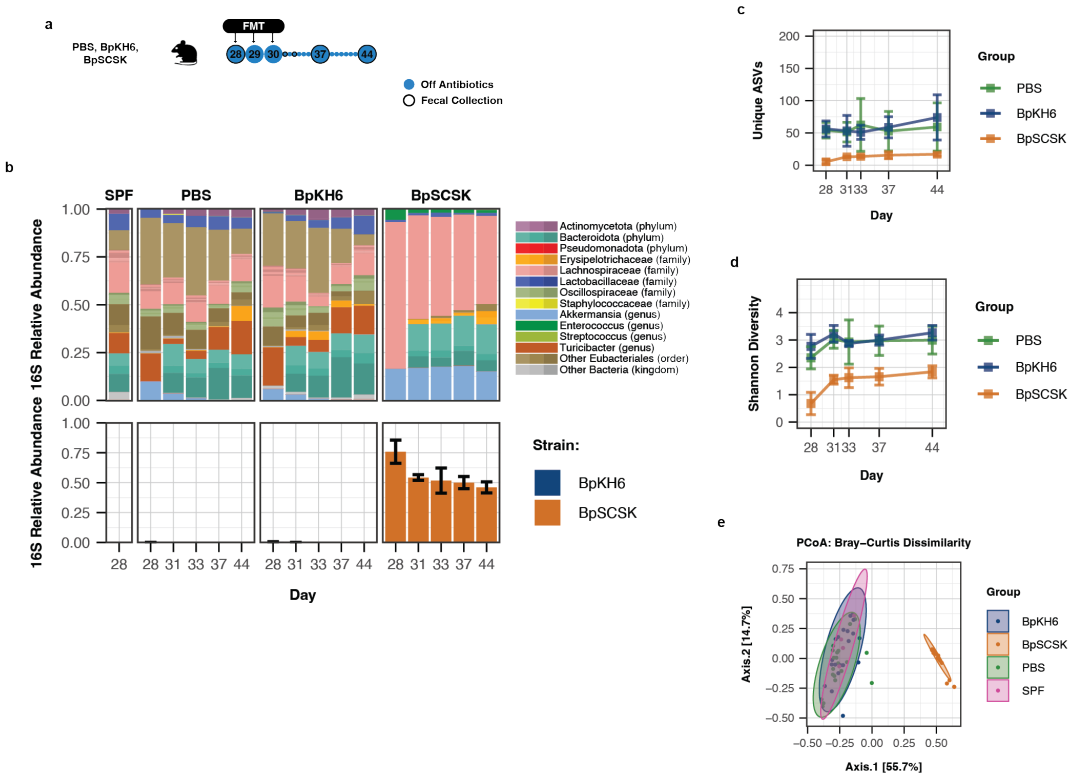

Figure 2.6: Fecal microbiota transplantation fails to restore gut microbiota diversity and key metabolite producers. a, Schematic of experimental groups and time points. 4 mice in each group from Figure 2.4 were subjected to an FMT from an SPF mouse for three days via oral gavage. **b,** Average fecal microbiota 16S rRNA gene relative abundance. ASVs with greater than >0.01% abundance are plotted. Specific ASVs for BpSCSK and BpKH6 are plotted below. Error bars indicate standard deviation. **c,** Average number of unique ASVs detected. Error bars indicate 95% confidence intervals. **d,** Average Shannon diversity. Error bars indicate 95% confidence intervals. **e,** Bray-Curtis dissimilarity principal coordinates analysis (PCoA) for all time points.

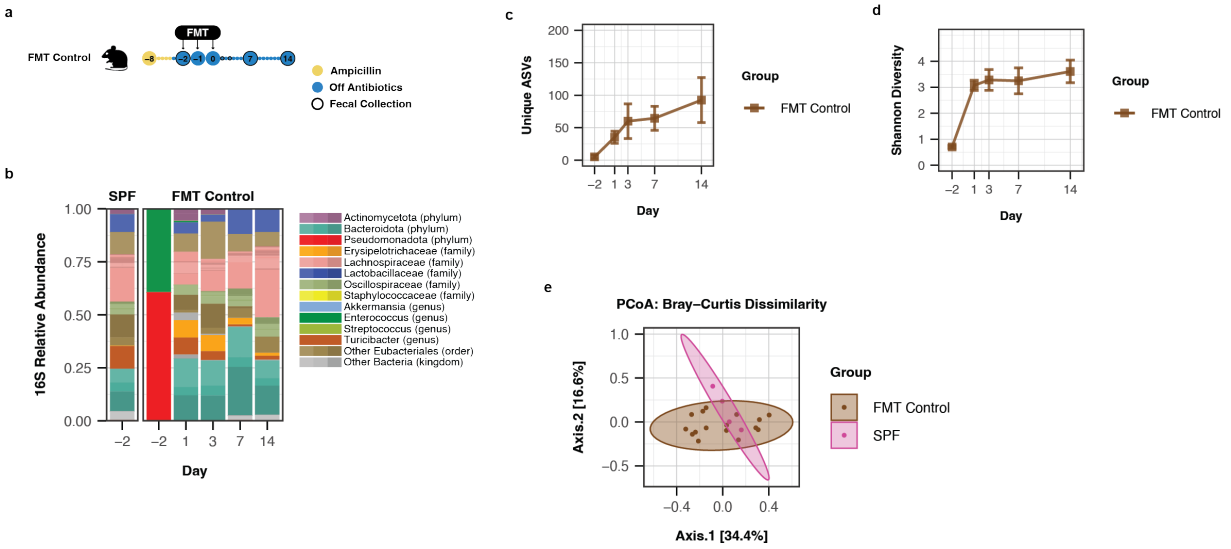

Figure 2.7: Colonization of FMT in antibiotic treated mice. a, Schematic of experimental groups and time points. 4 mice in the FMT control group were subjected to an FMT from an SPF mouse for three days via oral gavage. The FMT Control group were subject to 4 days ampicillin treatment starting 6 days before the first FMT. **b,** Average fecal microbiota 16S rRNA gene relative abundance. ASVs with greater than >0.01% abundance are plotted. **c,** Average number of unique ASVs detected. Error bars indicate 95% confidence intervals. **d,** Average Shannon diversity. Error bars indicate 95% confidence intervals. **e,** Bray-Curtis dissimilarity principal coordinates analysis (PCoA) for all time points.

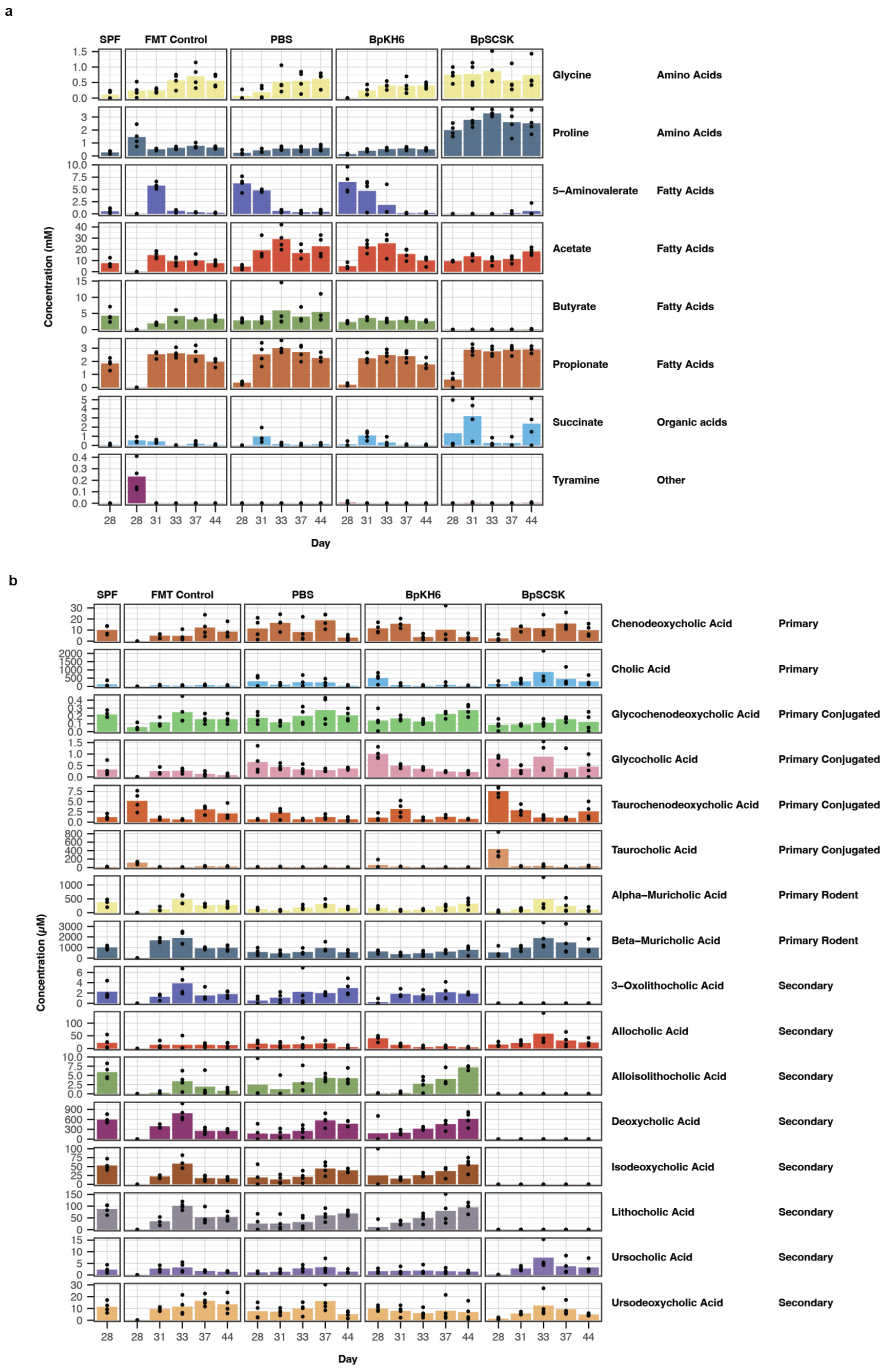

Figure 2.8: Metabolite concentrations after FMT treatment. a, b, Absolute concentrations of metabolites for mice from Figure 2.6 and 2.7. The bars represent the average concentration across the mice on each day. The dots are the individual values for each mouse.

2.5 Co-housing BpSCSK-colonized mice with SPF mice fails to restore gut diversity and key metabolite producers

To determine whether a more regular introduction of bacteria from SPF mice via coprophagia could overcome colonization resistance in the presence of BpSCSK, we co-housed BpSCSK-colonized mice with SPF mice. Each BpSCSK-colonized mouse was co-housed with one SPF mouse and fecal pellets were collected for 2 weeks for 16S rRNA gene sequencing and metabolomic profiling **(Fig. 2.9a)**.

The 16S rRNA gene sequencing revealed that, similar to the FMT, co-housing BpSCSK-colonized mice with SPF mice did not overcome the barrier to colonization established by BpSCSK. Over the two weeks, BpSCSK still remained approximately at 40% relative abundance in sequenced fecal pellets **(Fig. 2.9b)**. Likewise, the number of unique ASVs and α-diversity for BpSCSK-colonized mice remained at levels observed prior to co-housing **(Fig. 2.9c and 2.9d)**. The Bray-Curtis dissimilarity continued to show a clear separation from SPF mice as seen in previous experiments **(Fig. 2.9e)**. In addition to BpSCSK-treated mice, we sequenced fecal pellets from the SPF mice to determine whether co-housing would lead to colonization of BpSCSK. Although BpSCSK ASVs were detected in SPF mice, it was not consistently detected in mice over the course of the two weeks **(Fig. 2.9b)**. Therefore, it could not be determined whether BpSCSK actually colonized the mice or transiently passed through the gastrointestinal (GI) tract from coprophagia.

In conjunction with the continued lack of diversity, there were no notable changes in quantified metabolites between pre-co-housing and post-co-housing in BpSCSK-colonized mice except for alloisolithocholic and 3-oxolithocholic acid detected on the final day of collection at day 58 **(Fig. 2.10a and 2.10b)**. Similarly, there were no major changes among quantified metabolites for SPF mice after two weeks. Thus, even an FMT followed by co-housing was unable to restore important microbiota-derived metabolites in the presence of BpSCSK.

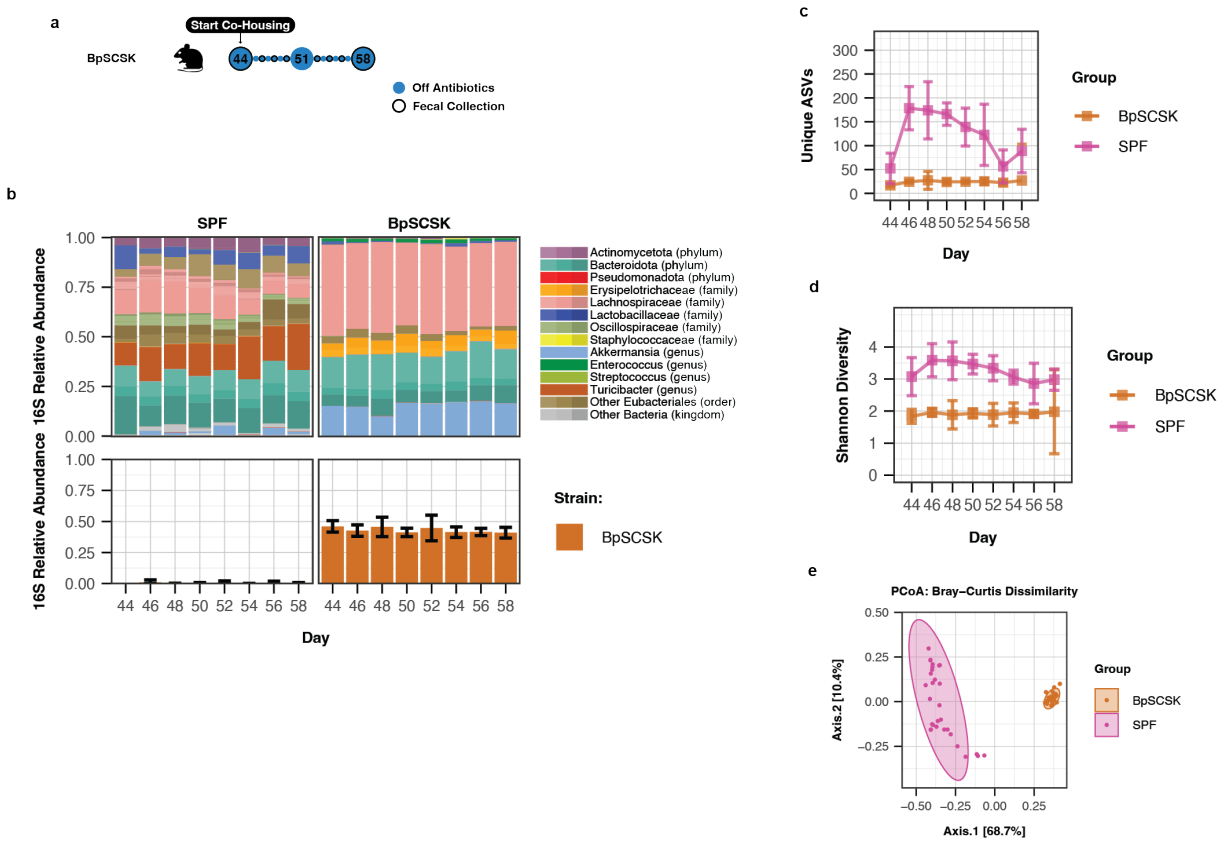

Figure 2.9: Co-housing BpSCSK-colonized mice with SPF mice fails to restore gut diversity and key metabolite producers. a, Schematic of experimental groups and time points. BpSCSK-treated mice from Figure 4 that received an FMT were co-housed with an SPF mouse for two weeks. **b,** Average fecal microbiota 16S rRNA gene relative abundance. ASVs with greater than >0.01% abundance are plotted. Specific ASVs for BpSCSK (orange) and BpKH6 (blue) are plotted below. Error bars indicate standard deviation. **c,** Average number of unique ASVs detected. Error bars indicate 95% confidence intervals. **d,** Average Shannon diversity. Error bars indicate 95% confidence intervals. **e,** Bray-Curtis dissimilarity principal coordinates analysis (PCoA) for all time points.

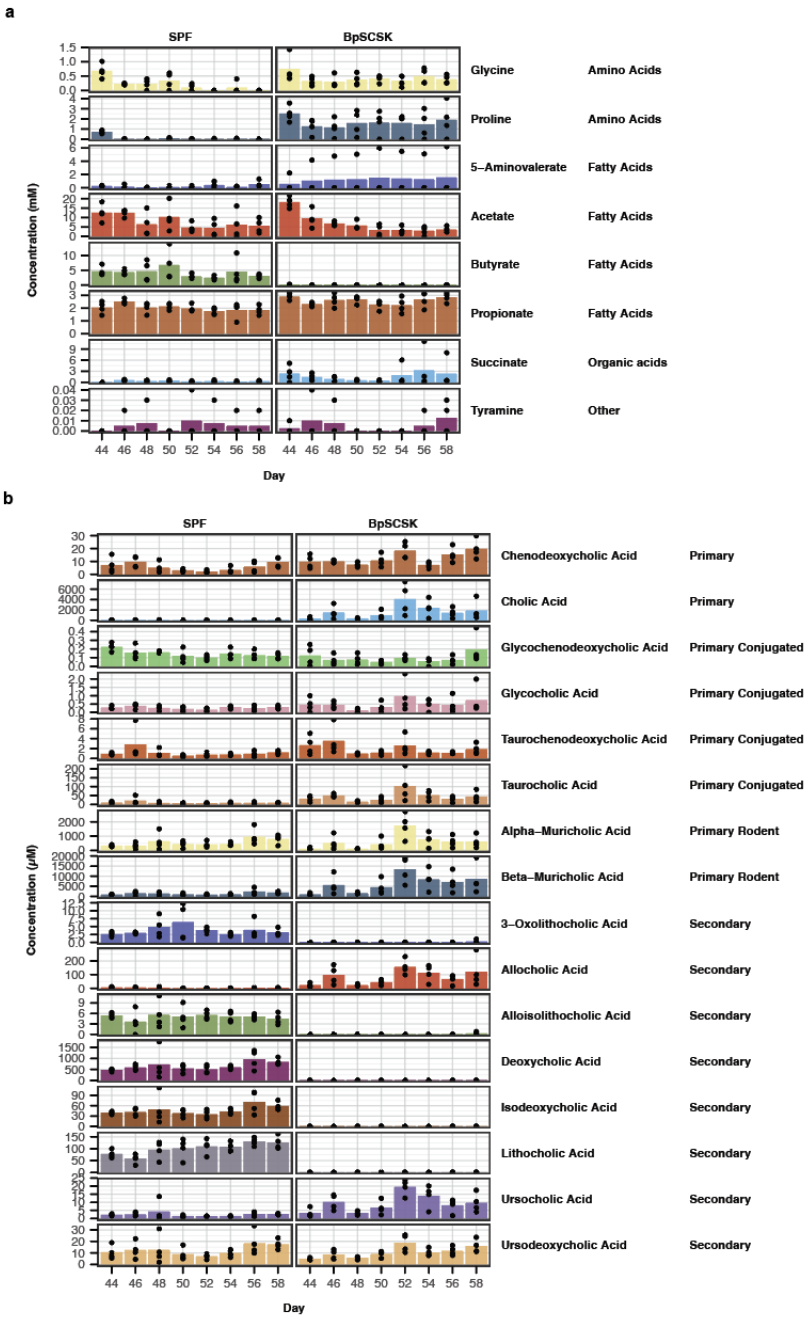

Figure 2.10: Metabolite concentrations after co-housing BpSCSK-colonized mice with SPF mice. a, b, Absolute concentrations of metabolites for mice from Figure 2.9. The bars represent the average concentration across the mice on each day. The dots are the individual values for each mouse.

2.6 A diverse ampicillin-resistant microbiota harboring BpSCSK

Continuous treatment of MyD88$^{-/-}$ C57BL/6 mice with Augmentin for over 10 years has led to the development of a unique ampicillin-resistant microbiota (ARM) capable of maintaining colonization in the presence of Augmentin or other β-lactams like ampicillin. The ARM shares little similarity with SPF as shown by 16S rRNA gene sequencing **(Fig. 2.11a)**. In fact, less than 5% of the relative abundance of the ARM is shared with SPF mice, and an even smaller percentage of ARM ASVs account for the SPF microbiota **(Fig. 2.11b)**. Bray-Curtis dissimilarity further highlights the difference between the ARM and SPF microbiota **(Fig. 2.11c)**. Despite their differences, however, the ARM of MyD88$^{-/-}$ mice still provides a similar level of α-diversity observed in SPF mice **(Fig. 2.11d)**.

Notably, ARM had fewer Bacillota and more species in the Bacteroidales order, especially with ASVs for *Muribaculaceae* and *Bacteroidaceae* **(Fig. 2.11a and Table 2.3)**. While the continuous antibiotic treatment likely played a role in this development, it is also possible that the lantibiotics produced by BpSCSK had an impact on the development of the ARM. Metabolomic profiling of fecal pellets from MyD88$^{-/-}$ mice revealed that the ARM contains proline and glycine consumers as well as butyrate and 5-aminovalerate producers **(Fig. 2.12a)**. The primary and conjugated primary bile acids were variable between the mice with the ARM, but secondary bile acids were largely absent compared to SPF mice **(Fig. 2.12b)**.

While ASVs found in BpSCSK were still detectable in each of the ARM samples, they were present in varying relative abundances between the four mice **(Fig. 2.11a)**. For ARM Mouse 3, BpSCSK ASVs were present but only represented approximately .008 (.8%) of the relative abundance. ARM Mouse 1-3 had another *Blautia* ASV that is not associated with BpSCSK, indicating that another species of *Blautia* may be present in the microbiota. To confirm that the BpSCSK detected still encoded the blauticin BGC, we performed short-read shotgun metagenomic sequencing on fecal pellets from MyD88$^{-/-}$ mice and mapped

the reads to the BpSCSK genome **(Fig. 2.13a)**. These mice also had varying degrees of BpSCSK ranging from around 1-8% of the total reads, but all four mice tested had the BpSCSK genome including the blauticin BGC. Although, there were four gap regions in the reads recruited to the BpSCSK genome. Many of these genes corresponded to phage genes, indicating that the BpSCSK strain in the ARM have now lost some phages. Interestingly, the lanthipeptide BGC 4, which had the overlapping *lanA* gene and *lanM* gene was also no longer detectable, while regions around the BGC were. Since the blauticin *lanA* genes were still in the genome, however, it is likely that the other bacteria have developed resistance and/or tolerance to blauticin.

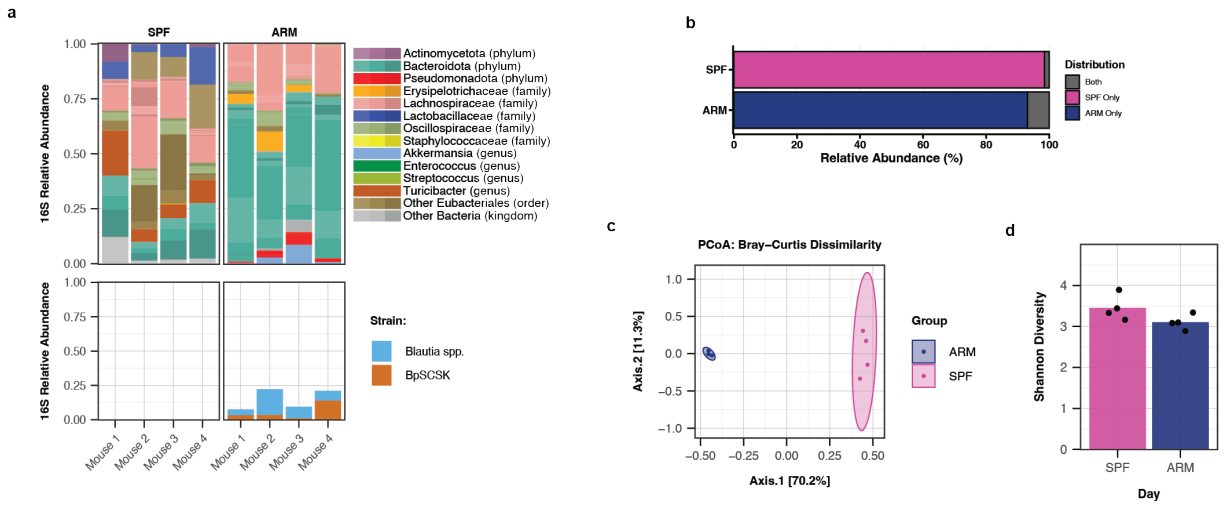

Figure 2.11: Metagenomic comparison of ARM to SPF mice. a, Fecal microbiota 16S rRNA gene relative abundance of individual mice ($n = 4$). ASVs with greater than >0.01% abundance are plotted. Specific ASVs for BpSCSK (orange) and other *Blautia* species (light blue) are plotted below. **b,** Relative abundance percentages of ASVs that belong to SPF only (pink), ARM only (blue), or both (gray). **c,** Bray-Curtis dissimilarity principal coordinates analysis (PCoA) for all SPF and ARM mice. **d,** Average Shannon diversity between SPF and ARM mice.

Phylum	Class	Order	Family	SPF	ARM
Actinomycetota	Actinobacteria	Bifidobacteriales	*Bifidobacteriaceae*	1	-
	Coriobacteriia	Coriobacteriales	*Atopobiaceae*	1	-
		Eggerthellales	*Eggerthellaceae*	2	1
Bacillota	Bacilli	Lactobacillales	*Enterococcaceae*	-	1
			Lactobacillaceae	1	-
	Clostridia	Eubacteriales	*Christensenellaceae*	2	1
			Clostridiaceae 1	3	-
			Eubacteriaceae	1	-
			Eubacteriales Family XIII Incertae Sedis	1	-
			Lachnospiraceae	141	10
			Oscillospiraceae	47	5
			Peptostreptococcaceae	2	2
			Unclassified	35	4
	Erysipelotrichia	Erysipelotrichales	*Coprobacillaceae*	1	-
			Erysipelotrichaceae	3	1
			Turicibacteraceae	3	-
			Unclassified	1	-
	Unclassified	Unclassified	Unclassified	1	1
Bacteroidota	Bacteroidia	Bacteroidales	*Bacteroidaceae*	-	4
			Muribaculaceae	8	36
			Porphyromonadaceae	-	3
			Prevotellaceae	-	3
			Rikenellaceae	-	2
			Unclassified	-	1
	Unclassified	Unclassified	Unclassified	-	1
Campylobacterota	Campylobacteria	Campylobacterales	*Helicobacteraceae*	-	1
Cyanobacteriota	Cyanophyceae	Unclassified	Unclassified	-	1
Deferribacterota	Deferribacteres	Deferribacterales	*Deferribacteraceae*	-	1
Mycoplasmatota	Mollicutes	Acholeplasmatales	*Acholeplasmataceae*	1	-
		Anaeroplasmatales	*Anaeroplasmataceae*	1	-
		Unclassified	Unclassified	3	-
Pseudomonadota	Alphaproteobacteria	Unclassified	Unclassified	-	2
	Betaproteobacteria	Burkholderiales	*Sutterellaceae*	-	2
	Deltaproteobacteria	Desulfovibrionales	*Desulfomicrobiaceae*	-	1
			Desulfovibrionaceae	-	2
	Gammaproteobacteria	Enterobacterales	*Enterobacteriaceae*	-	1
Unclassified	Unclassified	Unclassified	Unclassified	9	1
Verrucomicrobiota	Verrucomicrobiia	Verrucomicrobiales	*Akkermansiaceae*	-	1
			Total ASVs:	**266**	**89**

Table 2.3: ASVs in SPF and ARM mice. Taxonomic distribution of ASVs from 16S rRNA gene sequencing from mice in Figure 2.11. Values indicate the number of unique ASVs at the family level detected at >0.01% relative abundance.

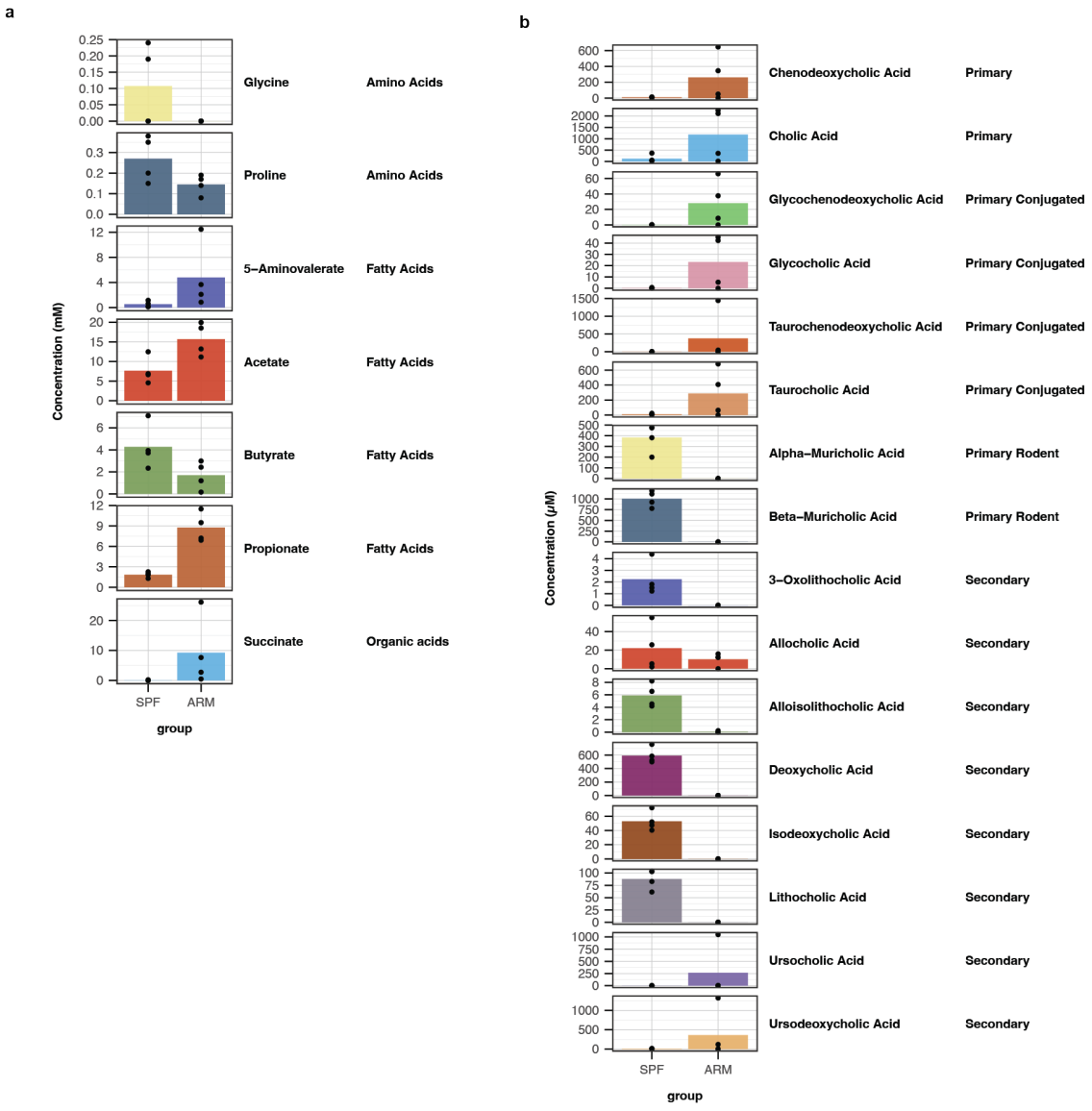

Figure 2.12: Metabolomic profiling of ARM and SPF mice. a, b, Absolute concentrations of metabolites for mice from Figure 2.11. The bars represent the average concentration across the mice on each day. The dots are the individual values for each mouse.

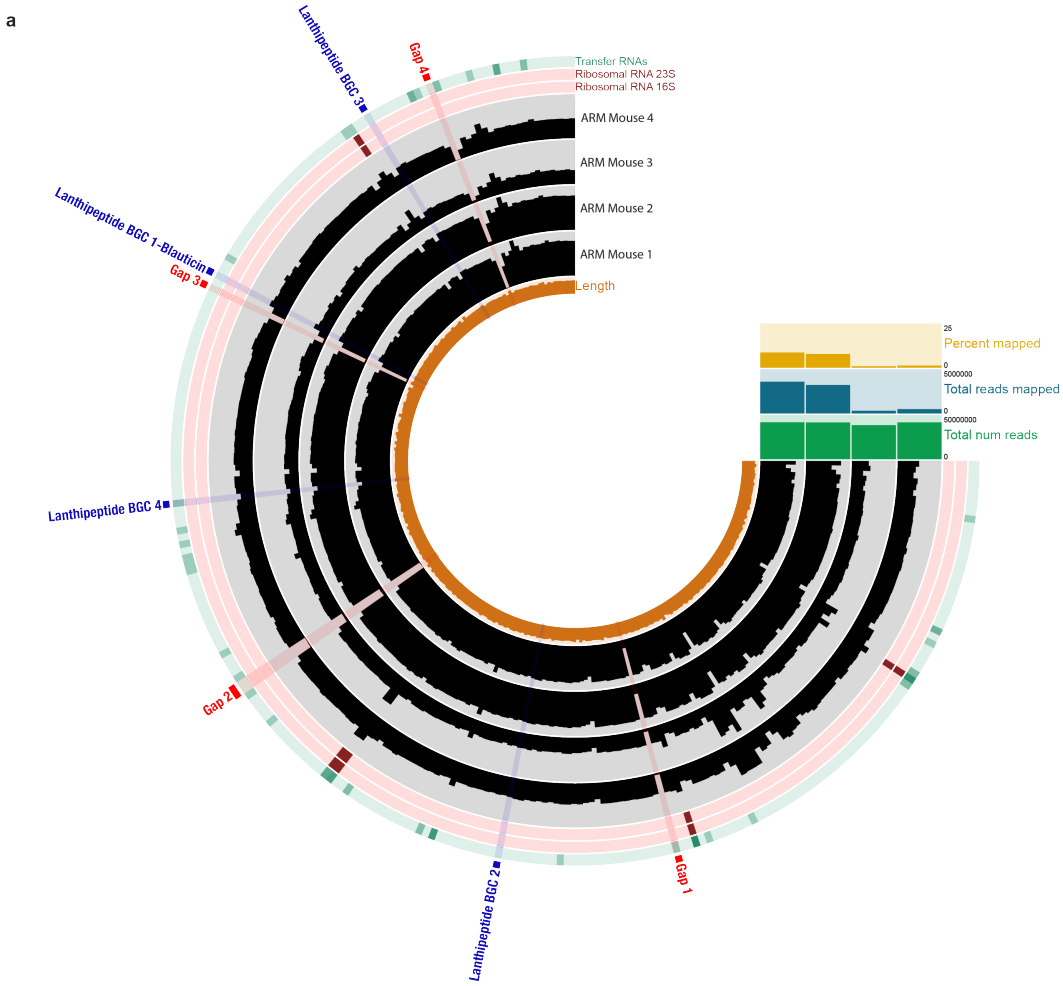

Figure 2.13: ARM shotgun sequencing reads mapped to BpSCSK genome. a, Fecal samples from four MyD88$^{-/-}$ mice with the ARM were shotgun sequenced and short-reads were mapped to the BpSCSK genome. Black bars represent the average coverage for an approximately 20,000 bp region of the genome. The gaps are regions with greater than 20,000 bp missing. Each of the regions containing the lanthipeptide BGCs in BpSCSK are denoted in blue.

2.7 BpSCSK-resistant microbiota can restore gut diversity and key metabolite producers

Because BpSCSK is in ARM, we hypothesized that the gut commensals from these mice would be capable of colonizing BpSCSK-dominated mice. To test this, we co-housed MyD88$^{-/-}$ C57BL/6 mice harboring the ARM with BpSCSK-colonized mice and sequenced fecal pellets over the following two weeks **(Fig. 2.14a)**. To reduce the impact of bacteria that were not associated with the ARM from colonizing, all mice were treated with ampicillin in drinking water throughout the experiment. Because BpSCSK is sensitive to ampicillin, we gavaged the previously described 4-mix consortia consisting of *Enterocloster* [*Clostridium*] *bolteae*, *Phocaeicola* [*Bacteroides*] *sartorii*, BpSCSK, and *Parabacteroides distasonis* (CBBP)[Caballero et al., 2017, Kim et al., 2019]. *P. distasonis* and *P. sartorii* encode β-lactamases that degrade ampicillin.

As expected, the ARM containing BpSCSK was able to transfer and colonize mice treated with ampicillin and subsequently given the CBBP consortia **(Fig. 2.14b)**. By day 14 of co-housing, the CBBP mice reached similar levels of unique ASVs as the ARM **(Fig. 2.14c)**. Additionally, Shannon diversity was no longer significantly different between the two groups **(Fig. 2.14d)**. Although BpSCSK was more abundant than in ARM, the average relative abundance of BpSCSK decreased from 41% at day 0 to approximately 18% by day 10 and 14 **(Fig. 2.14b)**. Importantly, metabolomic profiling revealed that 5-aminovalerate and butyrate were detectable in CBBP-colonized mice by day 6 **(Fig. 2.15a)**. Furthermore, proline levels decreased over the two-week period. While primary and secondary bile acids fluctuated between mice, some mice were able to modify bile acids **(Fig. 2.15b)**. Thus, a microbiota developed in the presence of BpSCSK can restore diversity, including butyrate and 5-aminovalerate producers, consumers of proline, and bile acid modifiers.

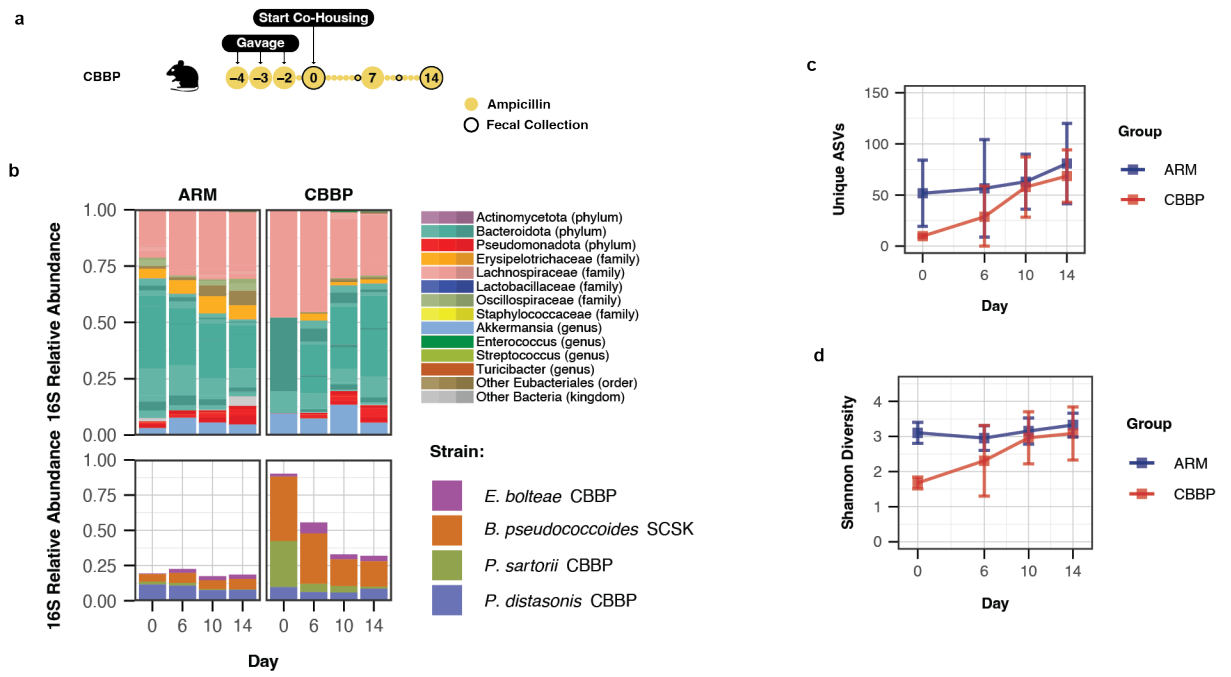

Figure 2.14: BpSCSK-resistant microbiota can restore gut diversity and key metabolite producers. a, Schematic of experimental groups and time points. 4 female C57BL/6 mice given CBBP (*Eubacteria bolteae* CBBP, *Phocaeicola sartorii* CBBP, *Blautia pseudococcoides* SCSK, and *Parabacteroides distasonis* CBBP) via oral gavage were co-housed with C57BL/6 MyD88-/- mice with an ampicillin resistant microbiota (ARM) for 2 weeks. Drinking water was supplemented with 0.5 g/L ampicillin throughout the experiment. **b,** Average fecal microbiota 16S rRNA gene relative abundance. ASVs with greater than >0.01% abundance are plotted. Specific ASVs found in the CBBP consortium are plotted below. **c,** Average number of unique ASVs detected. Error bars indicate 95% confidence intervals. **d,** Average Shannon diversity. Error bars indicate 95% confidence intervals.

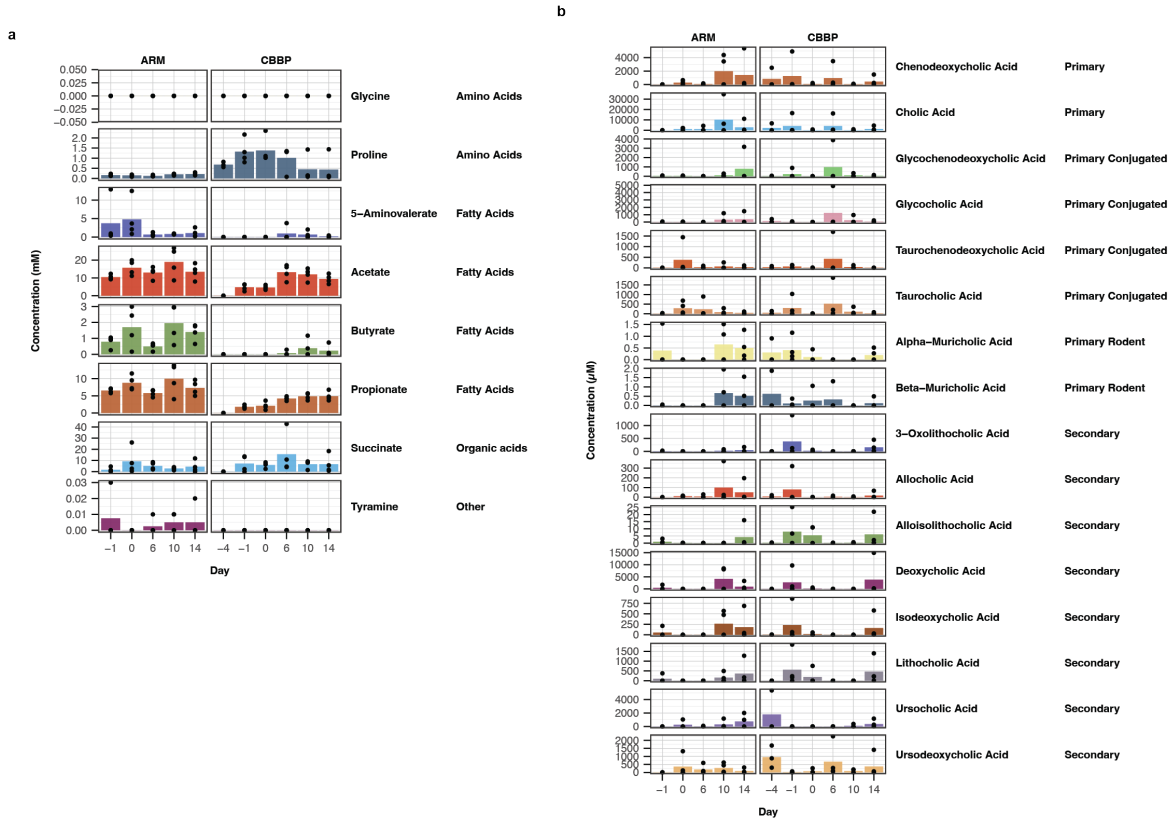

Figure 2.15: Metabolite concentrations after co-housing BpSCSK-colonized mice with ARM mice. a, b, Absolute concentrations of metabolites for mice from Figure 2.14. The bars represent the average concentration across the mice on each day. The dots are the individual values for each mouse.

2.8 Co-housing BpSCSK colonized mice with mice from different mouse vendor have mixed results on recolonization

In order to maintain consistency and reduce microbiota-driven differences between mouse experiments, all of our wild-type SPF mice were ordered from the same breeding room, AX8, at Jackson Laboratories. The gut commensals of mice from other breeding rooms may have different abilities at restoring diversity in BpSCSK-treated mice. To investigate, we individually co-housed Jackson Laboratories AX8 BpSCSK-treated mice with mice from the H47, K92, and R07 breeding rooms of Charles River and collected fecal pellets at day 0, 20, and 75 for 16S rRNA gene sequencing **(Fig. 2.16a)**.

For each of the three breeding rooms tested, the average relative abundance of BpSCSK decreased during co-housing **(Fig. 2.16b)**. On day 0, BpSCSK was greater than 75% of the average relative abundance for each group, but then decreased to approximately 25% by day 20. On day 75, BpSCSK-colonized mice cohoused with the H47 and K92 mice had less than 5% relative abundance of BpSCSK. However, BpSCSK-colonized mice with R07 mice still had an average relative abundance above 25%. All three groups regained butyrate production, but BpSCSK-colonized mice with R07 mice had the lowest butyrate production, which corresponded to its higher BpSCSK abundance **(Fig. 2.17a)**. In addition, the BpSCSK-colonized mice with R07 mice had elevated proline and glycine compared to the other groups. However, the natural R07 microbiota had high glycine. The bile acid profile appeared more similar between the nature microbiota and the BpSCSK colonized mice **(Fig. 2.17b)**.

While the microbiota from these mice appear to colonize better than the SPF microbiota from AX8 mice, the reduction in BpSCSK abundance happened gradually. A greater frequency in time points with a larger sample size would be needed to better understand the shift in BpSCSK.

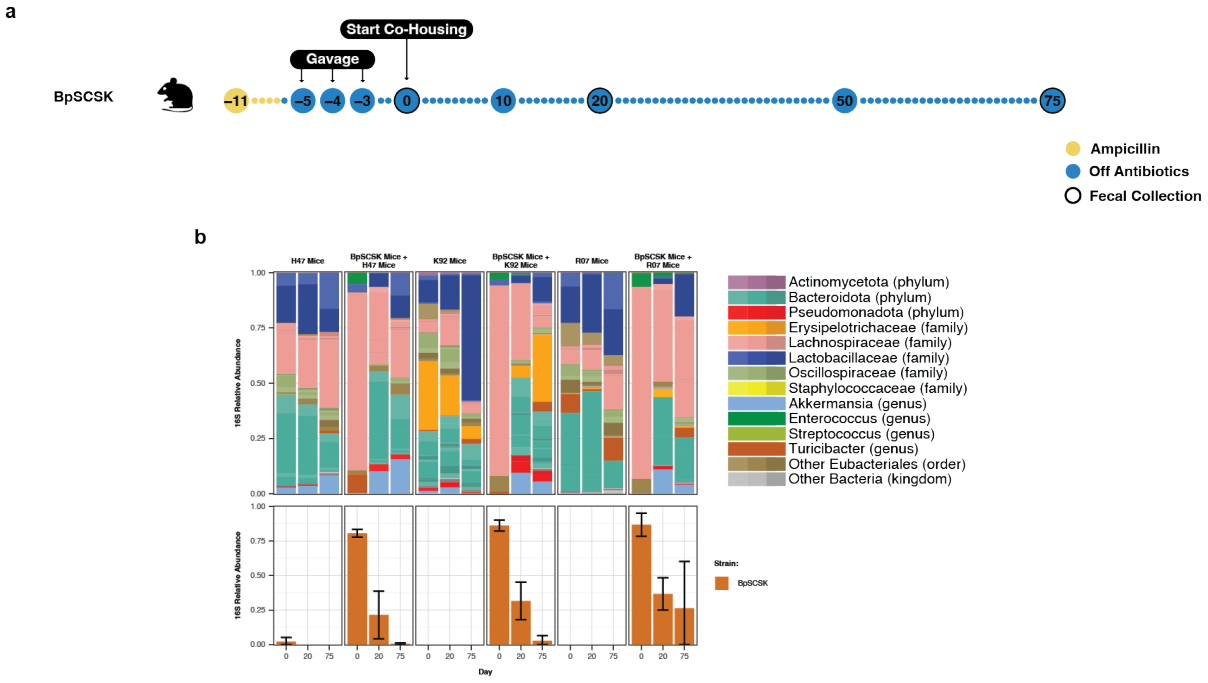

Figure 2.16: BpSCSK-colonized mice co-housed with mice from different mouse vendor. **a,** Schematic of experimental groups and time points. Female wild-type SPF C57BL/6 mice 9-10 weeks old from Jackson Laboratories were treated with ampicillin,colonized with BpSCSK, and co-housed individually with mice from different breeding rooms of Charles River. Fecal samples were collected at indicated timepoints. Each group contains 2 mice. **b,** Average fecal microbiota 16S rRNA gene relative abundance. ASVs with greater than >0.01% abundance are plotted. Specific ASVs for BpSCSK are plotted below. Error bars indicate standard deviation.

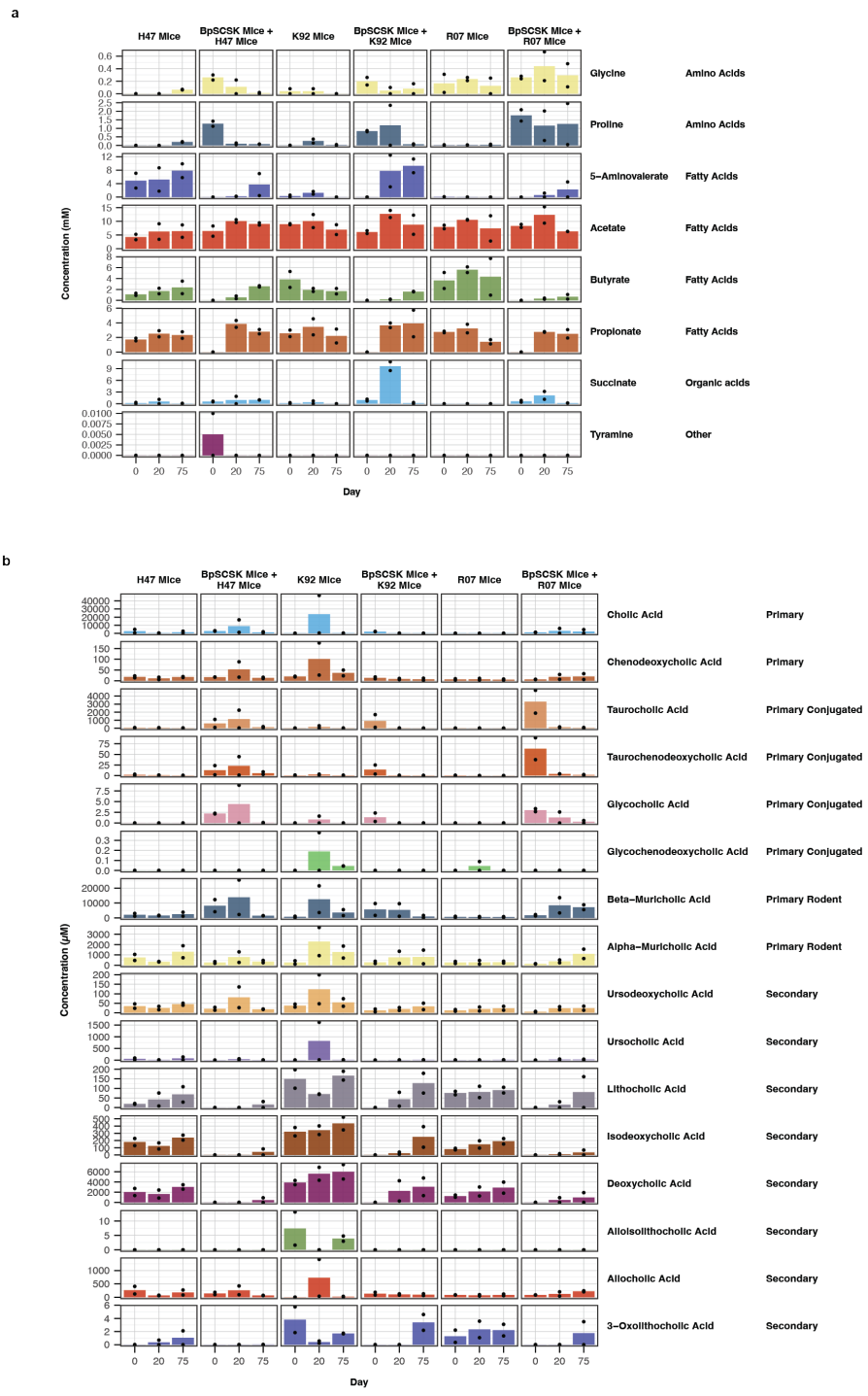

Figure 2.17: Metabolite concentrations after co-housing BpSCSK-colonized mice with mice from different vendor. a, b, Absolute concentrations of metabolites for mice from Figure 2.16. The bars represent the average concentration across the mice on each day. The dots are the individual values for each mouse.

CHAPTER 3

MURINE STUDIES ON LANTHIPEPTIDE IMPACTS ON INFECTION AND DISEASE SUSCEPTIBILITY

3.1 Mice colonized with BpSCSK are susceptible to *K. pneumoniae* infection

Lantibiotics typically have antibiotic activity against Gram-positive bacteria but are less effective against Gram-negative bacteria due to their outer membrane. Furthermore, butyrate depletion in the lower GI tract has been associated with increased oxygen concentrations at the epithelial barrier, which can provide facultative anaerobes with a growth advantage [Lee et al., 2024]. Therefore, we tested the susceptibility of BpSCSK-colonized mice to intestinal colonization with *Klebsiella pneumoniae* MH258, a multi-drug resistant strain originally isolated from the blood of a patient undergoing cancer treatment [Xiong et al., 2015].

Mice pre-treated with ampicillin and gavaged with PBS or BpSCSK were challenged 34 days later by gavage with 1000 colony-forming units (CFUs) of *K. pneumoniae* MH258 **(Fig. 3.1a)**. For the positive control, SPF mice were treated for 4 days with ampicillin starting 6 days prior to challenge. Based on 16S rRNA gene sequencing and CFUs for *K. pneumoniae* MH258, BpSCSK-colonized mice were more susceptible to *K. pneumoniae* MH258 colonization than PBS-treated mice **(Fig. 3.1b)**. Importantly, although SPF + ampicillin-treated mice had greater relative abundance and CFUs of *K. pneumoniae* MH258 at day 1, BpSCSK-treated mice consistently maintained greater than 1 x 10^8 CFU per gram of feces at day 1, 3, and 7 post infection **(Fig. 3.1c)**. In contrast, SPF + ampicillin-treated mice had reduced *K. pneumoniae* MH258 CFUs by day 3 that further decreased 7 days post infection.

Over the seven days of *K. pneumoniae* colonization, the metabolite concentrations of BpSCSK-treated mice remained similar to the starting concentrations before the infection

(Fig. 3.2a and 3.2b). Thus, it seems that *K. pneumoniae* has little to no impact on the metabolite production and consumption of the tested metabolites, despite the consistent colonization throughout the infection.

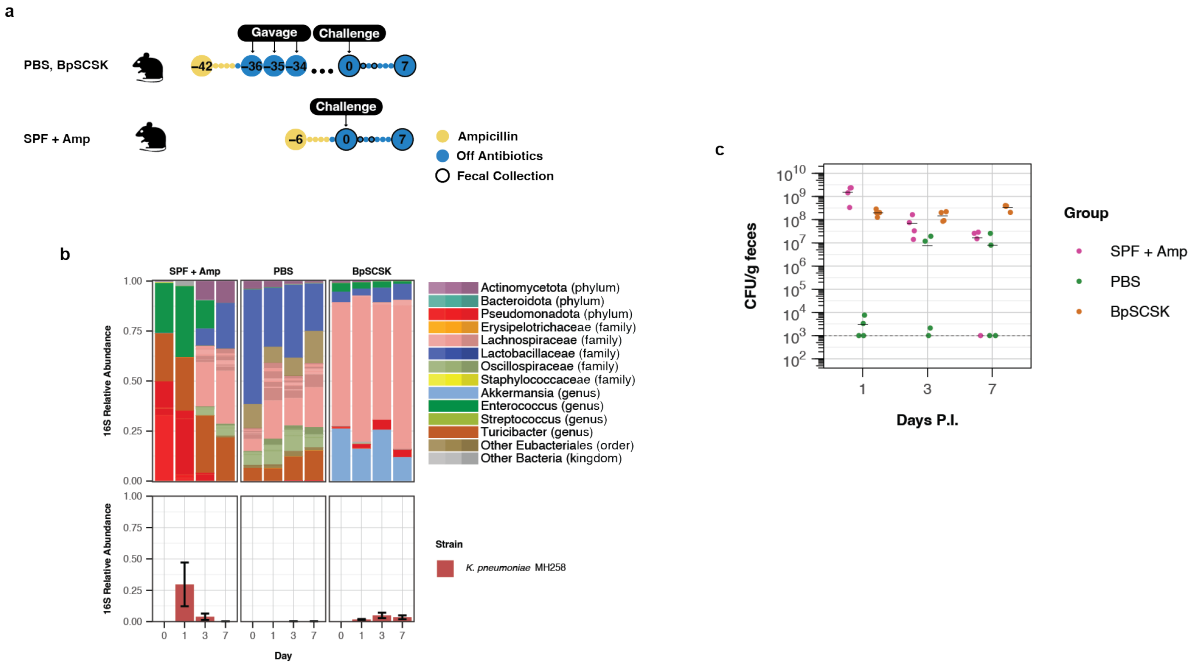

Figure 3.1: Mice colonized with BpSCSK are susceptible to *K. pneumoniae* infection. a, Schematic of experimental groups and time points. Female wild-type SPF C57BL/6 mice 9-10 weeks old were treated with 0.5 g/L ampicillin (Amp) in their drinking water for 4 days and given PBS or BpSCSK via oral gavage. On day 0, mice were challenged with approximately 1000 CFU of *K. pneumoniae* MH258 via oral gavage. The SPF + Amp group was treated with antibiotics just before *K. pneumoniae* challenge. Fecal samples were collected at indicated time points. Each group contained 4 mice. **b,** Average fecal microbiota 16S rRNA gene relative abundance. ASVs with greater than >0.01% abundance are plotted. Specific ASVs for *K. pneumoniae* MH258 are plotted below. Error bars indicate standard deviation. **c,** Colony-forming units (CFU) for *K. pneumoniae* MH258 post infection (P.I.). Black bars indicate the mean. Dashed line indicates the limit of detection.

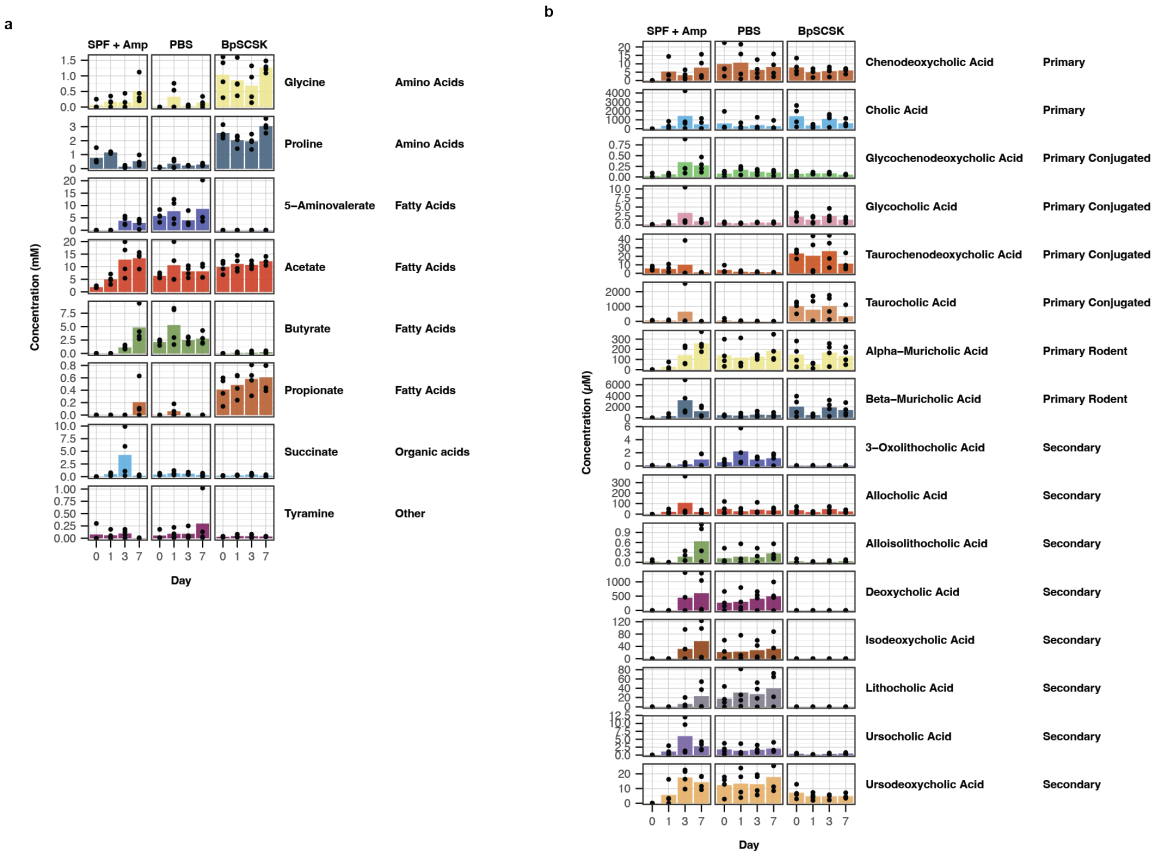

Figure 3.2: Metabolite concentrations of BpSCSK-colonized mice challenged with *K. pneumoniae*. a, b, Absolute concentrations of metabolites for mice challenged with *K. pneumoniae* from Figure 3.1. The bars represent the average concentration across the mice on each day. The dots are the individual values for each mouse.

3.2 Mice colonized with BpSCSK are susceptible to *C. difficile* infection

In addition to altered host responses to microbiota derived metabolites such as reduced hypoxia, some metabolites enhance host defenses against gut pathogens. Taurocholic acid, for example, induces germination in *Clostridioides difficile* while secondary bile acids and SCFAs can inhibit germination and vegetative growth [Abt et al., 2016]. *C. difficile* uses proline and glycine, which is often consumed by gut commensals, as reductive substrates to carry out Stickland fermentation for energy production and growth [Johnstone and Self, 2022]. *In vitro* minimum inhibitory concentration (MIC) testing of blauticin by Zhang et al. demonstrated that *C. difficile* VPI10463 had a higher MIC compared to some other gut commensals [Zhang et al., 2024b]. Together, the high concentrations of taurocholic acid, proline, and glycine combined with the low concentrations of butyrate and secondary bile acids in BpSCSK-colonized mice and potential resistance to concentrations of blauticin in the gut suggest that BpSCSK may maintain a permissive environment for *C. difficile* infection weeks after antibiotic treatment.

Infection and disease susceptibility were tested by challenging mice with *C. difficile* R20291 28 days following oral gavage of PBS or BpSCSK. Fecal samples were collected and sequenced 0, 1, and 7 days post infection **(Fig. 3.3a)**. SPF mice given an antibiotic cocktail of neomycin, metronidazole, vancomycin, and clindamycin (NMVC) to deplete most of the native microbiota prior to the challenge served as a positive control for infection. Although 16S rRNA gene sequences for *C. difficile* could be detected in some mice from all groups by day 7 post infection, all mice in the SPF + NMVC and BpSCSK-treated groups were colonized by *C. difficile* **(Fig. 3.3b)**. This was further supported by quantifying the CFUs of *C. difficile* R20291 in the fecal pellets **(Fig. 3.3c)**. Interestingly, over the 8 days that mouse weight was monitored post infection, BpSCSK-colonized mice showed similar weight loss to the positive control mice relative to the starting weight when challenged **(Fig. 3.3d)**.

On average, PBS-treated mice had less than a 5% loss from their initial weight. Consistent with proline and glycine reductase mediated Stickland fermentation in *C. difficile* R20291, SPF + NVMC and BpSCSK-treated mice exhibited decreased proline and glycine upon *C. difficile* R20291 infection **(Fig. 3.4a)**. Additionally, the concentration of 5-aminovalerate, the by-product of Stickland fermentation with proline, was increased.

These findings indicate that BpSCSK-colonized mice are vulnerable to colonization by pathogens like *K. pneumoniae* and *C. difficile*, remaining susceptible for months after cessation of antibiotic treatment.

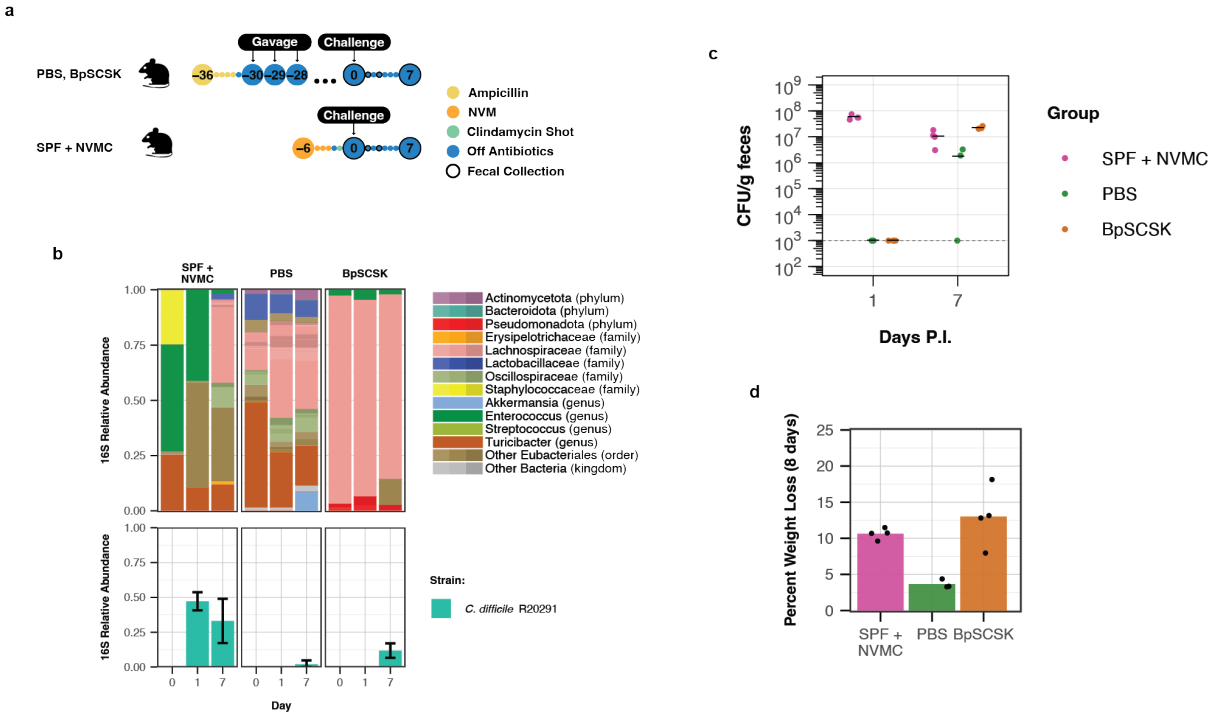

Figure 3.3: Mice colonized with BpSCSK are susceptible to *C. difficile* infection. **a,** Schematic of experimental groups and time points. Female wild-type SPF C57BL/6 mice 9-10 weeks old were treated with 0.5 g/L Ampicillin (Amp) in their drinking water for 4 days and given PBS or BpSCSK via oral gavage. Positive control mice were treated with neomycin, vancomycin, and metronidazole in the drinking water followed by an intraperitoneal injection of clindamycin. On day 0, mice were challenged with approximately 200 *Clostridioides difficile* R20291 spores via oral gavage. Fecal samples were collected at indicated time points. Each group contains 3-4 mice. **b,** Average fecal microbiota 16S rRNA gene relative abundance. ASVs with greater than >0.01% abundance are plotted. Specific ASVs for *C. difficile* R20291 are plotted below. Error bars indicate standard deviation. **c,** Colony-forming units (CFU) for *C. difficile* R20291 post infection (P.I.). Black bars indicate the mean. Dashed line indicates the limit of detection. **d,** Average maximum percentage of weight loss that mice experienced over the 8 days mice were monitored starting at day 0 P.I. Each dot represents an individual mouse.

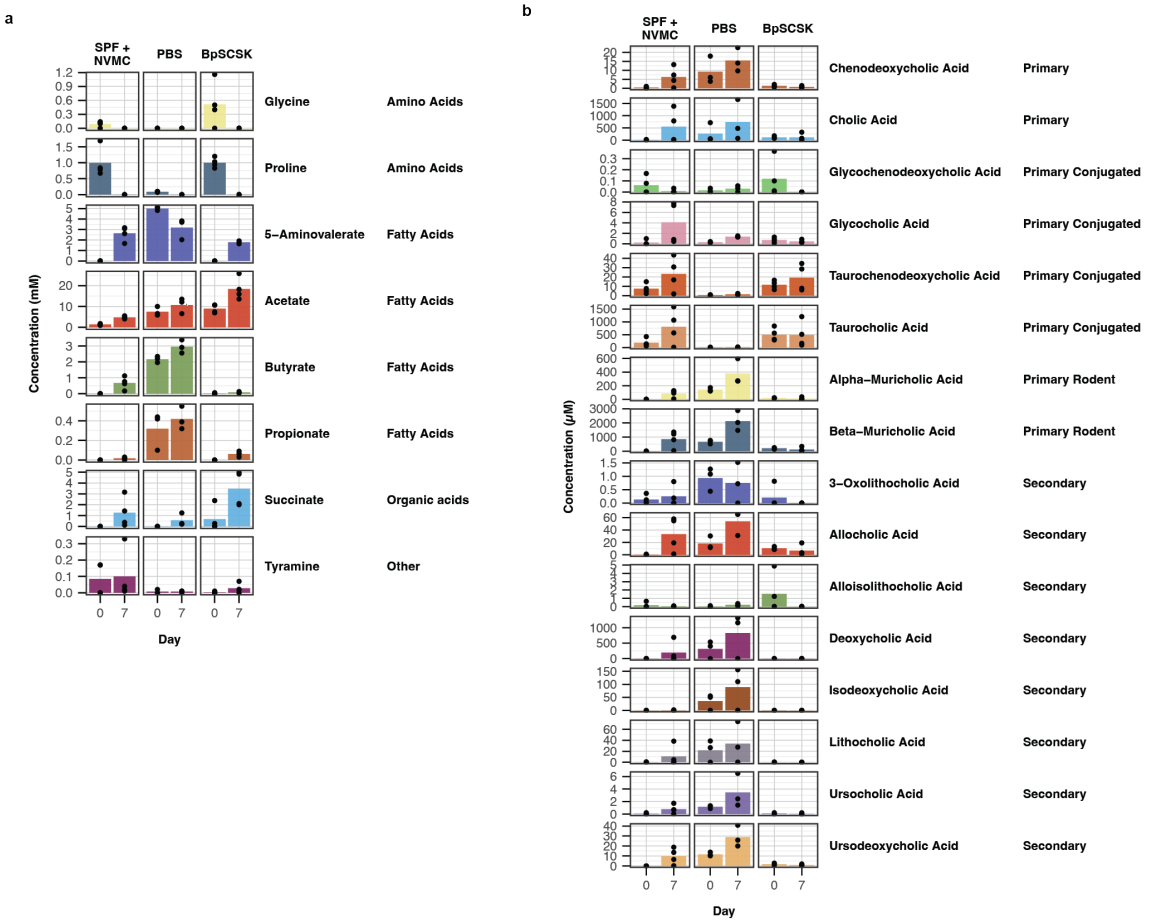

Figure 3.4: Metabolite concentrations BpSCSK-colonized mice challenged with *C. difficile*. **a, b,** Absolute concentrations of metabolites for mice challenged with *C. difficile* from Figure 3.3. The bars represent the average concentration across the mice on each day. The dots are the individual values for each mouse.

3.3 BpSCSK transmission between mice

During mouse experiments involving BpSCSK, mice that were treated with ampicillin followed by oral gavage of PBS or BpKH6 would occasionally get contaminated with BpSCSK **(Fig. 3.5a)**. In one experiment, for example, two mice in the PBS group and one mouse in the BpKH6 group were each contaminated with BpSCSK at different timepoints despite decontaminating the biosafety cabinet between each group before continuing with the next group **(Fig. 3.5b)**. Surprisingly, while BpSCSK was not able to colonize an SPF mouse, it was able to colonize an ampicillin treated mouse with a partially recovered microbiota as late as 13 days after ampicillin treatment had stopped. As with mice gavaged with BpSCSK, BpSCSK colonization in contaminated mice led to high abundance with few other species able to co-colonize. Furhtermore, the number of unique ASVs and α-diversity in contaminated mice began to drop to similar levels seen in the BpSCSK-colonized group **(Fig. 3.5c and 3.5d)**. Thus, BpSCSK is able to colonize a microbiota in an intermediate stage of recolonization post-antibiotic treatment and inhibit the growth of bacteria that had already begun to recolonize.

As BpSCSK quickly reached approximately 50% of the relative abundance of these mice, the metabolomic profile began to look similar to mice that received BpSCSK from the start **(Fig. 3.6a and 3.6b)**. Butyrate was soon diminished in these mice, and primary bile acids began to accumulate. This indicates that although the microbiota had already recovered some of its metabolite producers after ampicillin was removed from the drinking water, BpSCSK was able to inhibit their growth and restore the dysbiotic metabolomic profile.

At the time of these experiments, it was unknown to us that BpSCSK, like *C. difficile* forms spores. As a result, we were using a chlorine dioxide-based disinfectant (C-dox) provided by the University of Chicago animal facility to clean our biosafety cabinet. C-dox is known for not being strong enough to kill some spore-forming bacteria, which is why 10% bleach solution is recommended when working with bacteria like *C. difficile*. Once

we switched over to using bleach as our primary disinfectant, BpSCSK contamination was no longer an issue in mouse experiments. These findings suggest that BpSCSK, and other broad-spectrum lantibiotic-producers, may have several days after antibiotic treatment to colonize and dominate a gut microbiota. Additionally, the contamination and transmission we observed was likely the result of a few spores transferring between the mice, a transmission mechanism similar to *C. difficile* in the hospital settings.

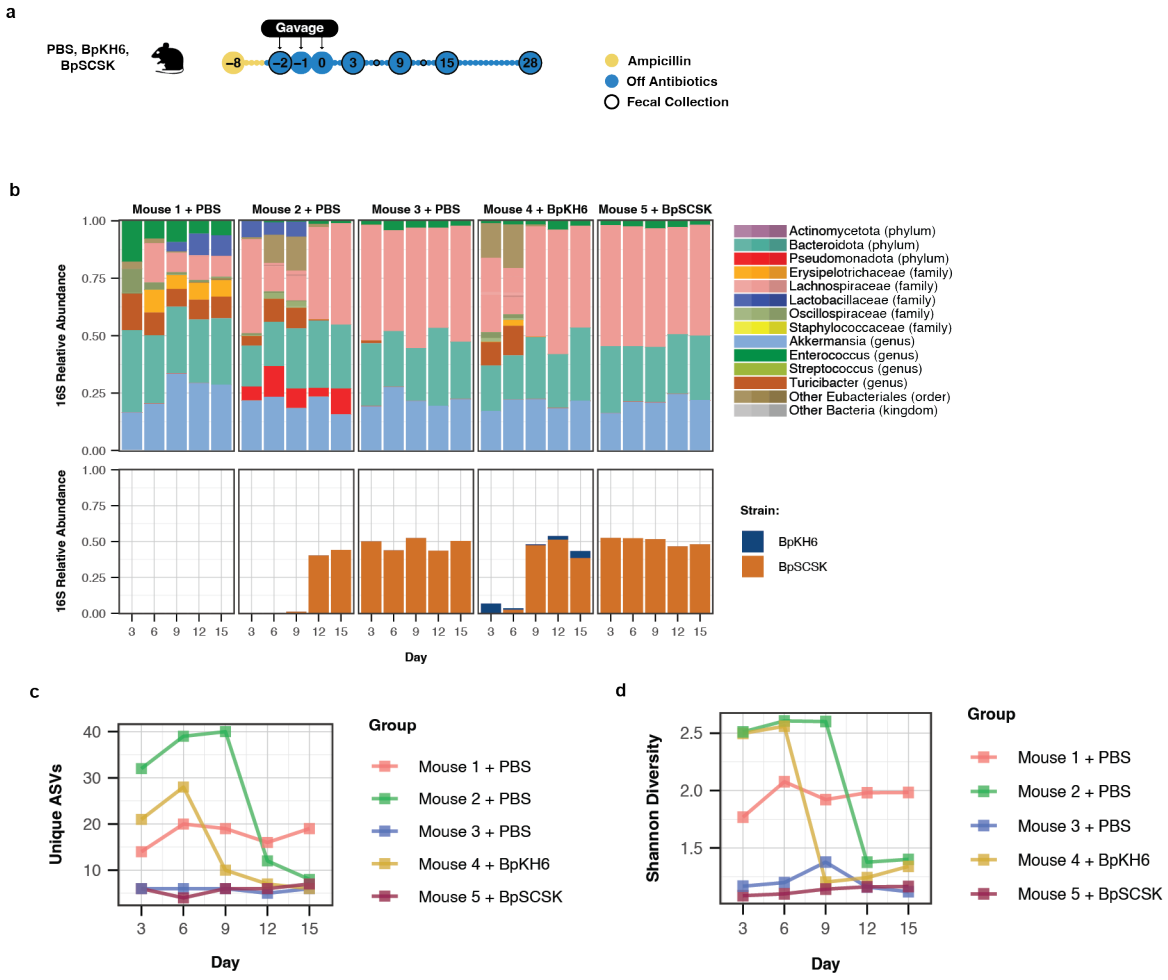

Figure 3.5: BpSCSK transmission between mice. a, Schematic of experimental groups and time points. Female wild-type SPF C57BL/6 mice 9-10 weeks old were treated with 0.5 g/L Ampicillin (Amp) in their drinking water for 4 days and given PBS or BpSCSK via oral gavage. Fecal samples were collected at indicated time points. **b,** Individual fecal microbiota 16S rRNA gene relative abundance. ASVs with greater than >0.01% abundance are plotted. Specific ASVs for BpSCSK (orange) are plotted below. **c, d,** Absolute concentrations of metabolites for mice. The bars represent the average concentration across the mice on each day.

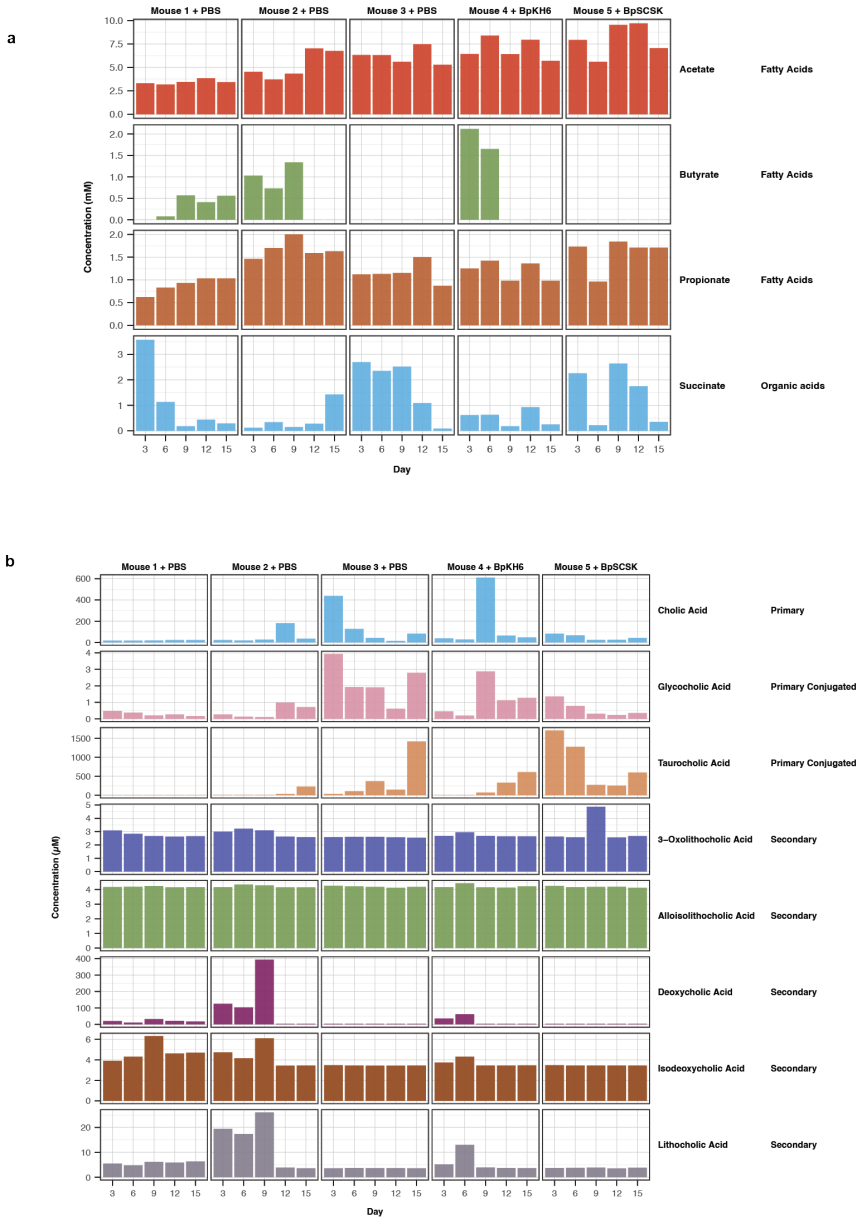

Figure 3.6: Metabolite concentrations of mice contaminated with BpSCSK. a, b, Absolute concentrations of metabolites for mice that were contaminated by BpSCSK at different timepoints from Figure 3.5. The bars represent the concentration for each mice on each day.

3.4 BpSCSK persistence in the gut microbiota

Like the ARM containing BpSCSK, we hypothesized that mice dominated with BpSCSK would eventually recolonize with bacteria that are either resist or tolerate the BpSCSK-mediated inhibition. Since we had only observed BpSCSK-treated mice up to 28 days, we decided to assess BpSCSK colonization for a longer duration. Mice were treated with ampicillin in drinking water and gavaged with the CBBP consortia that contains BpSCSK once a day for three days **(Fig. 3.7a)**. The mice were then monitored for a total of 90 days after the final gavage and fecal pellets were collected periodically throughout.

Even with the additional 60 days, BpSCSK and the other members of the CBBP consortia still dominated the gut with very little recolonization of other gut commensals **(Fig. 3.7b)**. On day 90, CBBP accounted for around 90% of the relative abundance, and BpSCSK had the greatest relative abundance among the mice. The primary genus that co-colonized the CBBP-treated mice during the 90-day period was *Akkermansia*, which is consistent with the previous observations of the other experiments. Therefore, BpSCSK appears to prolong dysbiosis for an extended period of time and likely leave mice more susceptible to infections well after antibiotic treatment is no longer administered. Further experiments extending beyond 90 days will be needed to fully understand recolonization.

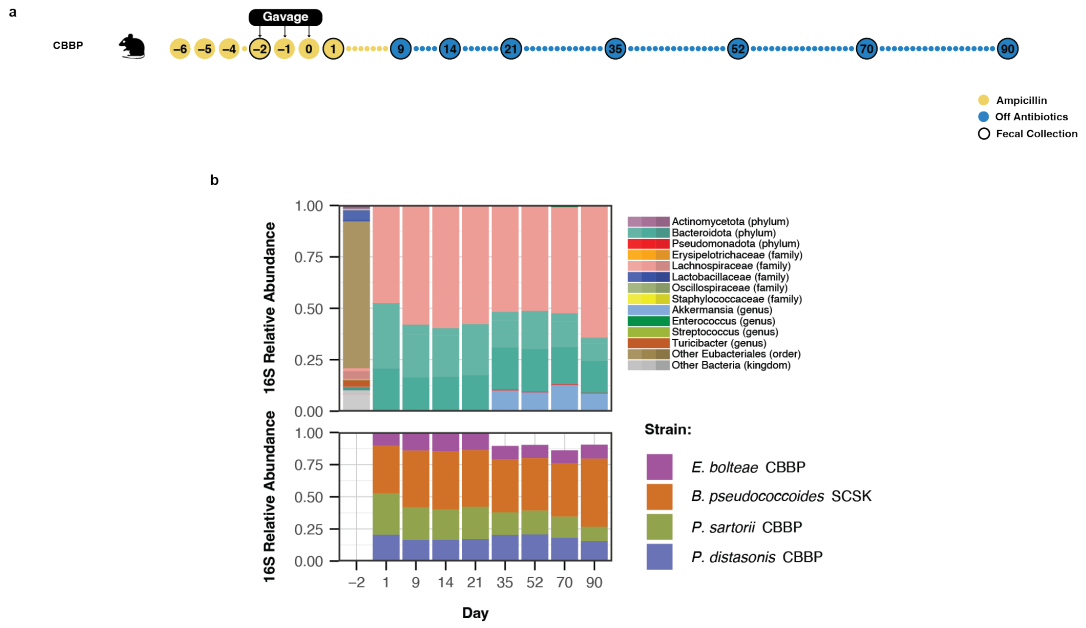

Figure 3.7: BpSCSK persistence in the gut microbiota. a, Schematic of experimental groups and time points. 4 female C57BL/6 mice were given CBBP (*Eubacteria bolteae* CBBP, *Phocaeicola sartorii* CBBP, *Blautia pseudococcoides* SCSK, and *Parabacteroides distasonis* CBBP) via oral gavage. Drinking water was supplemented with 0.5 g/L ampicillin until day 8. **b,** Average fecal microbiota 16S rRNA gene relative abundance. ASVs with greater than >0.01% abundance are plotted. Specific ASVs for the CBBP consortium are plotted below.

CHAPTER 4

LANTHIPEPTIDE GENES IN HUMAN MICROBIOMES

4.1 Lanthipeptides in isolates from healthy human donors

As part of an ongoing effort, the Duchossois Family Institute at the University of Chicago collects fecal samples from healthy human donors and has built a strain bank collection of over 1,600 isolates from these samples. Additionally, all isolates have been whole genome sequenced for genomic analysis. To determine whether any of these isolates contained lanthipeptides, all of the genomes were screened for lanthipeptides, biosynthesis genes, immunity genes, and lanthipeptide signaling genes.

Out of all the isolates screened, 66 isolates across 24 donors contained detectable *lanA* genes **(Table 4.1)**. Of these 66 isolates, 49 of them belonged to the family *Lachnospiraceae*, 7 belonged to *Bifidobacteriaceae*, 4 belonged to *Erysipelotricahaceae*, 2 belonged to *Streptococcaceae*. Other families that contained one isolate with lanthipeptide related genes were *Bacteroidaceae*, *Enterococcaceae*, and *Tissierellaceae*. Within *Lachnospiraceae*, *Blautia* was the most prevalent. The distribution of lanthipeptide genes in *Blautia* appear to vary, indicating that it is unlikely they are conserved at the genus or species level. Although some of the synthesis genes were not able to be detected, the *lanM* gene was detected in a total 21 isolates, while *lanC* was only found in 5 isolates. Therefore, it appears most of the lanthipeptide BGCs detected are for class II lanthipeptides.

This data confirms that lanthipeptide genes can be found throughout healthy donors. While more testing is needed to assess whether they have activity, their presence may have played a role in shaping the microbiota that they were isolated from, and they may contribute to the colonization resistance observed in a diverse microbiota.

Phylum	Class	Order	Family	Genus Species	Strain ID	Donor ID	lanA	lanB	lanC	lanM	lanKC	lanF	lanE	lanG	lanI	lanK	lanR	lanT	lanP
Actinomycetota	Actinobacteria	Bifidobacteriales	*Bifidobacteriaceae*	*Bifidobacterium longum*	DFI.4.163	DFI0004	1										1		
				Bifidobacterium longum	DFI.7.25	DFI0007	1										1		
				Bifidobacterium longum	MSK.13.5	FC0013	1										1		
				Bifidobacterium longum	MSK.19.27	FC0019	1										1		
				Bifidobacterium longum	MSK.7.30	FC0007	1										1		
				Bifidobacterium longum	MSK.8.8	FC0008	1										1		
				Bifidobacterium longum	DFI.2.45	DFI0002	1										1		
Bacillota	Bacilli	Lactobacillales	*Enterococcaceae*	*Enterococcus faecalis*	DFI.9.78	DFI0009	2			1							1		
			Streptococcaceae	*Lactococcus cremoris*	DFI.7.80	DFI0007	1	1	1			1	1		1	1	1	1	1
				Streptococcus oralis	DFI.7.26	DFI0007	1			1						1	1		1
Bacillota	Clostridia	Eubacteriales	*Lachnospiraceae*	*Anaerostipes hadrus*	MSK.14.9	FC0014	1					1	1	1	1	1	1		
				Blautia caecimuris	MSK.19.25	FC0019	1					2	2	2		1	1		
				Blautia faecis	DFI.1.205	DFI0001	2			1		1	1	1	1	2	2		
				Blautia faecis	DFI.3.67	DFI0003	1					1	1	1	1	1	1		
				Blautia faecis	DFI.9.7	DFI0009	1					1	1	1	1	1	1		
				Blautia faecis	MSK.11.45	FC0011	1					1	1	1	1	1	1		
				Blautia faecis	MSK.14.13	FC0014	4					2	2	2	1	1	1		
				Blautia faecis	MSK.17.74	FC0017	2					1	1	1	1	3	3		
				Blautia faecis	MSK.19.5	FC0019	1					1	1	1	1	2	2		
				Blautia glucerasea	DFI.3.54	DFI0003	1			1		2	2	2		3	3		
				Blautia glucerasea	DFI.5.14	DFI0005	1					1	1	1		2	2		
				Blautia glucerasea	DFI.6.21	DFI0006	1					1	1	1	1	1	1		
				Blautia hansenii	MSK.15.26	FC0015	3					2	1	1		2	2		
				Blautia luti	DFI.1.216	DFI0001	4			1		1	1	1	1	3	3		
				Blautia luti	DFI.3.45	DFI0003	1			1		3	3	3	1	2	2		
				Blautia luti	DFI.6.71	DFI0006	2			1		1	1	1	1	4	4		
				Blautia luti	MSK.15.26	FC0015	3					1	1	1	1	1	1		
				Blautia luti	MSK.20.44	FC0020	1			1		1	2	1	1	2	2		
				Blautia luti	MSK.22.56	FC0022	4			1		2	2	2	1	3	3		
				Blautia obeum	DFI.6.28	DFI0006	2												
				Blautia schinkii	DFI.6.59	DFI0006	2												
				Blautia schinkii	MSK.14.32	FC0014	3					2	1	1	2	3	3		
				Blautia schinkii	MSK.15.25	FC0015	3					2	2	1	2	3	3		
				Blautia wexlerae	DFI.4.9	DFI0004	4			1		1		1		1	1		
				Blautia wexlerae	DFI.5.15	DFI0005	2			1		2	2	2	1	4	4		
				Blautia wexlerae	DFI.6.104	DFI0006	2			1		1	1	1	1	4	4		
				Blautia wexlerae	MSK.15.15	FC0015	4					3	2	3	1	3	4		
				Blautia wexlerae	MSK.18.71	FC0018	1			1		2	2	1	1	3	3		
				Coprococcus comes	DFI.6.81	DFI0006	2					1	1	1		2	3		
				Dorea longicatena	DFI.6.91	DFI0006	1			1		1	1	1		3	4		
				Dorea longicatena	DFI.7.43	DFI0007	1					1	1	1		3	3	1	
				Dorea longicatena	DFI.9.58	DFI0009	1					1	1	1		2	2		
				Frisingicoccus caecimuris	DFI.3.63R	DFI0003	1					1	1	1		1	1		
				Lachnoclostridium hylemonae	SL.3.14	SL0003	1			1		1	1	1		2	2		
				Lachnoclostridium scindens	DFI.1.130	DFI0001	1			1		2	1	2		3	3		
				Lachnoclostridium scindens	DFI.5.44	DFI0005	1					2	1	1		3	3		
				Lachnospiraceae sp.	DFI.4.71	DFI0004	2					1	1	1		2	2	1	
				Lachnospiraceae sp.	DFI.5.19	DFI0005	1					2	1	1		3	3		
				Lactonifactor longoviformis	SL.2.30	SL0002	1	1	2			2	2	2		5	5	1	
				Mediterranebacter faecis	DFI.4.12	DFI0004	2					1	1	1		2	2	1	
				Mediterranebacter gnavus	MSK.11.9	FC0011	2		1			1	1	1		3	3		
				Mediterranebacter gnavus	MSK.15.54	FC0015	5			1		1	1	1		4	4		
				Mediterranebacter gnavus	MSK.23.63	FC0023	2			1		2	2	2		3	3		
				Mediterranebacter gnavus	SL.2.31	SL0002	3			1									
				unclassified	DFI.1.159	DFI0001	2			1		1	1	1	1	2	2		
				unclassified	DFI.5.30	DFI0005	1					1	1	1		3	3		
				unclassified	DFI.6.14	DFI0006	2												
				unclassified	MSK.13.4	FC0013	2	1				2	2	2	1	5	4		
				unclassified	MSK.16.77	FC0016	3					1	1	1	1	1	1		
				unclassified	MSK.18.27	FC0018	1					1	1	1	1	3	3		
Bacillota	Erysipelotrichia	Erysipelotrichales	*Erysipelotrichaceae*	*Erysipelatoclostridium ramosum*	DFI.2.15	DFI0002	1									1	1		
				Erysipelatoclostridium ramosum	MSK.14.25	FC0014	1									1	1		
				Erysipelatoclostridium ramosum	MSK.15.3	FC0015	1									1	1		
				unclassified	MSK.15.16	FC0015	1	1	1									1	
Bacillota	Tissierellia	Tissierellales	*Tissierellaceae*	*Tissierella carlieri*	DFI.7.95	DFI0007	1		1	1		1				3	3		
Bacteroidota	Bacteroidia	Bacteroidales	*Bacteroidaceae*	unclassified	MSK.18.37	MSK0018	1												

Table 4.1: Lanthipeptide genes in healthy human donor isolates. Isolates from healthy human donors that contained at least one *lanA* gene in their genome. Numbers under genes indicate the number of times the gene was detected in the genome of the isolate.

4.2 Healthy human and clinical patient cohorts

Patients hospitalized for respiratory failure, sepsis, or liver disease/transplantation are frequently treated with broad-spectrum antibiotics that disrupt the gut microbiota. Upon completion of antibiotic treatment, commensal bacterial species recolonize the gut at variable rates that are likely determined by the patient's environmental exposures and the composition of their residual microbiota. During the reconstitution phase, expression of lantibiotics by some strains may enhance their fitness in the gut lumen. We collected fecal samples from patients undergoing hospitalization for critical care, organ transplantation, and liver disease,

and subjected them to shotgun metagenomic sequencing as previously described [Odenwald et al., 2023, Lehmann et al., 2024, Stutz et al., 2022].

In total, there were 629 individuals comprised of 17 healthy donors and 612 clinical patients that provided fecal samples **(Table 4.2)**. The clinical patients were further divided depending whether they were receiving a heart transplant or liver transplant, treatment for liver disease, or admitted to the medical intensive care unit (MICU). Some patients spanned two or more of the cohorts throughout the course of their treatment. The amount individuals were sampled ranged from 1 to as much as 21 times resulting in 1872 samples overall.

During treatment, the hospitalized patients were prescribed various antibiotics to prevent or eliminate infections. Antibiotics can have varying effects on the gut microbiota depending on the type of antibiotic and the route it was administered. For example, antibiotics administered to the eyes or given topically will likely have little to no impact on gut commensals. Vancomycin was by far the most prevalent antibiotic used **(Fig. 4.1a)**. It was administered more than double the second most prescribed antibiotic, cefazolin. However, intravenous injection of vancomycin has markedly reduced impact on the gut microbiota compared to other routes such as oral administration. For simplicity, nasogastric/orogastric, gastrostomy, Dobhoff, and jejunostomy tubes are considered oral routes.

As expected based on antibiotic usage, the α-diversity of the hospitalized patients was typically lower than the healthy donors **(Fig. 4.2a)**. The heart transplant patients, however, were the closest to healthy donor levels of α-diversity. For the change in diversity between the first sample collected and the last sample collected for patients that provided two or more samples, most of the patients had a reduction in α-diversity over the course of their hospital visits **(Fig. 4.2b)**. Out of of the 405 patients with two or more samples, 263 had a lower Inverse Simpson index between their first and last visit.

Group	1x	2x	3x	4x	5x	6x	7x	8x	9x	10x	11x	12x	13x	14x	15x	16x	17x	19x	21x	Patients
Healthy Donor	17	-	-	-	-	-	-	-	-	-	-	-	-	-	-	-	-	-	-	17
Heart Transplant	5	8	9	6	9	7	4	6	1	-	1	-	-	-	-	-	1	-	1	58
Heart Transplant/Liver Disease	-	-	-	-	-	-	-	-	-	-	-	-	-	-	1	-	-	-	-	1
Heart Transplant/Liver Disease/Liver Transplant	-	-	-	-	-	-	-	1	-	-	-	1	-	-	-	-	-	-	-	2
Heart Transplant/Liver Transplant	2	1	-	-	-	-	1	-	-	-	-	1	-	-	-	-	1	-	-	6
Liver Disease	58	43	10	11	10	3	1	5	4	-	-	-	-	-	-	-	-	1	-	146
Liver Disease/Liver Transplant	4	7	3	5	5	1	-	-	1	-	-	-	2	-	-	-	-	-	-	28
Liver Disease/Liver Transplant/MICU	-	-	-	-	-	-	-	1	-	-	-	-	1	-	-	-	-	-	-	2
Liver Disease/MICU	1	1	2	-	1	1	-	-	-	-	-	-	-	-	-	-	-	-	-	6
Liver Transplant	13	9	6	5	5	5	4	2	-	1	-	-	-	2	-	-	-	-	-	52
Liver Transplant/MICU	-	-	1	-	2	-	1	1	-	-	-	-	-	1	-	1	-	-	-	7
MICU	143	80	36	22	13	6	3	-	-	1	-	-	-	-	-	-	-	-	-	304
																			Total:	629

Table 4.2: Sample distribution of clinical patient and healthy human donors. Patients are split based on the cohorts they were in and number of times the patients were sampled.

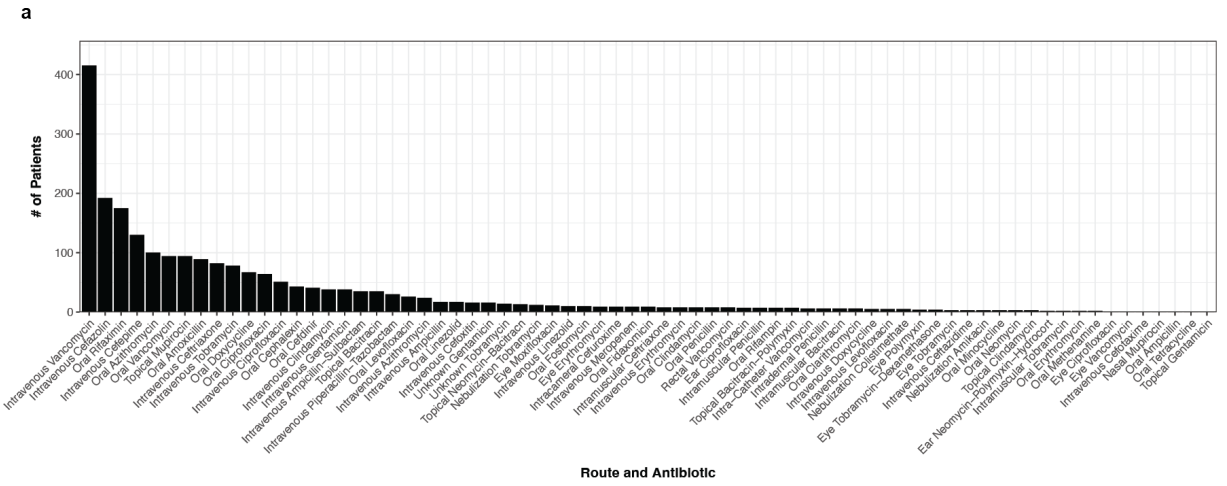

Figure 4.1: Antibiotic treatment regimens of clinical patients. a, The prescribed antibiotics given to patients over the course of their fecal sample collection, and the route that the antibiotic was administered.

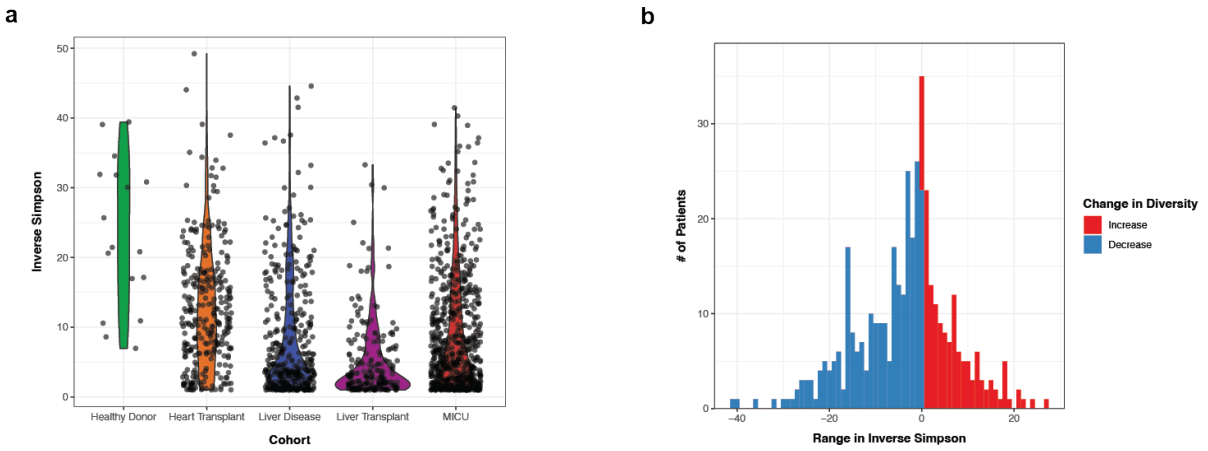

Figure 4.2: Diversity of clinical patient and healthy human donors. a, Inverse Simpson index of the four patient cohorts and healthy human donors. Only patients that belonged to a single cohort were included. **b,** Histogram of the ranges in Inverse Simpson index between the first sample and last fecal sample collected. Negative indicates a lower Inverse Simpson index than the start. Only patients with two or more samples were included.

4.3 Lanthipeptide genes identified in clinical patients

Using a combination of RODEO (Rapid ORF Description and Evaluation Online)[Tietz et al., 2017], previously identified lanthipeptide gene sequences, and specific lanthipeptide-associated Pfam domains [Walker et al., 2020, Paysan-Lafosse et al., 2025], we screened the 1872 fecal samples collected from the clinical patients and healthy donors for the presence of lanthipeptide genes associated with lanthipeptide BGCs.

Fecal microbiomes from 526 out of 612 hospitalized patients (~86%) contained at least one detectable lanthipeptide precursor encoding gene (*lanA*) **(Fig. 4.3a)**. Of the 1872 fecal samples screened, 71% contained at least one *lanA* gene, yielding 1015 unique lanthipeptide sequences. Lanthipeptide classes were determined on the basis of gene annotations, neighboring synthesis genes, or sequence similarity to known lanthipeptides. Although the classes of some lanthipeptides could not be determined, most of the *lanA* sequences detected belonged to class II lanthipeptides (640/1015) followed by class I (231/1015) and III (36/1015)

(Fig. 4.3b). All healthy donors contained at least one *lanA* sequence with 59 total unique sequences detected across the 17 healthy donor microbiomes.

Taxonomic classifications for *lanA* sequences were determined using NCBI BLAST on the contigs harboring *lanA* genes. Contigs that did not meet the inclusion thresholds or did not have any hits were labeled "Unclassified." Out of 5503 contigs, 3869 contigs were assigned a taxonomic classification. At the genus level, *Streptococcus*, *Blautia*, and *Mediterraneibacter* were the most prominent genera **(Fig. 4.3c)**. Most *lanA* sequences were predominantly detected in one species while some, such as lanA_1428 (RumB), lanA_1284, and lanA_338, were distributed across multiple species, suggesting they may have been acquired by horizontal gene transfer **(Fig. 4.3d)**. At the species level, *Blautia wexlerae* contained the most *lanA* sequences, followed by *Mediterraneibacter gnavus* and *Streptococcus thermophilus* **(Fig. 4.4a)**. *S. thermophilus* contained the most prevalent lanthipeptide, lanA_6, out of all the lanthipeptides detected **(Fig. 4.3d)**. It was detected in almost 200 of the 612 patients.

While *B. wexlerae* and *M. gnavus* are common human gut commensals, *S. thermophilus* is typically associated with fermented milk and is used in yogurt production. Other species with *lanA* genes that are commonly used as probiotics included *Bifidobacterium longum*, *Lactiplantabacillus plantarum*, *Lactococcus lactis*, *Ligilactobacillus salivarius*, and *Bifidobacterium breve* **(Fig. 4.4a and 4.4b)**. Most of the peptides were found in *S. thermophilus*, *B. longum*, and *L. lactis*, while *B. breve* and *L. plantarum* had much fewer lanthipeptides with only two class III and one class II lanthipeptide respectively. Lanthipeptides were also detected in oral microbiome associated bacteria such as *Streptococcus salivarious*, *Streptococcous parasanguinis*, *Streptococcos mutans*, and *Streptococcous pneumoniae* in addition to the nasal mucosal and dermal microbiome associated *Staphylococcus aureus* and *Staphylococcus epidermidis* **(Fig. 4.4a and 4.4c)**.

Whether bacterial strains encoding *lanA* genes impact microbiota composition, however, is unclear, since only a subset of lanthipeptides have been demonstrated to have antibacterial

activity and some encoded genes may not be transcribed in the gut. To determine whether lantibiotics provide a fitness advantage to bacterial species expressing them, we assessed the impact of the *lanA* genes in patient microbiomes by calculating the ratio of the average relative abundance of species with a *lanA* gene to the average relative abundance of the same species lacking the *lanA* gene. Since not all *lanA* contig taxonomic classifications could be matched to a species annotated by MetaPhlAn4[Blanco-Míguez et al., 2023] within a sequenced sample, only exact matches at the species level were considered. Moreover, only non-producing species and *lanA* genes that were present in at least 5 fecal samples were considered. Among the 1015 unique lanthipeptide sequences in patients, 102 sequences met the criteria for inclusion. We found that 80 out of the 102 lanthipeptide encoding strains had increased abundance compared to lanthipeptide lacking strains **(Fig. 4.5a)**. A UMAP of all the lanthipeptide sequences revealed that there was no clear clustering of lanthipeptides that provided a fitness advantage **(Fig. 4.5b)**. However, class I and class II lanthipeptides largely separated along the axis 2 of the UMAP.

Of the 1015 lanthipeptide sequences, 105 matched the core sequences of 33 previously characterized lanthipeptides. The most abundant were the two cytolysin L and S lanthipeptides associated with *Enterococcus faecalis***(Fig. 4.4c)**. Although exact matches to previously characterized lanthipeptides were detected, many of the peptides only shared the core sequence while encoding a different leader peptide. Unexpectedly, three of the lanthipeptides detected, lanA_605 (Blauticin-A1), lanA_623 (Blauticin-A5), and lanA_1622 (Blauticin-A6), were exact matches to the class I lantibiotic genes of BpSCSK. Only three patients, however, had at least one blauticin *lanA* gene, and only one of the patients had all three. Despite this, a variant of the BpSCSK may exist naturally in the human gut microbiota.

More work is needed to determine the overall impact lantibiotics may have on gut commensals and recolonization after antibiotic treatment. However, their presence in patients with varying degrees of dysbiosis indicate that they may have an important role. Like Bp-

SCSK, lantibiotic-producing bacteria could be prolonging dysbiosis in these patients.

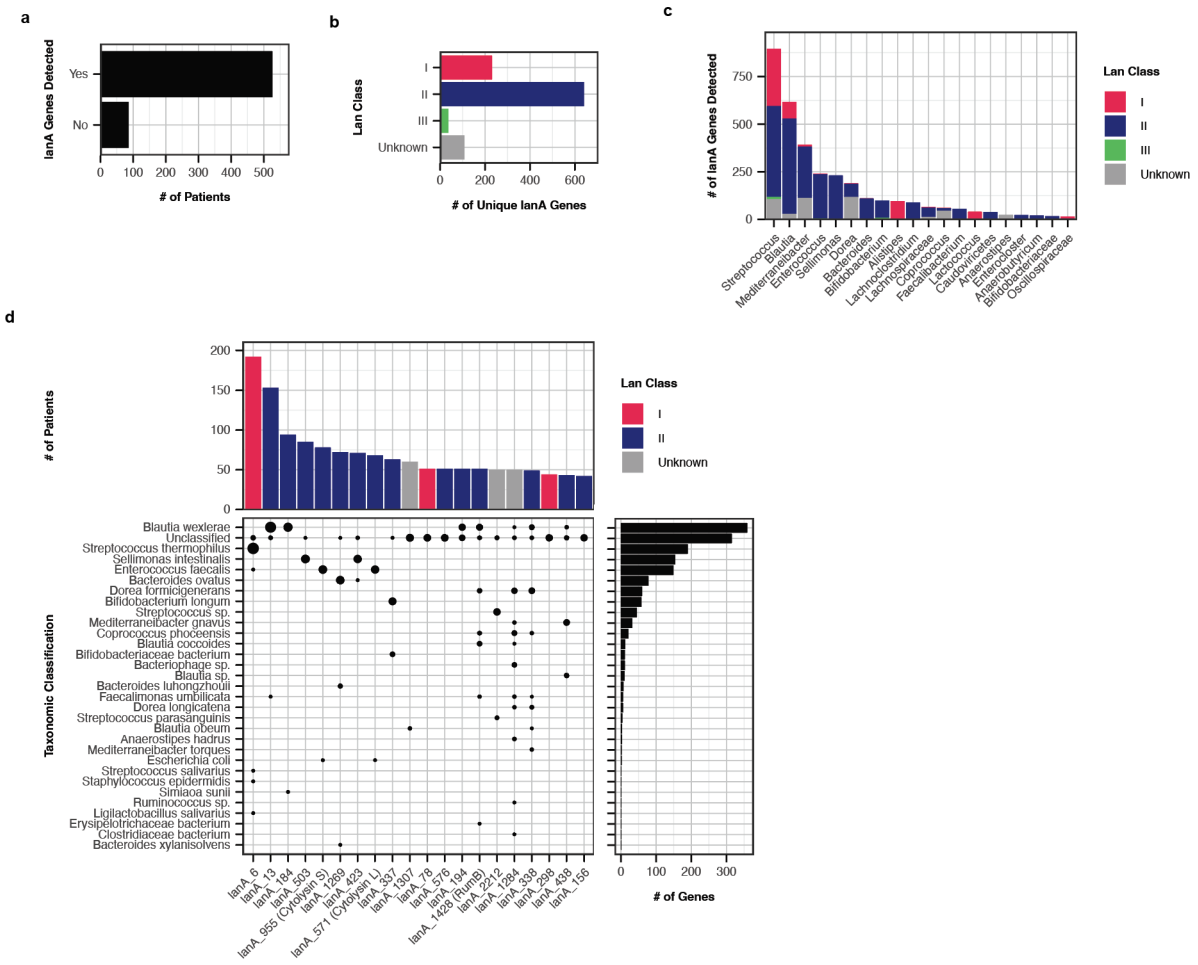

Figure 4.3: Lanthipeptide gene prevalence and diversity in patient microbiomes. A total of 1872 fecal samples were collected from 612 patients and screened for lanthipeptide genes. **a,** Patients that had a detectable lanthipeptide gene among fecal samples sequences. **b,** Lanthipeptide class distribution for unique lanthipeptides detected in patient samples (n = 1015). **c,** Distribution of detected lanthipeptide genes across the top 20 genera assigned to the encoding contig. **d,** Plot of the top 20 most abundant lanthipeptide genes. Vertical columns represent the number of times the lanthipeptide was detected. Horizontal bars represent the number of lanthipeptides were found in a given species. The dots represent the intersection between the two plots with the size of the dots representing the number of times a specific lanthipeptide was found in a specific species.

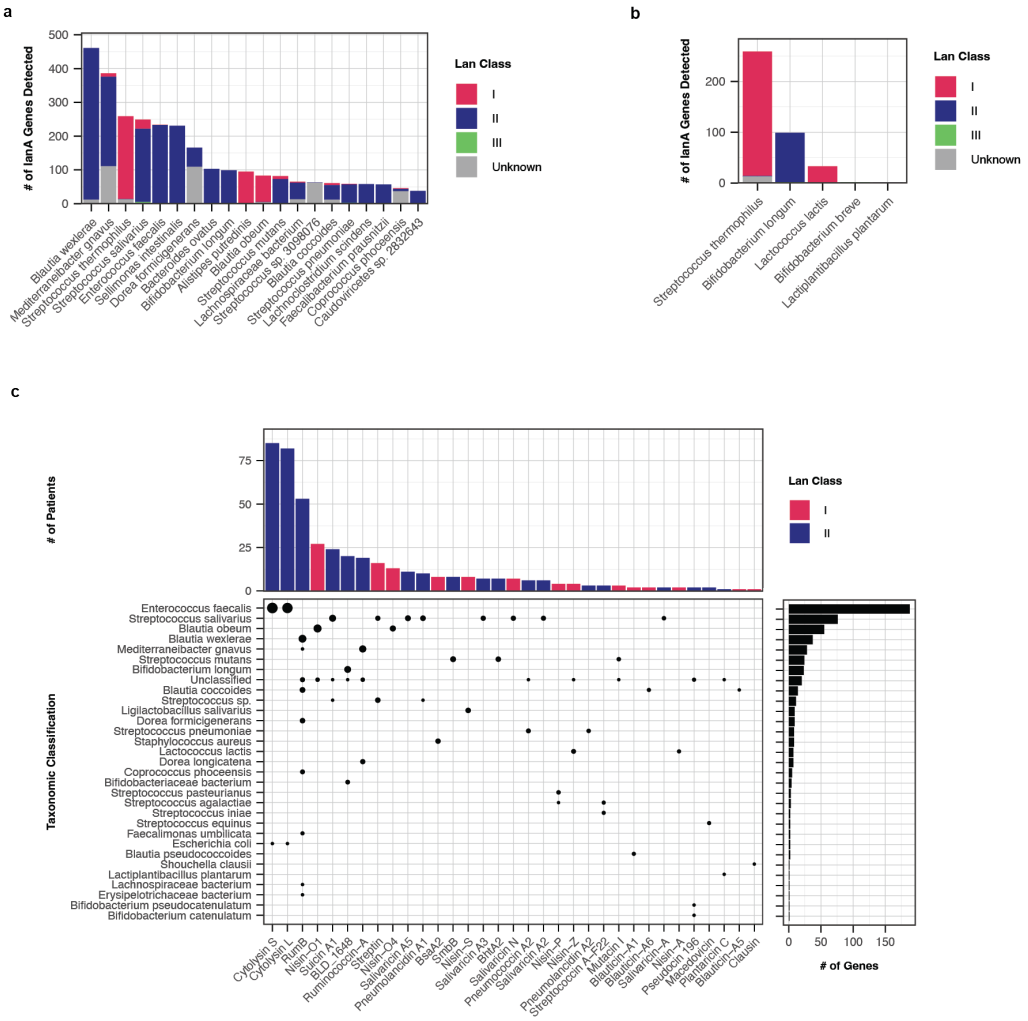

Figure 4.4: Species classification of lantibiotic-producers and previously characterized lanthipeptides in clinical patients. a, Distribution of detected lanthipeptide genes across the top 20 genera assigned to the encoding contig. **b,** Distribution of detected lanthipeptide genes across species commonly used as probiotics. **c,** Plot of the 32 previously characterized core lanthipeptide sequences detected. Vertical columns represent the number of times the lanthipeptide was detected. Horizontal bars represent the number of lanthipeptides found in each bacterial species. The dots represent the intersection between the two plots with the size of the dots representing the number of times a specific lanthipeptide was found in a specific species.

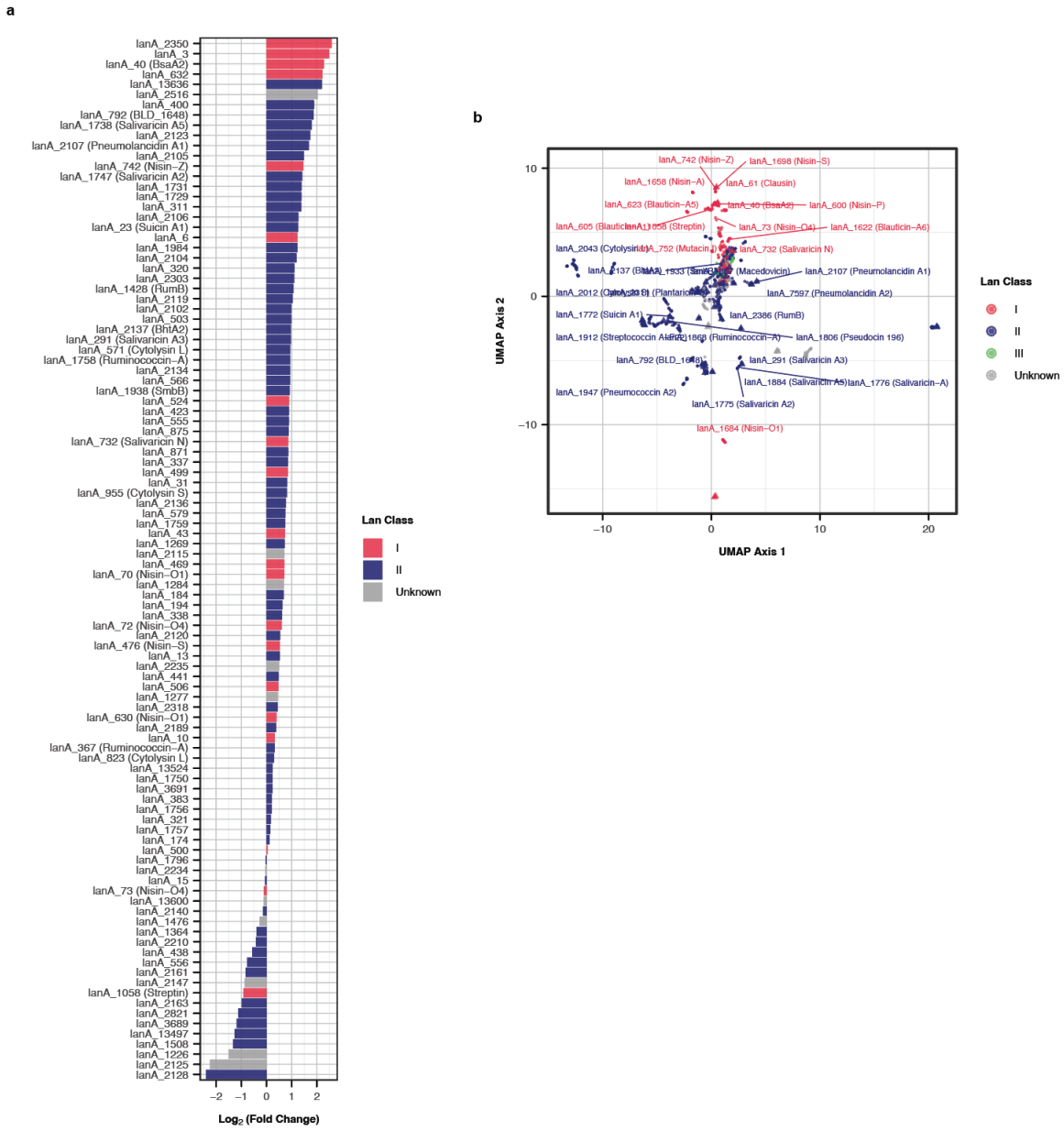

Figure 4.5: Fitness advantage of lanthipeptides in patient microbiomes. a, Fitness advantage of lanthipeptide genes calculated as the $\log_2$ fold change of the relative abundance of species with the lanthipeptide gene versus the relative abundance of the same species without the lanthipeptide gene. Only species that were found in at least 5 samples with and without the lanthipeptide gene were included. **b,** UMAP of all unique lanthipeptide genes detected across all samples. Triangles indicate lanthipeptide genes with a $\log_2$ fold change greater than 0. Previously published lanthipeptide core sequences that were a match to the identified lanthipeptide are specified in parentheses.

CHAPTER 5

DISCUSSION

5.1 Overview

The work outlined in this thesis demonstrates that BpSCSK, a strain of *Blautia* with a known class I lantibiotic-producing BGC, alters recolonization of the gut microbiota in mice with antibiotic-induced dysbiosis **(Fig. 5.1)**. As a result, important metabolites in the gut fail to return to concentrations observed in untreated SPF mice. While it is unknown how long this state can persist before diversity is restored, it appears that mice can remain dysbiotic for months after antibiotic treatment has stopped. Overcoming the strong barrier for colonization established by BpSCSK proved difficult as demonstrated by FMTs from SPF mice followed by co-housing was unable to restore diversity. However, recolonization seems to be microbiota dependent, since some commensals were better equipped at co-colonizing with BpSCSK. The SPF microbiota of mice from Charles River's breeding rooms proved better at restoring diversity, but none of the other methods were better than co-housing with mice that have the ARM, which already contains a blauticin producing strain of BpSCSK.

While there were no readily observable abnormalities in mice dominated with BpSCSK versus wild-type SPF mice and controls, the prolonged dysbiosis can have negative consequences for the host. BpSCSK-treated mice were just as susceptible to colonization by *K. pneumoniae* and *C. difficile* for a month as mice recently given antibiotics. While *K. pneumoniae* doesn't immediately cause disease, colonization can lead to increased chances of a systemic infection. In the case of *C. difficile* infection, BpSCSK-treated mice had similar weight loss, a hallmark symptom of *C. difficile* infection.

The prevalence of lanthipeptides in patient samples hint at the possibility that prolonged dysbiosis caused by lantibiotics could be occurring in people that undergo broad-spectrum antibiotic treatment. Lanthipeptide-producing bacteria appear to have a fitness advantage

over the same species lacking lanthipeptide genes. If one of them encode a broad-spectrum lantibiotic coupled with the ability to survive the harsh conditions outside the gut microbiome and easily transmit between people, it could lead to similar prolonged dysbiosis that was observed for BpSCSK. Interestingly, the blauticin *lanA* genes, as well as other well characterized lantibiotics, were detected among the patient samples, and the same lanthipeptide sequences could be detected across many patients. Unfortunately, infrequent sampling made it difficult to determine the impact they have on the microbiota.

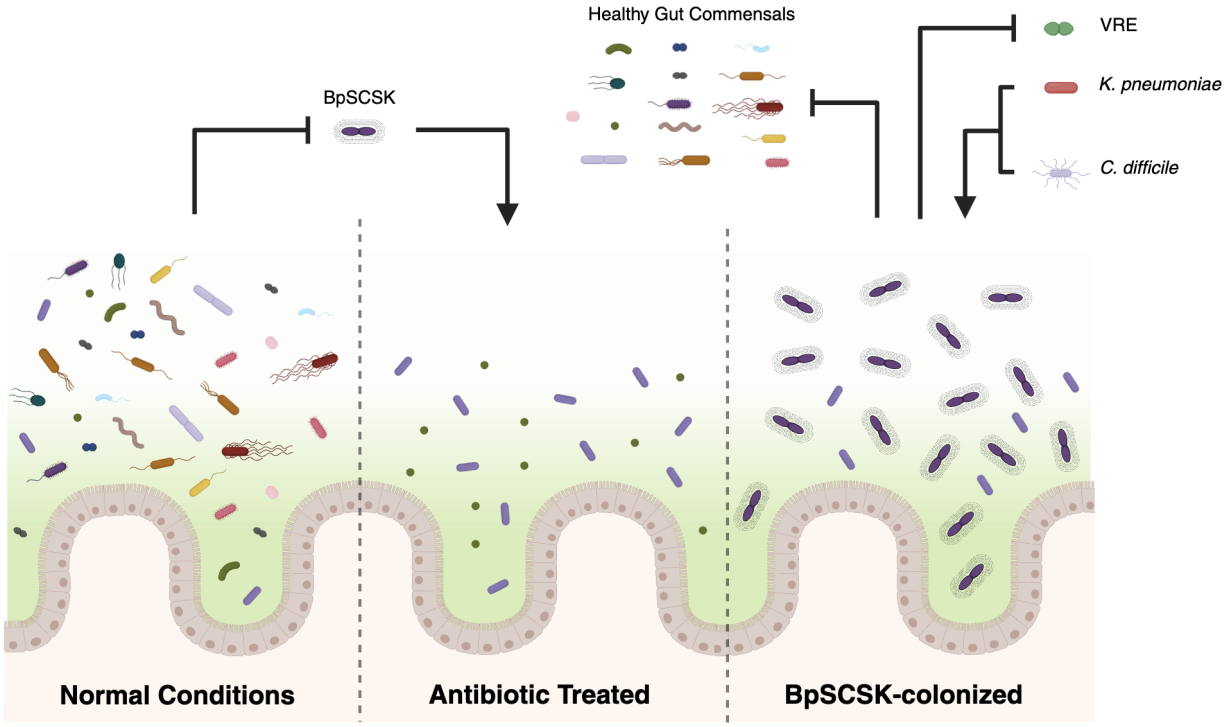

Figure 5.1: Overview of the impact of BpSCSK on the gut microbiome. BpSCSK is unable to colonize SPF mice under normal conditions with no antibiotic treatment. However, after treatment with antibiotics, BpSCSK is capable of colonizing which results in colonization resistant to healthy gut commensals. Although BpSCSK-colonized mice are resistant to VRE, they are susceptible to *K. pneumoniae* and *C. difficile* colonization.

5.2 Mechanisms of microbiome modulation by lantibiotic-producing bacteria

Previous studies demonstrated that BpSCSK culture supernatants inhibited Gram-positive but had poor activity against Gram-negative commensal bacterial strains [Kim et al., 2019]. Experiments performed by Zhang et al. with purified blauticin also support blauticin inhibition of Gram-positive gut commensals [Zhang et al., 2024b, 2023]. However, using an *in vivo* mouse model, the results described in this thesis demonstrate that many Gram-positive and Gram-negative commensal bacteria are suppressed by BpSCSK colonization in the GI tract. Thus, while direct inhibition by lantibiotics may serve as a major factor to colonization resistance, there are likely other factors contributing to indirect inhibition of bacteria that would otherwise be resistant to lantibiotics.

One possible mechanism in which indirect inhibition could be occurring is through the inhibition of keystone species, species that produce important metabolites or other products that are critical for the growth and support of neighboring bacteria. If, for example, there are bacteria that depend on a specific species in the microbiome to break down complex carbohydrates in the gut, then inhibiting the species responsible for carrying out that function would also inhibit the bacteria that depend on that carbohydrate source regardless of whether they are resistant to lantibiotics.

Inhibition of butyrate producers, in particular, can have many downstream consequences that result in indirect inhibition. Research by Lee et al. demonstrated that butyrate is used by epithelial cells as a major energy source in the GI tract via the Krebs cycle, and as a result, oxygen is consumed, reducing oxygen levels in the intestinal lumen [Lee et al., 2024]. Therefore, without butyrate producers, oxygen levels may rise to a level that inhibits any oxygen-sensitive commensal strains. This would have the additive effect of giving an advantage to facultative anaerobic bacteria, which may have been an important factor for colonization of *K. pneumoniae* in BpSCSK-treated mice.

Some bacteria also produce important anti-inflammatory products. In addition to the energy butyrate provides epithelial cells, it also can stimulate regulatory T-cell differentiation via the Foxp3 transcription factor [Iweala and Nagler, 2019]. Induced regulatory T-cells can also express RORγt, which is a transcription factor that modulates the T-helper 17 cells. Furthermore, butyrate has been shown to promote the production of IL-10, an anti-inflammatory cytokine, and it inhibits NF-κB, which dampens the pro-inflammatory cytokine IL-8 [Lee et al., 2017]. These properties of butyrate are important for maintaining barrier integrity, and any compromise in these areas can lead to inflammation in the gut that can impede bacterial growth of healthy gut commensals. It could also lead to greater risk of infection in the presence of pathobionts. Importantly, some lanthipeptides have been shown to directly have immune-regulatory properties [Staden et al., 2021].

Although some bacteria may have developed or contain natural resistance to lantibiotics, lantibiotics in the gut may work synergistically with other bacteriocins to inhibit bacteria. Whereas when acting alone, it does not have potent enough activity to cause inhibition. Gram-negative bacteria, for example, are generally resistant to lantibiotics due to their outer membrane layer, but if something were to disrupt the outer membrane permitting a lantibiotic to reach the inner membrane, then it may be more susceptible to inhibition. Host-derived antimicrobial peptides like LL-37 and defensins are another source of antimicrobials that could also potentially work synergistically with lantibiotics.

Lastly, inhibition could stem from directly from BpSCSK in a lantibiotic-independent manner. This is an especially important consideration since BpSCSK accounts for a large portion of the relative abundance and the overall bacterial titer is comparable to untreated SPF mice. BpSCSK may sequester or consume key nutrients that some commensals require for colonization in the gut. It may also utilize other bacteriocins in its genome including the other class II lanthipeptides that were found to be encoded by BpSCSK.

When it comes to the modulation of the microbiota, all of these factors are likely at play

in varying proportions. The impacts from loss of butyrate are particularly notable in the case of BpSCSK since BpSCSK colonization prevented butyrate producers from recolonizing. Introduction of a butyrate producer that can co-colonize with BpSCSK, which were present in the Charles River mice and the ARM, may alleviate much of the colonization resistance that it causes.

5.3 Importance of lantibiotic-mediated microbiome modulation

Bacteria have evolved strategies to compete with one another, such as nutrient competition, predation, and bacteriocin production. While narrow- and broad-spectrum bacteriocins have been identified, much is still unknown about their overall impact on microbiome compositions and functions. Purified lantibiotics such as nisin, as well as bacteria capable of producing lantibiotics, such as *S. thermophilus*, are used in the food industry and are being investigated for their potential to combat pathogens resistant to clinically available antibiotics. Previous studies have demonstrated that purified lantibiotics can impact gut commensals [Zhang et al., 2023, Riboulet-Bisson et al., 2012, O'Reilly et al., 2023], and lantibiotic-producing bacteria have been shown to inhibit human gut commensals *in vitro* [Colombo et al., 2023]. Since the use of bacteriocin-producing bacteria can lead to colonization and continuous production of bacteriocins within the microbiome, they may have a much greater impact than purified bacteriocins alone. Therefore, understanding their influence on the microbiome is becoming increasingly important, particularly when they are used to combat antibiotic-resistant pathogens.

Analysis of fecal samples collected from healthy individuals and hospitalized patients uncovered a high prevalence of lanthipeptide-encoding genes in their intestinal microbiomes, including previously characterized lantibiotics. While activity, specificity, and expression of lanthipeptides vary widely, we found many lanthipeptides correlate with a fitness advantage for the encoding species based on their greater relative abundance in the microbiota. The

presence of identical lanthipeptide genes across different patients may indicate that patients may be coming into contact with common bacterial sources. Some of the species, such as those found in *Blautia*, can form spores. The resliance of bacteria in spore form could be aiding in transmission similar to the transmission of *C. difficile*

Early colonization with a lantibiotic-producer in a developing or dysbiotic microbiota, has the potential to impair microbiota diversification. In these and other settings, bacteria expressing lantibiotics may serve as "co-pathogens," i.e. microbes that do not directly cause disease but establish a state of dysbiosis that enables pathogen persistence. Identifying narrower spectrum lantibiotics that resist pathogens while maintaining beneficial commensal bacterial species represents a significant challenge. Also, while this thesis work focuses on lantibiotics, any bacteriocin produced in the gut has the potential to have a similar impact on colonization. These include sactipeptides, thiopeptides, microcins, lasso peptides, and a wide range of others that are found in gut commensals [Heilbronner et al., 2021].

5.4 Lantibiotic-producing probiotics

Hindering gut recolonization of key-metabolite producers and consumers lead to prolonged suppression of metabolites that support a healthy gut environment. Despite BpSCSK's ability to provide colonization resistance against VRE, our study reveals that it enhances colonization and infection with *K. pneumoniae* and *C. difficile*. This finding highlights the importance of characterizing commensal bacterial strains that might be included in live biotherapeutic products designed to reestablish microbiome functions in patients with dysbiosis. Avoiding undesirable side effects such as prolonged dysbiosis and susceptibility to additional pathogens is critical. In addition to increasing susceptibility to pathobiont infections, BpSCSK also reduced FMT-mediated reconstitution with commensal microbes and as a result, key microbiota-derived metabolites remained below the limits of detection despite the attempts to restore the microbiota. This could potentially reduce the effectiveness

of an FMT at treating infections like recurrent *C. difficile*.

Suez et al., using an *in vivo* murine model and human volunteers, have shown that bacterial strains used as probiotics are capable of prolonging antibiotic-induced dysbiosis [Suez et al., 2018]. While a mechanism was not established, they found that the supernatant from the probiotics can inhibit bacteria cultured from human feces. The same species used in their probiotic treatment were identified in our study to contain lanthipeptide genes. They found that *Blautia*, *Enterococcus*, and *Lactococcus* could grow in the presence of the probiotic strains, which could be the result of lantibiotic resistance genes that often accompany lantibiotic-producing bacteria. In addition, *Akkermansia* was over-represented with probiotic colonization, which was a Genus that also was present in mice colonized with BpSCSK. Although more work needs to be done to establish a connection, the findings described herein suggest a possible mechanism for the prolonged dysbiosis caused by some probiotics.

Despite the negative impact of BpSCSK on microbiota resilience following antibiotic treatment, lantibiotic-producing strains may still find a role in reducing infections caused by highly antibiotic-resistant pathogens. Antibiotic resistant pathogens, such as VRE, colonize the gut at high density and can lead to systemic infections that are becoming increasingly resistant to the few remaining antibiotic options. Intestinal clearance of VRE with BpSCSK followed by antibiotic-mediated clearance of BpSCSK represents a potential two-step path to reducing the risk of system infection with nearly untreatable pathogens. Alternatively, designing consortia that can colonize with lantibiotic-producing bacteria like BpSCSK and account for the lack of metabolite producers is another viable approach. Just as the CBBP consortia was selected from MyD88$^{-/-}$ with the ARM, other commensals from the ARM or other microbiomes could be identified that can co-colonize and produce the metabolites missing in BpSCSK-colonized mice.

Further characterization of lantibiotics may reveal lantibiotic-producing gut commensals that express more targeted lantibiotics against pathogens with reduced activity against im-

portant gut commensals. In fact, this may be an important contribution to microbiome resilience in a healthy microbiota.Regardless, more work is needed to determine the therapeutic potential of lantibiotics and to better characterize the novel lantibiotics currently found in probiotics and microbiomes to mitigate off-target side-effects that could impair commensal bacterial functions.

5.5 Lantibiotic-producers in the infant microbiome

The effects of lantibiotic-producing bacteria in the human gut microbiome following antibiotic treatment is only one instance of microbiome influence. There are possibilities for lantibiotic-producing bacteria to act elsewhere in nature, especially when a new microbiome is generated.

One notable example where lantibiotics may be important is during the development of the microbiota following birth. One of the pioneering species to pass from the mother to infants is *Bifidobacterium longum*, which are known to sometimes encode lanthipeptide genes in their genes[Ferretti et al., 2018]. In this case, *B. longum* expressing lantibiotics may be integral to proper development of the microbiota by limiting the bacteria that can colonize. On the flip side, *B. longum* expressing a broad-spectrum lantibiotic could delay colonization of healthy commensals.

This may also be an important consideration when using probiotics with infants. In preterm infants, probiotics like *Lactobacillus* spp., *Bifidobacterium* spp., and *S. thermophilus* are sometimes considered to prevent or reduce risk of mortality in necrotizing enterocolitis [Preidis and Versalovic, 2009]. Butyrate has been implicated in preventing necrotizing enterocolitis. It has also been shown to be important in reduce development of food allergies [Iweala and Nagler, 2019]. Therefore, ensuring that a potent lantibiotic-producer that prevents butyrate-producers from colonizing may be critical as the microbiome develops in infants.

5.6 Limitations

While this work characterized the impact BpSCSK can have on recolonization of the gut microbiota in mice and discovered many novel lanthipeptide sequences through shotgun sequencing of human fecal samples, there are important limitations of note.

Since an isogenic mutant of BpSCSK lacking the blauticin BGC could not be created, it was not possible to determine exactly how much the lantibiotic contributes to the colonization resistance observed in mice. Although BpKH6, is closely related, it still has some differences that may or may not be significant to its inability to inhibit bacteria as BpSCSK. A possible work around would be to express the blauticin BGC heterogeneously. This was attempted in *Limosilactobacillus reuteri* through a collaboration with the Jan Peter van Pijkeren lab at the University of Wisconsin. However, the synthesis and immunity genes proved to be too toxic when expressed in *L. reuteri*.

For mouse experiments, 16S rRNA gene sequencing of fecal pellets was used to assess the microbiota compositions of the mice. This has the benefit of amplifying bacterial sequences that may have very low relative abundance, and it is a cheaper form of sequencing. However, it comes at the cost of resolution and the ability to interrogate genes beyond the 16S rRNA gene that is available in shotgun metagenomic data. Shotgun sequencing would also give the ability to determine bacteria that could colonize with BpSCSK at the strain level.

The FMT and co-housing experiments involving BpSCSK-treated mice and wild-type SPF mice from Jackson Laboratories was conducted in sequential order using the same group of mice. While this highlights how the two methods together could not overcome the colonization resistance of BpSCSK dominated mice, it is possible that the FMT influenced the ability of bacteria to colonize through co-housing. Therefore, conducting the experiments separately may prove worthwhile. Also, increasing the number of FMTs may have different outcomes on efficacy. For our experiments, we limited the number of FMTs to once per day for three days. In some mice that were co-housed with BpSCSK-colonized mice, some

BpSCSK ASVs could be detected. Although, it could not be determined whether BpSCSK actually colonized these mice or transiently passed through the GI tract via coprophagia. Separating the mice again after co-housing could potentially provide further insight.

The co-housing experiment with mice from Charles River was done with a very small sample size. In order to better determine the ability of the microbiota of these mice to colonize BpSCSK-treated mice, a larger sample size with more frequent sampling would be needed. Despite this, we were still able to see more diverse colonization in BpSCSK-treated mice that was not seen with the mice from Jackson Laboratories. The reason for this finding remains unknown.

The shotgun metagenomic data from healthy human donors and clinical patients provided a large source to screen for novel and previously characterized lanthipeptides. However, the infrequent samplings and variable antibiotic treatments made it difficult to confidentially assess correlations between the presence of lanthipeptides and diversity of the microbiota. Furthermore, many of the contigs harboring lanthipeptide genes were small, which made it difficult to assign taxonomy and lanthipeptide class. In fact, some of the lanthipeptide genes were the only gene present on contigs. This made it challenging to accurately identify lanthipeptides. Therefore, it is likely that some lanthipeptides were missed, and some of the identified lanthipeptide genes may be false positives. Also, lanthipeptide-producers may have been at vary low abundance in some samples, which prevented detection of some lanthipeptide genes. With greater sequencing depth beyond the shallow-shotgun sequencing that was conducted for all samples, it may be possible to detect more lanthipeptide BGCs. Furthermore, repeated gene sequences like the blauticin genes in BpSCSK can make it challenging to assemble lanthipeptide BGCs. Long-read sequencing may another way to yield better lanthipeptide BGC assemblies.

5.7 Future Directions

The ability of BpSCSK to heavily impact colonization of the gut microbiota serves as a model describing how one strain can have dramatic impact on the microbiota. However, examples of this occurring naturally remain poorly described. Despite the advances in metagenomic mining capabilities, much of the analysis has been on large datasets that focus on healthy humans. The clinical samples from hospitalized patients analyzed in this study provide a great start to better understanding lantibiotics, and other bacteriocins, in the gut microbiota. Furthermore, a benefit to this dataset is the fact that the fecal samples of the patients have been preserved. Therefore, it is possible to go back and isolate strains that have been identified in the metagenomic data. This would allow testing isolates *in vitro* and *in vivo* using mouse models in the same manner as BpSCSK. Not only could this yield more information about lantibiotic-producing bacteria, but it could also be a great source for therapeutic lantibiotics with a more desirable activity profile.

It would also be interesting to understand more about the other dynamics involved with BpSCSK-mediated inhibition. The same experiments, for example, could be performed in gnotobiotic immune deficient mice to eliminate the immune component. Butyrate producers or butyrate itself could be supplemented in mice to see how much butyrate is impacting colonization. Additionally, finding a suitable candidate for heterologous expression of the blauticin BGC would allow greater control of blauticin to understand its impact. It would also make lanthipeptides from metagenomic sequences in bacteria that have not yet been isolated more accessible for expression and testing.

Lastly, further investigating lantibiotics-and bacteriocins more generally-would be helpful in improving our methods of detection. Studies that purely look at correlations between taxonomy and diseases may be missing bacteriocin-mediated mechanisms, such as those observed in BpSCSK, where some strains may encode a bacteriocin while others may not. Without gene level resolution and detection of bacteriocins, coming across a *Blautia* strain

in a microbiome would not be uncommon. However, these common commensals could be acting as “co-pathogens" or maybe even pathogens themselves under certain circumstances.

Overall, there are many directions that can build upon this work. I think in the coming years we will be able to harness the specific properties of bacteria, like lantibiotic production, to improve human health. I look forward to continuing my career in microbiome research to help advance this goal.

CHAPTER 6

MATERIALS AND METHODS

6.1 Phylogenetic tree of *Blautia* isolates

The phylogenetic tree was constructed as previously described [Zhang et al., 2024a]. Briefly, single-copy core genes (SCGs) were identified with the Anvi'o pan-genome bioinformatic workflow [Eren et al., 2021] through Hidden Markov Models (HMM) of a list of 71 bacterial SCGs. SCGs that were present in all *Blautia* isolates in addition to the *Escherichia coli* K12 MG1655 outgroup used to root the tree. The amino acid sequences encoded by these genes were extracted and concatenated using the 'anvi-get-sequences-for-hmm-hits'. A Newick file was generated using the 'anvi-gen-phylogenomic-tree' function, which utilizes FastTree 2.1.11 [Price et al., 2010]. The tree was visualized in R using the ggtree R package [Yu et al., 2017].

6.2 Mice

All mouse studies were approved by The University of Chicago Institutional Animal Care and Use Committee (protocol 72599). Wild-type C57BL/6 mice were ordered from the AX8 breeding room at Jackson Laboratories, or they were ordered from H47, K92, R07 breeding rooms of Charles River where noted. MyD88$^{-/-}$ C57BL/6 mice are maintained as a colony at the University of Chicago under continuous treatment of augmentin (NorthStarx NDC:16714-293-01), which contains 0.48 g/L amoxicillin and 0.07 mg/L clavulanate, added to drinking water. For experiments, female mice aged 9 to 10 weeks old and 37 to 44 weeks old for wild-type and MyD88$^{-/-}$ mice, respectively. All mice were housed in a BSL2 animal room under specific-pathogen-free (SPF) conditions at the University of Chicago. Mice were fed a standard chow diet and given autoclaved acidified drinking water. All mice were randomized and single housed in cages, except where specified, containing corncob bedding. Cages were

changed every 2 weeks. When working with the mice, a 10% bleach solution was used to disinfect surfaces to prevent contamination from spores.

6.3 Bacterial consortia strains and growth conditions

Frozen stocks for *Enterocloster bolteae* CBBP, *Phocaeicola sartorii* CBBP, *Parabacteroides distasonis* CBBP, *Blautia pseudococcoides* SCSK, and *Blautia producta* KH6 were streaked out on Columbia blood agar plates with 5% sheep's blood (BBL 221263) and incubated at 37 °C in an anaerobic chamber for 2 days. Single colonies were mixed in 500 µL of Dulbecco's phosphate buffered saline (DPBS) (Gibco 14190-144) and 200 µL were streaked in a lawn on a fresh plate. Plates were again incubated for 2 days. Next, lawns were scrapped up with a sterile inoculating loop and suspended in 1.2 mL DPBS. For the CBBP consortia, each strain was mixed into the same 1.2 mL DPBS. 200 µL was administered via oral gavage for colonization in mice. These steps were repeated for each day the bacteria were administered.

6.4 FMT and Co-housing

For the FMT, one fecal pellet was collected from four female SPF C57BL/6 mice. The fecal pellets were pooled into one tube and kept on ice until transferred to an anaerobic chamber within 30 minutes from collection. All four fecal pellets were combined and suspended in 4 mL of reduced DPBS. Then, the fecal pellets were crushed, mixed, and aliquoted in 200 µL volumes for gavage. Mice were gavaged with 200 µL. This process was then repeated on subsequent days for a total of three gavages. Mice used for the FMT control were treated with ampicillin (Athenex NDC:70860-118-99) for four days starting six days before the first gavage. After two weeks, each mouse colonized with BpSCSK was then co-housed with a female SPF C57BL/6 mouse for an additional two weeks. Fecal pellets were collected for metagenomic and metabolomic analysis throughout the experiments.

In a separate experiment, BpSCSK colonized mice were individually co-housed with female MyD88$^{-/-}$ C57BL/6 mice. All mice were kept on 0.5 g/L ampicillin in the drinking water throughout the experiment. Fecal pellets were collected for metagenomic and metabolomic analysis. The same experimental setup was used for the co-housing experiment with Charles River mice.

6.5 Antibiotic treatment

Mice treated with ampicillin to deplete the native gut microbiota were given 0.5 g/L ampicillin in their drinking water starting 6 days prior to their first gavage and returned to their normal drinking water two days before their first gavage. MyD88$^{-/-}$ and mice colonized with the CBBP consortia were continuously treated with 0.5 g/L ampicillin prepared every 4 days. Mice treated with a cocktail of antibiotics were given 0.25 g/L neomycin (Fisher BioReagents BP2669), vancomycin (SAGENT Pharmaceuticals NDC:25021-158-99), and metronidizole (Sigma-Aldrich M3761) in their drinking water starting five days from infection with *C. difficile*. They were returned to normal drinking water 2 days prior to infection and given an intraperitoneal (IP) injection of 100µL of 2 g/L clindamycin (Sigma-Aldrich C5269) 24 hours prior to infection.

6.6 *C. difficile* spore preparation

C. difficile spore preparation was carried out as previously described with slight modifications[Dong et al., 2023]. Using isolated colonies grown on BHIS agar, which consists of 37 g/L Brain-Heart infusion powder (BD Bacto 237500), 5 g/L yeast extract (BD Bacto 212750), 15 g/L agar (BD Bacto 214040), and 0.1% (w/v) L-cysteine powder (Sigma cat# C7352), *C. difficile* was inoculated into pre-reduced BHIS broth and incubated anaerobically in a 50 mL conical tube at 37 °C. After 40-50 days, the suspended cells were harvested via

centrifugation with five washes with ice-cold water. The cell pellet was then re-suspended in 20% HistoDenz (w/v) (Sigma, St. Louis, MO) and layered onto a 50% (w/v) HistoDenz solution. Purified spores were collected via centrifugation at 15,000 g for 15 min 3 times. The resulting spore pellet was again washed with ice-cold water 4 times to remove traces of HistoDenz. Finally, the spore pellet was re-suspended in sterile water. To kill any remaining vegetative cells, the re-suspended spores were heated on a heat block for 20 minutes at 60 °C. A portion of the spore stocks were diluted and plated on BHIS agar to confirm that there is less than 1 vegetative cell per 200 spores. Another portion was plated on BHIS agar containing 0.1% (w/v) taurocholic acid (BHIS-TA) for numeration.

6.7 *C. difficile* infection

Mice were challenged via oral gavage of approximately 200 *C. difficile* R20291 spores suspended in 200 µL of DPBS. Fecal samples were collected prior to challenge followed by day 1 and 7 post infection for CFU counts, 16S rRNA gene sequencing, and metabolomics. Mice were also weighed daily for 8 days and compared to their weight prior to challenge.

6.8 *K. pneumoniae* infection

K. pneumoniae MH258 was grown aerobically at 37 °C overnight in LB broth supplemented with 100 µg/mL carbenicillin (Fisher BioReagents BP2648) and 50 µg/mL neomycin. Overnight culture was serial diluted to 5 CFU/µL in DPBS. Mice were challenged via oral gavage of approximately 1000 CFU (200 µL) of *K. pneumoniae*. Fecal samples were collected prior to infection in addition to day 1, 3, and 7 post infection for CFU and 16S rRNA gene sequencing.

6.9 Quantification of *C. difficile* and *K. pneumoniae* shedding

Fecal pellets were collected from mice on the indicated dates in micro-centrifuge tubes and stored on ice. After weighing samples, 1 mL of DPBS was added to each tube and fecal pellets were broken up using an inoculating loop. Then, samples were vortexed for 5 seconds and aliquoted to a 96-well flat-bottom plate for serial dilutions. Each sample was serial diluted in DPBS to 10^{-5} in 10-fold steps using a total of 300 µL volumes for each dilution. Next, 10 µL of each dilution was plated in rows on agar media and incubated at overnight at 37 °C within 1 hour of collection. For *C. difficile*, serial dilutions and culturing were conducted in an anaerobic chamber and plated on CC-BHIS-TA containing 0.25 g/L D-cycloserine (Acros Organics 228480250), and 0.016 g/L cefoxitin (Sigma C4786). *K. pneumoniae* was grown on LB (BD 244620) agar containing 100 g/mL carbenicillin, 50 g/mL neomycin, and 25 g/mL chloramphenicol (Fisher BioReagents BP904) antibiotics. Colonies were counted at the least diluted concentration that colonies could be accurately counted at and reported as CFU per gram of feces.

6.10 Quantitative metabolomics

Mouse fecal pellets were collected in 2 mL cryogenic microcentrifuge tubes (Sarstedt 72.694.006) on collection days and placed on dry ice until transferred to a -80 °C freezer DNA sequencing. Fecal samples were weighed and extraction solvent, 80% methanol spiked with internal standards, was added to make a ratio of 100 mg of material/mL of extraction solvent. Samples were then homogenized at 4 °C using a Bead Mill 24 Homogenizer (Fisher; 15-340-163) set at 1.6 m/s with six x 30 s cycles, 5 seconds off per cycle. Next, samples were centrifuged at -10 °C, 20,000 x g for 15 min. The supernatant was used for subsequent metabolomic analysis.

Short-chain fatty acids (SCFAs), amino acids, and phenolic metabolites were quantified

via derivatization with pentafluorobenzl-bromide (PFBBr). Methanol containing internal standards was added to fecal samples at 4 volumes per mg of feces. Samples were subjected to centrifugation followed by addition of 100 µL of 100 mM borate buffer at a pH of 10. Next, 400 µL 100 mM PFBBr suspended in acetonitrile was added to the samples and incubated at 65 °C for 1 hour. Lastly, metabolites were extracted with hexanes and subjected to gas chromatography-mass spectrometry (GC-MS) (Agilent 8890/5977B and 7890B/5977B) with chemical ionization and negative mode detection.

Bile acids were quantified via liquid chromatography-mass spectrometry (LC-MS). First, 75 µL was added to mass spectrometry autosampler vials (Microliter; 09-1200) and subsequently dried using a nitrogen stream of 30 L/min (top) and 1 L/min (bottom) at 30 °C (Biotage SPE Dry 96 Dual; 3579M). Dried samples were then re-suspended in 750 µL of a 50:50 water:methanol mixture. The vials were added to a thermomixer (Eppendorf) to re-suspend analytes under the following conditions: 4 °C, 1000 rpm for 15 min with infinite hold at 4 °C. To remove insoluble debris, samples were centrifuged in microcentrifuge tubes at 20,000 x g for 15 mins at 4 °C. Next, 700 µL was transferred to a new mass spectrometry autosampler vial and analyzed in negative mode on an LC system (Agilent 1290 infinity II) coupled to a quadrupole time-of-flight (QTOF) mass spectrometer (Agilent 6546) equipped with an Agilent Jet Stream Electrospray Ionization source. Then, 5 µL of sample was then injected onto an XBridge BEH C18 column (3.5 µm, 2.1 x 100 mm; Waters Corporation, PN) fitted with an XBridge BEH C18 guard (Waters Corportation, PN) at 45 °C. Elution started with 72% A (Water, 0.1% formic acid) and 28% B (Acetone, 0.1% formic acid) with a flow rate of 0.4 mL/min for 1 min and linearly increased to 33% B over 5 min, then linearly increased to 65% B over 14 min. Then the flow rate was increased to 0.6 mL/min and B was increased to 98% over 0.5 min and these conditions were held constant for 3.5 min. Finally, re-equilibration at a flow rate of 0.4 mL/min of 28% B was performed for 3 min. The electrospray ionization conditions were set with the capillary voltage at 3.5 kV, nozzle

voltage at 2 kV, and detection window set to 100-1700 m/z with continuous infusion of a reference mass (Agilent ESI TOF Biopolymer Analysis Reference Mix) for mass calibration. A 10-point calibration curve was used for quantification. Data analysis was performed using MassHunter Profinder Analysis software (version B.10, Agilent Technologies) and confirmed by comparison with authentic standards. Normalized peak areas were calculated by dividing raw peak areas of targeted analytes by averaged raw peak areas of internal standards.

Log_2 Fold changes were calculated for metabolites by taking the ratio of the average metabolite concentration for a given metabolite within each group to the average metabolite concentration of SPF mice across all timepoints.

6.11 Hospitalized patient fecal sample collection

Metagenomic data for clinical patients have been previously described [Odenwald et al., 2023, Lehmann et al., 2024, Stutz et al., 2022]. Briefly, fecal samples for clinical patients were collected by nurses in inpatient wards and medical intensive care units. Upon collection, samples were immediately sent for storage at 4 °C via a pneumatic tubing system. The samples in storage at 4 °C were then aliquoted and stored at -80 °C within 24 hours after initial collection. In addition to samples, history of inpatient prescribed antibiotics was collected. Samples collected between June 2020 to October 2021 were included in the anaysis.

6.12 Healthy human donor fecal sample collection

Fecal sample collection for healthy human donors was conducted as previously described [Zhang et al., 2024a]. were enrolled in a prospective fecal collection protocol. Donor age and sex were not reported. The prospective fecal collection protocol was approved by the institutional review boards at Memorial Sloan Kettering Cancer Center and at The University of Chicago. All donors provided written and informed consent for IRB-approved biospec-

imen collection and analysis (protocols 06-107; IRB20-1384). The study was conducted in accordance with the Declaration of Helsinki. In total, 17 donors samples were included.

6.13 Shallow shotgun sequencing

Human fecal samples were suspended in lysis buffer and broken up with a bead beater (BioSpec Product). DNA was purified with the QIAamp PowerFecal Pro DNA kit (Qiagen). Sequencing was performed using the Illumina HiSEq platform. This produced approximately 7-8 million paired-end reads for each sample with a read length of 150 bp. After trimming adapters from raw reads, the quality of reads was assessed and controlled with Trimmomatic[Bolger et al., 2014] (version 0.39). Reads that map to the human genome were removed with kneaddata (version 0.7.10). In order to assign taxonomy, the filtered reads were run through MetaPhlAn4[Blanco-Míguez et al., 2023]. All reads were then assembled into contigs using MEGAHIT[Li et al., 2015] (version 1.2.9). α-diversity was assessed using the asbio R package.

Shotgun sequencing for fecal pellets from four ARM mice were processed as described above. Instead of assembling contigs, the reads were recruited to the BpSCSK genome using the Anvi'o[Eren et al., 2021] metagenomic workflow.

6.14 16S rRNA gene sequencing

Mouse fecal pellets were collected in 2 mL cryogenic microcentrifuge tubes (Sarstedt) on collection days and placed on dry ice until transferred to a -80 °C freezer until sequenced. Fecal samples were suspended in lysis buffer and broken up with a bead beater (BioSpec Product). DNA was purified with the QIAamp PowerFecal PRo DNA kit (Qiagen). With the purified DNA, the V4-V5 region of the 16S rRNA gene was amplified using universal primers 563F (5'-nnnnnnnn-NNNNNNNNNNNN-AYTGGGYDTAAA-GNG-3') and 926R (5'-nnnnnnnn-

NNNNNNNNNNNN-CC GTCAATTYHT-TTRAGT-3'), where 'N' represents the barcodes and 'n' are additional nucleotides added to offset primer sequencing. Amplicons containing approximately 412 bp regions were purified in a spin column (Minelute, Qiagen). Purified amplicons were quantified using a Qubit 2.0 fluorometer and pooled at equimolar concentrations. Unique Dual Index adapters were ligated to the amplicons with QIAseq 1-step amplicon library kit (Qiagen). Library quality control was performed using Qubit and TapeStation. Results were analyzed as using the Phyloseq[McMurdie and Holmes, 2013] R package. Taxonomy for amplicon sequence variants (ASVs) were assigned with Ribosomal Database Project (RDP) classifier 2.14 [Cole et al., 2013]. α-diversity was calculated using the estimate_richness() function, Bray-Curtis dissimilarity was calculated and plotted in R using the ordinate() and plot_ordination() functions.

6.15 16S rRNA gene qPCR

An aliquot of the samples prepared for 16S rRNA gene sequencing were diluted to 20 ng/µL. The primers 563F (5'-AYTGGGYDTAAAGNG-3') and 926R (5'-CCGTCAATTYHTTTRAGT-3') for the V4-V5 region of the 16S rRNA gene were used for amplification. A standard curve was created with a V4-V5 region on a linearized TOPO pcr2.1TA vector isolated from *Eschericha coli* DH5α cells. The vector was serially diluted 5-fold ranging from 10^8 to 10^3 copies/µL. qPCR was performed on a QuantStudio 6 Pro (Applied Biosystems) using PowerTrack SYBR Green Master Mix (A46109) with the following cycling conditions: 95 °C for 10 min, followed by 40 cycles of 95 °C for 30 s, 52 °C for 30 s,and 72 °C for 1 min. Design and Analysis v2 software was used to calculate the copy numbers for each sample. Copy numbers were normalized based on the weight of fecal pellets the DNA was extracted from.

6.16 Lanthipeptide detection

Anvi'o[Eren et al., 2021] was used to manage gene annotations. Anvi'o contig databases were generated from fasta files containing shotgun sequencing reads assembled into contigs by MEGAHIT[Li et al., 2015] (version 1.2.9) using 'anvio-gen-contigs-database.' Genes in the Anvi'o contigs databases were called using Prodigal[Hyatt et al., 2010] (version 2.6.3) with default parameters. Specific Pfam domains[Paysan-Lafosse et al., 2025] were annotated using 'anvi-run-hmms' with custom Hidden Markov Model (HMM) profile[Eddy, 2011]. The following Pfam domains were used for the search: PF00005, PF00069, PF00072, PF00082, PF00106, PF00196, PF00330, PF00486, PF00512, PF00664, PF00672, PF00929, PF01532, PF01895, PF01964, PF02052, PF02463, PF02492, PF02518,PF03572, PF03663, PF03902, PF04369, PF04604, PF04738, PF05147, PF07470, PF07714, PF07944, PF08130, PF08279, PF08659, PF10439, PF12121, PF12730, PF13304, PF13384, PF13555, PF13561, PF13575, PF13581, PF13589, PF13699, PF13817, PF14028, PF14501, PF14867, PF16934, PF18218, PF18923, PF18937, PF19398, PF20693, PF22146. Contigs were also run through the RODEO (Rapid ORF Description and Evaluation Online)[Tietz et al., 2017] program to identify lanthipeptide genes. All contigs that contained an annotated Pfam domain, previously identified lanthipeptide from Walker et al.[Walker et al., 2020], a lanthipeptide gene identified by RODEO, or lanthipeptides in the InterPro[Blum et al., 2025] and KEGG[Kanehisa et al., 2025] databases were extracted and converted into a new fasta file. The contigs were then made into a new Anvi'o contig database and annotated with 'anvi-run-pfams.' Additionally, the fasta file containing filtered contigs was run separately through Bakta[Schwengers et al., 2021] and genes were extracted from the Anvi'o contig database to run through GhostKOALA[Kanehisa et al., 2016] for gene annotations. Any newly identified lanthipeptides from the gene annotations detected were added to the list of lanthipeptides and were re-screened to identify any additional contigs containing the gene. Genes of interest were also run through NCBI BLASTp to further identify and confirm lanthipeptide sequences

[Camacho et al., 2009]. Only the top 5 hits from BLASTp were considered. Lanthipeptide class was assigned based on annotations or surrounding synthesis genes.

The same method was used to detect lanthipeptide genes in BpSCSK and other isolates from healthy donors. Biosynthetic gene clusters were visualized using the gggenes R package.

6.17 Taxonomic classification of lanthipeptide containing contigs

Taxonomic classification for contigs containing lanthipeptides was determined by running contig sequences through the NCBI Nucleotide database[Camacho et al., 2009]. Hits were limited to the top five results. A single taxonomic classification was assigned to a contig if the evalue was less than 1 x 10^{-3}, percent identity was greater than 75%, and query coverage was greater than 60%. If there were more than one result remaining, the result with the highest bitscore was used. Contigs that did not have a taxonomic classification that met the thresholds were labeled “Unclassified."

6.18 Lanthipeptide fitness advantage assessment

Taxonomic annotations for contigs were matched to identical genus and species taxonomic classifications determined by MetaPhlAn4[Blanco-Míguez et al., 2023]. For species that were annotated as "sp.", the taxids were appended to the taxonomic classification for matching purposes. Only lanthipeptides that had at least five matches were considered. Relative abundances of species that did not contain a match to a lanthipeptide were averaged together. Fold changes were calculated as the ratio of the relative abundances of bacteria that contained the lanthipeptide genes to the average relative abundances of the same species that did not contain the lanthipeptide gene. Next, the fold changes of lanthipeptides were averaged together to get the mean fold change for each lanthipeptide gene. Results were plotted as the $\log_2$ mean fold change.

6.19 UMAP analysis of lanthipeptides

Lanthipeptide sequences were aligned in R using MUSCLE[Edgar, 2022] in the msa[Bodenhofer et al., 2015] R package. A distance matrix as generated using dist.alignment() in the seqinr[Charif and Lobry, 2007] package. Next, the uniform manifold approximation and projection (UMAP)[McInnes et al., 2018] conducted using the umap R package.

6.20 Bacterial isolates from healthy human donors

Bacterial strains from healthy donors were isolated as previously described [Sorbara et al., 2019]. Isolation and growth of commensal bacteria was performed under anaerobic conditions with 5% H 2 , 5% CO 2 and 90% N2 in an anaerobic chamber (Coy Labs). Fresh donor fecal samples were transferred into anaerobic conditions within 1 h of collection. Fecal samples were resuspended in pre-reduced PBS and plated on Columbia agar with 5% sheep blood (BBL, BD) or brain-heart infusion (BHI – Difco, BD) agar in three serial 10-fold dilutions and incubated at 37 °C for 48 – 96 h. Isolated colonies were re-streaked for purity onto Columbia blood agar and frozen in pre-reduced 10% glycerol in PBS. For broth cultures, isolates were grown in pre-reduced BHI supplemented with 5g/L yeast extract (Difco, BD) and 0.1% L-cysteine (Sigma) (BHIS).

6.21 Growth curve of *Blautia pseudococcoides* SCSK and *Blautia producta* KH6

BpSCSK and BpKH6 were both grown anaerobically in six batches of 4 mL of BHIS liquid media at 37 °C for two days. The cultures were back diluted to an OD_{600} of .01 in pre-reduced BHIS liquid media using a flat-bottom 96-well plate (Greiner Bio-One). The total volume for each well was 300 µL. For the co-culturing, 150 µL of each culture at OD_{600} of .01 was combined to make 300 µL total. In 12 wells, 300 µL of BHIS alone was added to

serve as the blank. A clear seal was stuck to the top of the lid to prevent evaporation. The 96-well plate was then loaded in to an Epoch 2 plate reader and the cultures were grown anaerobically at 37 °C with orbital shaking. OD measurements were taken at OD_{600}, OD_{975}, and OD_{970} every 15 minutes for approximately 35 hours. Pathlength for OD readings were corrected using Beer-Lambert's law.

6.22 Gut metabolite modules for *Blautia pseudococcoides* SCSK and *Blautia producta* KH6

Genes for BpSCSK and BpKH6 were called using Prodigal[Hyatt et al., 2010] (version 2.6.3) with default parameters. Amino acid sequences were annotated with KEGG accessions using GhostKOALA[Kanehisa et al., 2016]. Gut Metabolic Modules (GMMs) were determined with the R package omixer-rpmR [Vieira-Silva et al., 2016]. Pathways were visualized using pheatmap in R.

6.23 External images

Chemical structures used in 1.1 were made using the desktop version of ChemDraw 23.1.2 (https://revvitysignals.com/products/research/chemdraw). Figure 5.1 was made using images from BioRender. (https://app.biorender.com/)

REFERENCES

Michael C Abt, Peter T McKenney, and Eric G Pamer. Clostridium difficile colitis: pathogenesis and host defence. *Nature Reviews Microbiology*, 2016. ISSN 1740-1526. doi:10.1038/nrmicro.2016.108.

Zainab Alkhatib, André Abts, Antonino Mavaro, Lutz Schmitt, and Sander H.J. Smits. Lantibiotics: How do producers become self-protected? *Journal of Biotechnology*, 159(3): 145–154, 2012. ISSN 0168-1656. doi:10.1016/j.jbiotec.2012.01.032.

Paul G. Arnison, Mervyn J. Bibb, Gabriele Bierbaum, Albert A. Bowers, Tim S. Bugni, Grzegorz Bulaj, Julio A. Camarero, Dominic J. Campopiano, Gregory L. Challis, Jon Clardy, Paul D. Cotter, David J. Craik, Michael Dawson, Elke Dittmann, Stefano Donadio, Pieter C. Dorrestein, Karl-Dieter Entian, Michael A. Fischbach, John S. Garavelli, Ulf Göransson, Christian W. Gruber, Daniel H. Haft, Thomas K. Hemscheidt, Christian Hertweck, Colin Hill, Alexander R. Horswill, Marcel Jaspars, Wendy L. Kelly, Judith P. Klinman, Oscar P. Kuipers, A. James Link, Wen Liu, Mohamed A. Marahiel, Douglas A. Mitchell, Gert N. Moll, Bradley S. Moore, Rolf Müller, Satish K. Nair, Ingolf F. Nes, Gillian E. Norris, Baldomero M. Olivera, Hiroyasu Onaka, Mark L. Patchett, Joern Piel, Martin J. T. Reaney, Sylvie Rebuffat, R. Paul Ross, Hans-Georg Sahl, Eric W. Schmidt, Michael E. Selsted, Konstantin Severinov, Ben Shen, Kaarina Sivonen, Leif Smith, Torsten Stein, Roderich D. Süssmuth, John R. Tagg, Gong-Li Tang, Andrew W. Truman, John C. Vederas, Christopher T. Walsh, Jonathan D. Walton, Silke C. Wenzel, Joanne M. Willey, and Wilfred A. van der Donk. Ribosomally synthesized and post-translationally modified peptide natural products: overview and recommendations for a universal nomenclature. *Natural Product Reports*, 30(1):108–160, 2012. ISSN 0265-0568. doi:10.1039/c2np20085f.

Aitor Blanco-Míguez, Francesco Beghini, Fabio Cumbo, Lauren J. McIver, Kelsey N. Thompson, Moreno Zolfo, Paolo Manghi, Leonard Dubois, Kun D. Huang, Andrew Maltez Thomas, William A. Nickols, Gianmarco Piccinno, Elisa Piperni, Michal Punčochář, Mireia Valles-Colomer, Adrian Tett, Francesca Giordano, Richard Davies, Jonathan Wolf, Sarah E. Berry, Tim D. Spector, Eric A. Franzosa, Edoardo Pasolli, Francesco Asnicar, Curtis Huttenhower, and Nicola Segata. Extending and improving metagenomic taxonomic profiling with uncharacterized species using MetaPhlAn 4. *Nature Biotechnology*, 41(11):1633–1644, 2023. ISSN 1087-0156. doi:10.1038/s41587-023-01688-w.

Matthias Blum, Antonina Andreeva, Laise Cavalcanti Florentino, Sara Rocio Chuguransky, Tiago Grego, Emma Hobbs, Beatriz Lazaro Pinto, Ailsa Orr, Typhaine Paysan-Lafosse, Irina Ponamareva, Gustavo A Salazar, Nicola Bordin, Peer Bork, Alan Bridge, Lucy Colwell, Julian Gough, Daniel H Haft, Ivica Letunic, Felipe Llinares-López, Aron Marchler-Bauer, Laetitia Meng-Papaxanthos, Huaiyu Mi, Darren A Natale, Christine A Orengo, Arun P Pandurangan, Damiano Piovesan, Catherine Rivoire, Christian J A Sigrist, Narmada Thanki, Françoise Thibaud-Nissen, Paul D Thomas, Silvio C E Tosatto, Cathy H Wu, and Alex Bateman. InterPro: the protein sequence classification resource in 2025. *Nucleic acids research*, 53(D1):D444–D456, 2025. ISSN 0305-1048. doi:10.1093/nar/gkae1082.

Ulrich Bodenhofer, Enrico Bonatesta, Christoph Horejš-Kainrath, and Sepp Hochreiter. msa: an R package for multiple sequence alignment. *Bioinformatics*, 31(24):3997–3999, 2015. ISSN 1367-4803. doi:10.1093/bioinformatics/btv494.

Anthony M. Bolger, Marc Lohse, and Bjoern Usadel. Trimmomatic: a flexible trimmer for Illumina sequence data. *Bioinformatics*, 30(15):2114–2120, 2014. ISSN 1367-4803. doi:10.1093/bioinformatics/btu170.

Sandrine Brugiroux, Markus Beutler, Carina Pfann, Debora Garzetti, Hans-Joachim Ruscheweyh, Diana Ring, Manuel Diehl, Simone Herp, Yvonne Lötscher, Saib Hussain, Boyke Bunk, Rüdiger Pukall, Daniel H. Huson, Philipp C. Münch, Alice C. McHardy, Kathy D. McCoy, Andrew J. Macpherson, Alexander Loy, Thomas Clavel, David Berry, and Bärbel Stecher. Genome-guided design of a defined mouse microbiota that confers colonization resistance against Salmonella enterica serovar Typhimurium. *Nature Microbiology*, 2(2):16215, 2016. doi:10.1038/nmicrobiol.2016.215.

Silvia Caballero, Sohn Kim, Rebecca A. Carter, Ingrid M. Leiner, Bože Sušac, Liza Miller, Grace J. Kim, Lilan Ling, and Eric G. Pamer. Cooperating Commensals Restore Colonization Resistance to Vancomycin-Resistant Enterococcus faecium. *Cell Host & Microbe*, 21(5):592–602.e4, 2017. ISSN 1931-3128. doi:10.1016/j.chom.2017.04.002.

Christiam Camacho, George Coulouris, Vahram Avagyan, Ning Ma, Jason Papadopoulos, Kevin Bealer, and Thomas L Madden. BLAST+: architecture and applications. *BMC Bioinformatics*, 10(1):421, 2009. doi:10.1186/1471-2105-10-421.

Delphine Charif and Jean R. Lobry. *SeqinR 1.0-2: A Contributed Package to the R Project for Statistical Computing Devoted to Biological Sequences Retrieval and Analysis*, pages 207–232. Springer Berlin Heidelberg, Berlin, Heidelberg, 2007. ISBN 978-3-540-35306-5. doi:10.1007/978-3-540-35306-5_10.

James R Cole, Qiong Wang, Jordan A Fish, Benli Chai, Donna M McGarrell, Yanni Sun, C Titus Brown, Andrea Porras-Alfaro, Cheryl R Kuske, and James M Tiedje. Ribosomal Database Project: data and tools for high throughput rRNA analysis. *Nucleic acids research*, 42(Database issue):D633–42, 2013. ISSN 0305-1048. doi:10.1093/nar/gkt1244.

Natalia S. Ríos Colombo, Mariana Perez-Ibarreche, Lorraine A. Draper, Paula M. O'Connor, Des Field, R. Paul Ross, and Colin Hill. Impact of bacteriocin-producing strains on bacterial community composition in a simplified human intestinal microbiota. *Frontiers in Microbiology*, 14:1290697, 2023. ISSN 1664-302X. doi:10.3389/fmicb.2023.1290697.

Qiwen Dong, Huaiying Lin, Marie-Maude Allen, Julian R. Garneau, Jonathan K. Sia, Rita C. Smith, Fidel Haro, Tracy McMillen, Rosemary L. Pope, Carolyn Metcalfe, Victoria Burgo, Che Woodson, Nicholas Dylla, Claire Kohout, Anitha Sundararajan, Evan S. Snitkin, Vincent B. Young, Louis-Charles Fortier, Mini Kamboj, and Eric G. Pamer. Virulence and genomic diversity among clinical isolates of ST1 (BI/NAP1/027) Clostridioides difficile. *Cell Reports*, 42(8):112861, 2023. ISSN 2211-1247. doi:10.1016/j.celrep.2023.112861.

Mohamed S. Donia, Peter Cimermancic, Christopher J. Schulze, Laura C. Wieland Brown, John Martin, Makedonka Mitreva, Jon Clardy, Roger G. Linington, and Michael A. Fischbach. A Systematic Analysis of Biosynthetic Gene Clusters in the Human Microbiome Reveals a Common Family of Antibiotics. *Cell*, 158(6):1402–1414, 2014. ISSN 0092-8674. doi:10.1016/j.cell.2014.08.032.

Lorraine A. Draper, Paul D. Cotter, Colin Hill, and R. Paul Ross. Lantibiotic Resistance. *Microbiology and Molecular Biology Reviews*, 79(2):171–191, 2015. ISSN 1092-2172. doi:10.1128/mmbr.00051-14.

Sean R. Eddy. Accelerated Profile HMM Searches. *PLoS Computational Biology*, 7(10): e1002195, 2011. ISSN 1553-734X. doi:10.1371/journal.pcbi.1002195.

Robert C. Edgar. Muscle5: High-accuracy alignment ensembles enable unbiased assessments of sequence homology and phylogeny. *Nature Communications*, 13(1):6968, 2022. doi:10.1038/s41467-022-34630-w.

A. Murat Eren, Evan Kiefl, Alon Shaiber, Iva Veseli, Samuel E. Miller, Matthew S. Schechter, Isaac Fink, Jessica N. Pan, Mahmoud Yousef, Emily C. Fogarty, Florian Trigodet, Andrea R. Watson, Özcan C. Esen, Ryan M. Moore, Quentin Clayssen, Michael D. Lee, Veronika Kivenson, Elaina D. Graham, Bryan D. Merrill, Antti Karkman, Daniel Blankenberg, John M. Eppley, Andreas Sjödin, Jarrod J. Scott, Xabier Vázquez-Campos, Luke J. McKay, Elizabeth A. McDaniel, Sarah L. R. Stevens, Rika E. Anderson, Jessika Fuessel, Antonio Fernandez-Guerra, Lois Maignien, Tom O. Delmont, and Amy D. Willis. Community-led, integrated, reproducible multi-omics with anvi'o. *Nature Microbiology*, 6 (1):3–6, 2021. doi:10.1038/s41564-020-00834-3.

Chang Soo Eun, Yoshiyuki Mishima, Steffen Wohlgemuth, Bo Liu, Maureen Bower, Ian M. Carroll, and R. Balfour Sartor. Induction of Bacterial Antigen-Specific Colitis by a Simplified Human Microbiota Consortium in Gnotobiotic Interleukin-10-/- Mice. *Infection and Immunity*, 82(6):2239–2246, 2014. ISSN 0019-9567. doi:10.1128/iai.01513-13.

Leonides Fernández, Susana Delgado, Helena Herrero, Antonio Maldonado, and Juan M. Rodríguez. The Bacteriocin Nisin, an Effective Agent for the Treatment of Staphylococcal Mastitis During Lactation. *Journal of Human Lactation*, 24(3):311–316, 2008. ISSN 0890-3344. doi:10.1177/0890334408317435.

Pamela Ferretti, Edoardo Pasolli, Adrian Tett, Francesco Asnicar, Valentina Gorfer, Sabina Fedi, Federica Armanini, Duy Tin Truong, Serena Manara, Moreno Zolfo, Francesco Beghini, Roberto Bertorelli, Veronica De Sanctis, Ilaria Bariletti, Rosarita Canto, Rosanna Clementi, Marina Cologna, Tiziana Crifò, Giuseppina Cusumano, Stefania Gottardi, Claudia Innamorati, Caterina Masè, Daniela Postai, Daniela Savoi, Sabrina Duranti, Gabriele Andrea Lugli, Leonardo Mancabelli, Francesca Turroni, Chiara Ferrario, Christian Milani, Marta Mangifesta, Rosaria Anzalone, Alice Viappiani, Moran Yassour, Hera Vlamakis, Ramnik Xavier, Carmen Maria Collado, Omry Koren, Saverio Tateo, Massimo Soffiati, Anna Pedrotti, Marco Ventura, Curtis Huttenhower, Peer Bork, and Nicola

Segata. Mother-to-Infant Microbial Transmission from Different Body Sites Shapes the Developing Infant Gut Microbiome. *Cell Host & Microbe*, 24(1):133–145.e5, 2018. ISSN 1931-3128. doi:10.1016/j.chom.2018.06.005.

Des Field, Miguel Fernandez de Ullivarri, R Paul Ross, and Colin Hill. After a century of nisin research - where are we now? *FEMS Microbiology Reviews*, 47(3):fuad023, 2023. ISSN 0168-6445. doi:10.1093/femsre/fuad023.

Michael A Funk and Wilfred A van der Donk. Ribosomal Natural Products, Tailored To Fit. *Accounts of Chemical Research*, 50(7):1577–1586, 2017. ISSN 0001-4842. doi:10.1021/acs.accounts.7b00175.

Yile He, Aili Fan, Meng Han, Hongwei Li, Mengzhe Li, Huahao Fan, Xiaoping An, Lihua Song, Shaozhou Zhu, and Yigang Tong. Mammalian Commensal Streptococci Utilize a Rare Family of Class VI Lanthipeptide Synthetases to Synthesize Miniature Lanthipeptide-type Ribosomal Peptide Natural Products. *Biochemistry*, 62(2):462–475, 2023. ISSN 0006-2960. doi:10.1021/acs.biochem.2c00534.

Simon Heilbronner, Bernhard Krismer, Heike Brötz-Oesterhelt, and Andreas Peschel. The microbiome-shaping roles of bacteriocins. *Nature Reviews Microbiology*, 19(11):726–739, 2021. ISSN 1740-1526. doi:10.1038/s41579-021-00569-w.

Colin Hill, Lorraine Draper, R Ross, and Paul Cotter. Lantibiotic Immunity. *Current Protein & Peptide Science*, 9(1):39–49, 2008. ISSN 1389-2037. doi:10.2174/138920308783565750.

Thomas Hindré, Jean-Paul Le Pennec, Dominique Haras, and Alain Dufour. Regulation of lantibiotic lacticin 481 production at the transcriptional level by acid pH. *FEMS Microbiology Letters*, 231(2):291–298, 2004. ISSN 0378-1097. doi:10.1016/s0378-1097(04)00010-2.

Doug Hyatt, Gwo-Liang Chen, Philip F LoCascio, Miriam L Land, Frank W Larimer, and Loren J Hauser. Prodigal: prokaryotic gene recognition and translation initiation site identification. *BMC Bioinformatics*, 11(1):119–119, 2010. doi:10.1186/1471-2105-11-119.

Onyinye I. Iweala and Cathryn R. Nagler. The Microbiome and Food Allergy. *Annual Review of Immunology*, 37(1):377–403, 2019. ISSN 0732-0582. doi:10.1146/annurev-immunol-042718-041621.

Michael A. Johnstone and William T. Self. d-Proline Reductase Underlies Proline-Dependent Growth of Clostridioides difficile. *Journal of Bacteriology*, 204(8):e00229–22, 2022. ISSN 0021-9193. doi:10.1128/jb.00229-22.

Minoru Kanehisa, Yoko Sato, and Kanae Morishima. BlastKOALA and GhostKOALA: KEGG Tools for Functional Characterization of Genome and Metagenome Sequences. *Journal of Molecular Biology*, 428(4):726–731, 2016. ISSN 0022-2836. doi:10.1016/j.jmb.2015.11.006.

Minoru Kanehisa, Miho Furumichi, Yoko Sato, Yuriko Matsuura, and Mari Ishiguro-Watanabe. KEGG: biological systems database as a model of the real world. *Nucleic acids research*, 53(D1):D672–D677, 2025. ISSN 0305-1048. doi:10.1093/nar/gkae909.

Sohn G. Kim, Simone Becattini, Thomas U. Moody, Pavel V. Shliaha, Eric R. Littmann, Ruth Seok, Mergim Gjonbalaj, Vincent Eaton, Emily Fontana, Luigi Amoretti, Roberta Wright, Silvia Caballero, Zhong-Min X. Wang, Hea-Jin Jung, Sejal M. Morjaria, Ingrid M. Leiner, Weige Qin, Ruben J. J. F. Ramos, Justin R. Cross, Seiko Narushima, Kenya Honda, Jonathan U. Peled, Ronald C. Hendrickson, Ying Taur, Marcel R. M. van den Brink, and Eric G. Pamer. Microbiota-derived lantibiotic restores resistance against vancomycin-resistant Enterococcus. *Nature*, 572(7771):665–669, 2019. ISSN 0028-0836. doi:10.1038/s41586-019-1501-z.

Andrew M. King, Zhengan Zhang, Emerson Glassey, Piro Siuti, Jon Clardy, and Christopher A. Voigt. Systematic mining of the human microbiome identifies antimicrobial peptides with diverse activity spectra. *Nature Microbiology*, 8(12):2420–2434, 2023. doi:10.1038/s41564-023-01524-6.

Shinya Kodani, Michael E. Hudson, Marcus C. Durrant, Mark J. Buttner, Justin R. Nodwell, and Joanne M. Willey. The SapB morphogen is a lantibiotic-like peptide derived from the product of the developmental gene ramS in Streptomyces coelicolor. *Proceedings of the National Academy of Sciences*, 101(31):11448–11453, 2004. ISSN 0027-8424. doi:10.1073/pnas.0404220101.

Changhyun Lee, Byeong Gwan Kim, Jee Hyun Kim, Jaeyoung Chun, Jong Pil Im, and Joo Sung Kim. Sodium butyrate inhibits the NF-kappa B signaling pathway and histone deacetylation, and attenuates experimental colitis in an IL-10 independent manner. *International Immunopharmacology*, 51:47–56, 2017. ISSN 1567-5769. doi:10.1016/j.intimp.2017.07.023.

Jee-Yon Lee, Connor R. Tiffany, Scott P. Mahan, Matthew Kellom, Andrew W.L. Rogers, Henry Nguyen, Eric T. Stevens, Hugo L.P. Masson, Kohei Yamazaki, Maria L. Marco, Emiley A. Eloe-Fadrosh, Peter J. Turnbaugh, and Andreas J. Bäumler. High fat intake sustains sorbitol intolerance after antibiotic-mediated Clostridia depletion from the gut microbiota. *Cell*, 187(5):1191–1205.e15, 2024. ISSN 0092-8674. doi:10.1016/j.cell.2024.01.029.

Christopher J Lehmann, Nicholas P Dylla, Matthew Odenwald, Ravi Nayak, Maryam Khalid, Jaye Boissiere, Jackelyn Cantoral, Emerald Adler, Matthew R Stutz, Mark Dela Cruz, Angelica Moran, Huaiying Lin, Ramanujam Ramaswamy, Anitha Sundararajan, Ashley M Sidebottom, Jessica Little, Eric G Pamer, Andrew Aronsohn, John Fung, Talia B Baker, and Aalok Kacha. Fecal metabolite profiling identifies liver transplant recipients at risk for postoperative infection. *Cell Host & Microbe*, 32(1):117–130.e4, 2024. ISSN 1931-3128. doi:10.1016/j.chom.2023.11.016.

Dinghua Li, Chi-Man Liu, Ruibang Luo, Kunihiko Sadakane, and Tak-Wah Lam. MEGAHIT: an ultra-fast single-node solution for large and complex metagenomics assem-

bly via succinct de Bruijn graph. *Bioinformatics*, 31(10):1674–1676, 2015. ISSN 1367-4803. doi:10.1093/bioinformatics/btv033.

Jonathan B. Lynch, Erika L. Gonzalez, Kayli Choy, Kym F. Faull, Talia Jewell, Abelardo Arellano, Jennifer Liang, Kristie B. Yu, Jorge Paramo, and Elaine Y. Hsiao. Gut microbiota Turicibacter strains differentially modify bile acids and host lipids. *Nature Communications*, 14(1):3669, 2023. doi:10.1038/s41467-023-39403-7.

José Luis Maturana and Juan P. Cárdenas. Insights on the Evolutionary Genomics of the Blautia Genus: Potential New Species and Genetic Content Among Lineages. *Frontiers in Microbiology*, 12:660920, 2021. ISSN 1664-302X. doi:10.3389/fmicb.2021.660920.

Leland McInnes, John Healy, and James Melville. UMAP: Uniform Manifold Approximation and Projection for Dimension Reduction. *arXiv*, 2018. doi:10.48550/arxiv.1802.03426.

Paul J. McMurdie and Susan Holmes. phyloseq: An R Package for Reproducible Interactive Analysis and Graphics of Microbiome Census Data. *PLoS ONE*, 8(4):e61217, 2013. doi:10.1371/journal.pone.0061217.

Matthew A Odenwald, Huaiying Lin, Christopher Lehmann, Nicholas P Dylla, Cody G Cole, Jake D Mostad, Téa E Pappas, Ramanujam Ramaswamy, Angelica Moran, Alan L Hutchison, Matthew R Stutz, Mark Dela Cruz, Emerald Adler, Jaye Boissiere, Maryam Khalid, Jackelyn Cantoral, Fidel Haro, Rita A Oliveira, Emily Waligurski, Thomas G Cotter, Samuel H Light, Kathleen G Beavis, Anitha Sundararajan, Ashley M Sidebottom, K Gautham Reddy, Sonali Paul, Anjana Pillai, Helen S Te, Mary E Rinella, Michael R Charlton, Eric G Pamer, and Andrew I Aronsohn. Bifidobacteria metabolize lactulose to optimize gut metabolites and prevent systemic infection in patients with liver disease. *Nature Microbiology*, 8(11):2033–2049, 2023. doi:10.1038/s41564-023-01493-w.

Elvis Legala Ongey, Hüseyin Yassi, Stephan Pflugmacher, and Peter Neubauer. Pharmacological and pharmacokinetic properties of lanthipeptides undergoing clinical studies. *Biotechnology Letters*, 39(4):473–482, 2017. ISSN 0141-5492. doi:10.1007/s10529-016-2279-9.

Chayanid Ongpipattanakul, Emily K. Desormeaux, Adam DiCaprio, Wilfred A. van der Donk, Douglas A. Mitchell, and Satish K. Nair. Mechanism of Action of Ribosomally Synthesized and Post-Translationally Modified Peptides. *Chemical Reviews*, 122(18): 14722–14814, 2022. ISSN 0009-2665. doi:10.1021/acs.chemrev.2c00210.

Catherine O'Reilly, Ghjuvan M. Grimaud, Mairéad Coakley, Paula M. O'Connor, Harsh Mathur, Veronica L. Peterson, Ciara M. O'Donovan, Peadar G. Lawlor, Paul D. Cotter, Catherine Stanton, Mary C. Rea, Colin Hill, and R. Paul Ross. Modulation of the gut microbiome with nisin. *Scientific Reports*, 13(1):7899, 2023. doi:10.1038/s41598-023-34586-x.

Typhaine Paysan-Lafosse, Antonina Andreeva, Matthias Blum, Sara Rocio Chuguransky, Tiago Grego, Beatriz Lazaro Pinto, Gustavo A Salazar, Maxwell L Bileschi, Felipe

Llinares-López, Laetitia Meng-Papaxanthos, Lucy J Colwell, Nick V Grishin, R Dustin Schaeffer, Damiano Clementel, Silvio C E Tosatto, Erik Sonnhammer, Valerie Wood, and Alex Bateman. The Pfam protein families database: embracing AI/ML. *Nucleic acids research*, 53(D1):D523–D534, 2025. ISSN 0305-1048. doi:10.1093/nar/gkae997.

Geoffrey A. Preidis and James Versalovic. Targeting the Human Microbiome With Antibiotics, Probiotics, and Prebiotics: Gastroenterology Enters the Metagenomics Era. *Gastroenterology*, 136(6):2015–2031, 2009. ISSN 0016-5085. doi:10.1053/j.gastro.2009.01.072.

Morgan N. Price, Paramvir S. Dehal, and Adam P. Arkin. FastTree 2 – Approximately Maximum-Likelihood Trees for Large Alignments. *PLoS ONE*, 5(3):e9490, 2010. doi:10.1371/journal.pone.0009490.

Dulce Ramírez-Rendón, Fernando Guzmán-Chávez, Carlos García-Ausencio, Romina Rodríguez-Sanoja, and Sergio Sánchez. The untapped potential of actinobacterial lanthipeptides as therapeutic agents. *Molecular Biology Reports*, 50(12):10605–10616, 2023. ISSN 0301-4851. doi:10.1007/s11033-023-08880-w.

Lindsay M Repka, Jonathan R Chekan, Satish K Nair, and Wilfred A van der Donk. Mechanistic Understanding of Lanthipeptide Biosynthetic Enzymes. *Chemical Reviews*, 117(8): 5457–5520, 2017. ISSN 0009-2665. doi:10.1021/acs.chemrev.6b00591.

Eliette Riboulet-Bisson, Mark H. J. Sturme, Ian B. Jeffery, Michelle M. O'Donnell, B. Anne Neville, Brian M. Forde, Marcus J. Claesson, Hugh Harris, Gillian E. Gardiner, Patrick G. Casey, Peadar G. Lawlor, Paul W. O'Toole, and R. Paul Ross. Effect of Lactobacillus salivarius Bacteriocin Abp118 on the Mouse and Pig Intestinal Microbiota. *PLoS ONE*, 7 (2):e31113, 2012. doi:10.1371/journal.pone.0031113.

Sandra M Roy, Margaret A Riley, and Joseph H Crabb. The Bacteriocins: Current Knowledge and Future Prospects - Treating Bovine Mastitis with Nisin: A Model for the Use of Protein Antimicrobials in Veterinary Medicine. *Caister Academic Press*, pages 127–140, 2016. doi:10.21775/9781910190371.07.

Oliver Schwengers, Lukas Jelonek, Marius Alfred Dieckmann, Sebastian Beyvers, Jochen Blom, and Alexander Goesmann. Bakta: rapid and standardized annotation of bacterial genomes via alignment-free sequence identification. *Microbial Genomics*, 7(11):000685, 2021. doi:10.1099/mgen.0.000685.

Matthew T Sorbara, Eric R Littmann, Emily Fontana, Thomas U Moody, Claire E Kohout, Mergim Gjonbalaj, Vincent Eaton, Ruth Seok, Ingrid M Leiner, and Eric G Pamer. Functional and Genomic Variation between Human-Derived Isolates of Lachnospiraceae Reveals Inter- and Intra-Species Diversity. *Cell host & microbe*, 28(1):134–146.e4, 2019. ISSN 1931-3128. doi:10.1016/j.chom.2020.05.005.

Anton Du Preez van Staden, Winschau F. van Zyl, Marla Trindade, Leon M. T. Dicks, and Carine Smith. Therapeutic Application of Lantibiotics and Other Lanthipeptides: Old and

New Findings. *Applied and Environmental Microbiology*, 87(14):e00186–21, 2021. ISSN 0099-2240. doi:10.1128/aem.00186-21.

Matthew R Stutz, Nicholas P Dylla, Steven D Pearson, Paola Lecompte-Osorio, Ravi Nayak, Maryam Khalid, Emerald Adler, Jaye Boissiere, Huaiying Lin, William Leiter, Jessica Little, Amber Rose, David Moran, Michael W Mullowney, Krysta S Wolfe, Christopher Lehmann, Matthew Odenwald, Mark De La Cruz, Mihai Giurcanu, Anne S Pohlman, Jesse B Hall, Jean-Luc Chaubard, Anitha Sundararajan, Ashley Sidebottom, John P Kress, Eric G Pamer, and Bhakti K Patel. Immunomodulatory fecal metabolites are associated with mortality in COVID-19 patients with respiratory failure. *Nature Communications*, 13(1):6615, 2022. doi:10.1038/s41467-022-34260-2.

Jotham Suez, Niv Zmora, Gili Zilberman-Schapira, Uria Mor, Mally Dori-Bachash, Stavros Bashiardes, Maya Zur, Dana Regev-Lehavi, Rotem Ben-Zeev Brik, Sara Federici, Max Horn, Yotam Cohen, Andreas E. Moor, David Zeevi, Tal Korem, Eran Kotler, Alon Harmelin, Shalev Itzkovitz, Nitsan Maharshak, Oren Shibolet, Meirav Pevsner-Fischer, Hagit Shapiro, Itai Sharon, Zamir Halpern, Eran Segal, and Eran Elinav. Post-Antibiotic Gut Mucosal Microbiome Reconstitution Is Impaired by Probiotics and Improved by Autologous FMT. *Cell*, 174(6):1406–1423.e16, 2018. ISSN 0092-8674. doi:10.1016/j.cell.2018.08.047.

Zhizeng Sun, Jin Zhong, Xiaobo Liang, Jiale Liu, Xiuzhu Chen, and Liandong Huan. Novel Mechanism for Nisin Resistance via Proteolytic Degradation of Nisin by the Nisin Resistance Protein NSR. *Antimicrobial Agents and Chemotherapy*, 53(5):1964–1973, 2009. ISSN 0066-4804. doi:10.1128/aac.01382-08.

Jonathan I. Tietz, Christopher J. Schwalen, Parth S. Patel, Tucker Maxson, Patricia M. Blair, Hua-Chia Tai, Uzma I. Zakai, and Douglas A. Mitchell. A new genome-mining tool redefines the lasso peptide biosynthetic landscape. *Nature chemical biology*, 13(5):470–478, 2017. ISSN 1552-4450. doi:10.1038/nchembio.2319.

Fabricio L. Tulini, Christopher T. Lohans, Karla C.F. Bordon, Jing Zheng, Eliane C. Arantes, John C. Vederas, and Elaine C.P. De Martinis. Purification and characterization of antimicrobial peptides from fish isolate Carnobacterium maltaromaticum C2: Carnobacteriocin X and carnolysins A1 and A2. *International Journal of Food Microbiology*, 173:81–88, 2014. ISSN 0168-1605. doi:10.1016/j.ijfoodmicro.2013.12.019.

Shona Uniacke-Lowe, Catherine Stanton, Colin Hill, and R. Paul Ross. The Marine Fish Gut Microbiome as a Source of Novel Bacteriocins. *Preprints*, page 202405.1215.v1, 2024. doi:10.20944/preprints202405.1215.v1.

Katy Vaillancourt, Geneviève LeBel, Michel Frenette, Marcelo Gottschalk, and Daniel Grenier. Suicin 3908, a New Lantibiotic Produced by a Strain of Streptococcus suis Serotype 2 Isolated from a Healthy Carrier Pig. *PLoS ONE*, 10(2):e0117245, 2015. doi:10.1371/journal.pone.0117245.

Sara Vieira-Silva, Gwen Falony, Youssef Darzi, Gipsi Lima-Mendez, Roberto Garcia Yunta, Shujiro Okuda, Doris Vandeputte, Mireia Valles-Colomer, Falk Hildebrand, Samuel Chaffron, and Jeroen Raes. Species–function relationships shape ecological properties of the human gut microbiome. *Nature Microbiology*, 1(8):16088, 2016. doi:10.1038/nmicrobiol.2016.88.

Mark C. Walker, Sara M. Eslami, Kenton J. Hetrick, Sarah E. Ackenhusen, Douglas A. Mitchell, and Wilfred A. van der Donk. Precursor peptide-targeted mining of more than one hundred thousand genomes expands the lanthipeptide natural product family. *BMC Genomics*, 21(1):387, 2020. doi:10.1186/s12864-020-06785-7.

Calum J. Walsh, Caitriona M. Guinane, Colin Hill, R. Paul Ross, Paul W. O'Toole, and Paul D. Cotter. In silico identification of bacteriocin gene clusters in the gastrointestinal tract, based on the Human Microbiome Project's reference genome database. *BMC Microbiology*, 15(1):183, 2015. doi:10.1186/s12866-015-0515-4.

Philip A. Wescombe, Mathew Upton, Karen P. Dierksen, Nancy L. Ragland, Senthuran Sivabalan, Ruth E. Wirawan, Megan A. Inglis, Chris J. Moore, Glenn V. Walker, Chris N. Chilcott, Howard F. Jenkinson, and John R. Tagg. Production of the Lantibiotic Salivaricin A and Its Variants by Oral Streptococci and Use of a Specific Induction Assay To Detect Their Presence in Human Saliva. *Applied and Environmental Microbiology*, 72(2): 1459–1466, 2006. ISSN 0099-2240. doi:10.1128/aem.72.2.1459-1466.2006.

Huizhong Xiong, Rebecca A Carter, Ingrid M Leiner, Yi-Wei Tang, Liang Chen, Barry N Kreiswirth, and Eric G Pamer. Distinct Contributions of Neutrophils and CCR2 + Monocytes to Pulmonary Clearance of Different Klebsiella pneumoniae Strains. *Infection and Immunity*, 83(9):3418–3427, 2015. ISSN 0019-9567. doi:10.1128/iai.00678-15.

Guangchuang Yu, David K. Smith, Huachen Zhu, Yi Guan, and Tommy Tsan-Yuk Lam. ggtree: an r package for visualization and annotation of phylogenetic trees with their covariates and other associated data. *Methods in Ecology and Evolution*, 8(1):28–36, 2017. ISSN 2041-210X. doi:10.1111/2041-210x.12628.

Zhenrun J. Zhang, Cody G. Cole, Huaiying Lin, Chunyu Wu, Fidel Haro, Emma McSpadden, Wilfred A van der Donk, and Eric G. Pamer. Exposure and resistance to lantibiotics impact microbiota composition and function. *bioAxiv*, 2023. doi:10.1101/2023.12.30.573728.

Zhenrun J. Zhang, Cody G. Cole, Michael J. Coyne, Huaiying Lin, Nicholas Dylla, Rita C. Smith, Téa E. Pappas, Shannon A. Townson, Nina Laliwala, Emily Waligurski, Ramanujam Ramaswamy, Che Woodson, Victoria Burgo, Jessica C. Little, David Moran, Amber Rose, Mary McMillin, Emma McSpadden, Anitha Sundararajan, Ashley M. Sidebottom, Eric G. Pamer, and Laurie E. Comstock. Comprehensive analyses of a large human gut Bacteroidales culture collection reveal species- and strain-level diversity and evolution. *Cell Host & Microbe*, 32(10):1853–1867.e5, 2024a. ISSN 1931-3128. doi:10.1016/j.chom.2024.08.016.

Zhenrun J Zhang, Chunyu Wu, Ryan Moreira, Darian Dorantes, Téa Pappas, Anitha Sundararajan, Huaiying Lin, Eric G Pamer, and Wilfred A van der Donk. Activity of Gut-Derived Nisin-like Lantibiotics against Human Gut Pathogens and Commensals. *ACS Chemical Biology*, 19(2):357–369, 2024b. ISSN 1554-8929. doi:10.1021/acschembio.3c00577.

Xiling Zhao and Wilfred A. van der Donk. Structural Characterization and Bioactivity Analysis of the Two-Component Lantibiotic Flv System from a Ruminant Bacterium. *Cell Chemical Biology*, 23(2):246–256, 2016. ISSN 2451-9456. doi:10.1016/j.chembiol.2015.11.014.

Jinshui Zheng, Michael G. Gänzle, Xiaoxi B. Lin, Lifang Ruan, and Ming Sun. Diversity and dynamics of bacteriocins from human microbiome. *Environmental Microbiology*, 17 (6):2133–2143, 2015. ISSN 1462-2912. doi:10.1111/1462-2920.12662.